MONTHLY NOTICES

OF THE

ROYAL ASTRONOMICAL SOCIETY

Volume 120 No. 1 1960

Published and Sold by the

ROYAL ASTRONOMICAL SOCIETY
BURLINGTON HOUSE
LONDON, W.1

Price £1 4*s.* 0*d.*; *in U.S.A.* $3·50

Subscription for volume: £6 ; *in U.S.A.* $18

The Geophysical Journal

OF THE

ROYAL ASTRONOMICAL SOCIETY

Editors

A. H. Cook
M.A., Ph.D., F.R.A.S., F.G.S.
National Physical Laboratory
Teddington

T. F. Gaskell
M.A., Ph.D., F.R.A.S.
British Petroleum Company
London

Price £1 per number; in U.S.A. $3. Annual Subscription £3; in U.S.A. $9

Volume 2 No. 4 December 1959

CONTENTS

K. M. Creer, A.C. demagnetization of unstable Triassic Keuper Marls from S.W. England.

T. Rikitake, Anomaly of geomagnetic variations in Japan.

K. F. Bowden, L. A. Fairbairn and P. Hughes, The distribution of shearing stresses in a tidal current

K. M. Creer, E. Irving and A. E. M. Nairn, Palaeomagnetism of the Great Whin Sill.

A. L. Hales and D. I. Gough, Gravity anomalies and crustal structure in South Africa.

J. E. Jackson, Observations with the Cambridge pendulum apparatus in North, Central and South America in 1958.

B. Gutenberg, Wave velocities below the Mohorovičič discontinuity.

R. W. Girdler, A palaeomagnetic study of some Lower Jurassic rocks of N.W. Europe.

J. MacDowall, A note on the relation between wind velocity and the amplitude of microseisms on the coast of Antarctica.

Report on the Moscow Meeting of the Joint Commission on Solar and Terrestrial Relationships, August 1958.

Orders should be addressed to:

The Assistant Secretary

Royal Astronomical Society, Burlington House, London, W.1

MONTHLY NOTICES

OF THE

ROYAL ASTRONOMICAL SOCIETY

Vol. 120 No. 1

MEETING OF 1960 JANUARY 8

Professor R. O. Redman, President, in the Chair

The President announced that the Council had awarded the Gold Medal of the Society to Professor Viktor Amazaspovich Ambartsumian for his numerous important contributions to both theoretical and observational astronomy.

The President announced that the Council had awarded the Eddington Medal to Dr Robert d'Escourt Atkinson for his pioneering paper on atomic synthesis and stellar energy.

The President announced that the Council had awarded the Jackson Gwilt Medal and Gift jointly to Mr Frank Malne Bateson and Mr Albert Francis Arthur Lofley Jones for their work on variable stars in the southern hemisphere.

The election by the Council of the following Fellows was duly confirmed:—

Colin Benjamin Baxter, 25 Swallowbeck Avenue, Lincoln (proposed by R. R. S. Cox);

Maudslay Baynes, Flat 89A, Whitehall Court, London, S.W.1 (proposed by R. A. Lyttleton);

Henry Brinton, Old Mill House, Selsey, Sussex (proposed by P. Moore);

Stace Victor Murray Clube, Winchester College, Winchester (proposed by H. H. Plaskett);

David L. Crawford, Dyer Observatory, Vanderbilt University, Nashville, Tenn., U.S.A. (proposed by R. Hardie);

James Cuffey, Department of Astronomy, University of Indiana, Bloomington, Indiana, U.S.A. (proposed by M. H. Wrubel);

*John Keith Welwyn Davies, 12 Farm Lane, Cobbs Quarry Estate, Appleton, nr. Warrington, Lancs. (proposed by F. D. Kahn);

Keith Malcolm Donald, 53 Elm Tree Close, Northolt, Mddx. (proposed by F. W. Cousins);

Hugh Alastair Gebbie, Basic Physics Division, National Physical Laboratory, Teddington, Mddx. (proposed by A. H. Cook);

*David J. Harris, 148 Windsor Avenue, Penn, Wolverhampton, Staffs. (proposed by C. Lloyd);

Roger Davis Harrison, Department of Extra-Mural Studies, King's College, Newcastle upon Tyne, 1 (proposed by C. Gilbert);

*Muriel Hodgkinson, 78 Hardy Lane, Chorlton-cum-Hardy, Manchester 21 (proposed by Z. Kopal);

James Trevor Hornabrook, Exploration Department, British Petroleum Co. Ltd., Ropemaker Street, London, E.C.2 (proposed by L. H. Tarrant);

* Transferring from Junior Membership.

*Derek Hugh Powell Jones, Royal Greenwich Observatory, Herstmonceux Castle, Hailsham, Sussex (proposed by O. J. Eggen);

Herbert Joy, 33 Milman Road, Reading, Berks. (proposed by G. E. S. Kendall);

*Peter Calvin Kendall, 2c Hall Drive, London, S.E.26 (proposed by V. C. A. Ferraro);

Arlo Udell Landolt, Goethe Link Observatory, Indiana University, Bloomington, Indiana, U.S.A. (proposed by R. L. Sears);

Clarence Roger Lynds, National Radio Astronomy Observatory, Green Bank, W. Virginia, U.S.A. (proposed by A. B. Underhill);

*Brian Geoffrey Marsden, Yale University Observatory, 135 Prospect Street, New Haven, Conn., U.S.A. (proposed by A. Beer);

*Derek McNally, Department of Mathematics, Royal Holloway College, Englefield Green, Surrey (proposed by W. H. McCrea);

*Christopher J. Millns, 21 The Brow, The Brecks, Rotherham, Yorks. (proposed by Z. Kopal);

Kenneth Ashe Payne, 22 Addiscombe Grove, Croydon, Surrey (proposed by C. W. Allen);

Kenneth Samuel George Stocker, 12 Oxford Road, Wallington, Surrey (proposed by F. H. G. Best); and

Herbert Norman Douglas Wright, 96 Elmbourne Road, London, S.W.17 (proposed by F. H. G. Best).

* Transferring from Junior Membership.

The election by the Council of the following Junior Members was duly confirmed:—

Charles Reginald Dickens, 6 Taddington Road, Eastbourne, Sussex (proposed by C. W. Allen);

Leon Brian Lucy, 34 Athol Road, Whalley Range, Manchester 16 (proposed by F. D. Kahn);

John Christopher Marsh, 22 The Lawns, London, S.E.19 (proposed by F. H. G. Best); and

Ian Gerhard Van Breda, 20 St. Barnabas Road, Woodford Green, Essex (proposed by D. E. Blackwell).

ON THE MEAN ABSORPTION COEFFICIENT IN THE COMPUTATION OF MODEL STELLAR ATMOSPHERES OF SOLAR TYPE STARS

Antoni Przybylski

(Received 1959 May 14)

Summary

The problem of reducing the general case to the grey one in the computation of model stellar atmospheres was investigated for solar type stars. It was found that:

(i) the " absorption " mean defined by the equation $\kappa_a = (1/\bar{I}) \int_0^\infty \kappa_\nu \bar{I}_\nu \, d\nu$ and the " emission " mean $\kappa_e = (1/B) \int_0^\infty \kappa_\nu B_\nu \, d\nu$ are numerically equal within about 1 per cent throughout the whole atmosphere and consequently the equation

$$\bar{I}(\bar{\tau}) = B(\bar{\tau}),$$

which is strictly valid for the grey case, is also satisfied for the non-grey solar atmosphere within about 1 per cent;

(ii) the radiation pressure mean $\kappa p_r = (1/F) \int_0^\infty \kappa_\nu F_\nu \, d\nu$ and the Rosseland mean require only small corrections to the grey temperature distribution in the computation of model stellar atmospheres;

(iii) if these corrections are disregarded both means lead to model stellar atmospheres sufficiently accurate to account for all visible features of stellar spectra;

(iv) other mean absorption coefficients require large corrections to the grey temperature distribution; and

(v) at the optical depth $\bar{\tau} = 11{\cdot}6$ the weight function of the Rosseland mean is practically identical with that of the radiation pressure mean and similarly the weight functions of the " absorption " mean and the " emission " mean approach each other very closely.

---

1. *Introduction*

Whilst the problem of a grey atmosphere can now be considered as a closed chapter in the theory of stellar atmospheres, since the exact solution is known, our present knowledge of the theory of a non-grey atmosphere is still inadequate. The obvious reason for this is the fact that non-grey atmospheres cannot be treated mathematically in a general way and therefore recourse must be made to numerical methods, which lack the precision of general methods and, in addition, require much computational work.

The most promising approach to the problem of computing non-grey stellar atmospheres consists of an attempt to reduce the general case to the grey one. Were this possible, the relation between the Planck function $B(\tau)$ and the optical depth τ:

$$B(\tau) = \tfrac{3}{4} F . \{\tau + q(\tau)\}, \qquad (1)$$

valid for the grey case, would remain valid in the general case if the optical depth is measured in terms of a suitable mean value $\bar{\kappa}$ of the absorption coefficient κ_ν. For many years it was believed that such a mean value of the absorption coefficient existed and that in fact it was identical to the radiation pressure mean κ_{pr} defined by the equation

$$\kappa_{pr} = \frac{1}{F}\int_0^\infty \kappa_\nu F_\nu \, d\nu, \tag{2}$$

in which F is the (constant) net flux and F_ν the monochromatic flux of energy. This view, however, was erroneous, as pointed out by Michard (1) in 1949. Indeed, equation (1) fixes the surface temperature T_0 as a function of the net flux F:

$$\frac{\sigma}{\pi} T_0^4 = B(0) = \frac{3}{4} F \cdot q(0) = \frac{\sqrt{3}}{4} F, \tag{3}$$

whereas the surface temperature of a non-grey atmosphere, as shown by Hopf (2), depends on the variation of the absorption coefficient with the wave-length. It is therefore impossible to reduce the general case to the grey one in full mathematical strictness and consequently no *true* mean absorption coefficient exists. In view of this difficulty, all that can be done is to search for the best possible mean and in the present investigations this is done for model stellar atmospheres of solar type stars.

2. *Different kinds of mean absorption coefficients*

2.1. *Primary mean absorption coefficients.*—The weight function, $W(\nu)$, used in the computation of the mean absorption coefficient:

$$\kappa = \int_0^\infty \kappa_\nu W(\nu)\, d\nu,$$

cannot be arbitrary but (apart from being normalized to unity) must have some physical justification. The possible weight functions $W(\nu)$ are determined by physical processes which involve the coefficient of absorption and have a bearing on the state of the stellar atmosphere, i.e. the radiation pressure, the process of the absorption of energy and that of emission. Each of these three physical phenomena defines its own mean absorption coefficient and therefore, instead of one single mean as in the grey case, we have three kinds of mean absorption coefficient in the general or non-grey case. This point was first put clearly by Kourganoff (3). The three means in question will be called subsequently in this paper the radiation pressure mean κ_{pr}, the absorption mean κ_a, and the emission mean κ_e, and are defined by the equations:

$$\kappa_{pr} = \frac{1}{F}\int_0^\infty \kappa_\nu F_\nu \, d\nu,$$

$$\kappa_a = \frac{1}{\bar{I}}\int_0^\infty \kappa_\nu \bar{I}_\nu \, d\nu, \tag{4}$$

$$\kappa_e = \frac{1}{\mathcal{J}}\int_0^\infty \kappa_\nu \mathcal{J}_\nu \, d\nu, \tag{5}$$

in which the designation $\bar{I}_\nu$ is used for the (geometric) monochromatic mean intensity, $\mathcal{J}_\nu$ for the monochromatic source function and $\bar{I}$, $\mathcal{J}$ for the corresponding integrated values. In the case of local thermodynamic equilibrium

(which, after all, is assumed in all practical applications of the theory of radiative transfer) the last mean is identical to the Planck mean κ_P defined by the equation:

$$\kappa_P = \frac{1}{B}\int_0^\infty \kappa_\nu B_\nu \, d\nu. \tag{6}$$

In the grey case all means have, of course, the same value equal to the constant absorption coefficient; in the general case, however, they differ, and therefore the law of the temperature distribution depends on the kind of mean absorption coefficient used in the construction of the model stellar atmosphere.

As already stated in Section 1, all three possible laws of the temperature distribution must differ from that of the grey case given by equation (1), but the present investigations show that the corresponding law for the radiation pressure mean differs only slightly from it. In practice, therefore, it is possible to reduce the general case to the grey one within the limits of the accuracy of computations.

The application of any mean absorption coefficient defined by equations (2), (4) and (5) in the computation of model stellar atmospheres is, however, hardly possible since they are not known until the definitive structure of the stellar atmosphere is known; the only exception is to a certain extent the "emission" mean κ_e which can be computed in the case of local thermodynamic equilibrium by means of equation (6) as the Planck mean κ_P. In view of this difficulty, recourse must be made to some approximations to a chosen mean, which can be computed *a priori* without the knowledge of the definitive structure of the model stellar atmosphere. Such approximations have been found by Rosseland and Chandrasekhar for the radiation pressure mean, which for a long time was considered to be the true mean in spite of the fact that the radiation pressure has only a negligible effect on the structure of stellar atmospheres.

2.2. *Chandrasekhar's mean.*—In the first approximation Chandrasekhar replaces the monochromatic fluxes F_ν in equation (2) by the fluxes $F_\alpha^{(1)}$ computed for a grey atmosphere and obtains in that way:

$$\kappa_{Ch} = \frac{1}{F}\int_0^\infty \kappa_\nu F_\alpha^{(1)} \, d\alpha,$$

where $\alpha = h\nu/kT_e$, T_e being the effective temperature of the star. The function $F_\alpha^{(1)}$ has been tabulated by Chandrasekhar (4). Chandrasekhar's mean can be a good approximation to the radiation pressure mean κ_{pr} only if the monochromatic fluxes F_ν do not differ greatly from the fluxes computed for a grey atmosphere or, as explained in subsequent sections, if the deviations of the monochromatic absorption coefficient κ_ν from the mean value are not too large. This condition is, however, not fulfilled for most stars and therefore Chandrasekhar's mean is only a poor approximation to the radiation pressure mean.

2.3. *Unsöld's and Rosseland's means.*—Another approximation to the radiation pressure mean can be obtained if in the equation for $F_\nu(\tau_\nu)$:

$$F_\nu(\tau_\nu) = \Phi_{\tau_\nu}(B_\nu) = 2\int_{\tau_\nu}^\infty B_\nu(t)E_2(t-\tau_\nu)\,dt - 2\int_0^{\tau_\nu} B_\nu(t)E_2(\tau_\nu - t)\,dt,$$

or

$$F_\nu(\tau_\nu) = 2\int_0^\infty B_\nu(\tau_\nu + x)E_2(x)\,dx - 2\int_0^\infty B_\nu(\tau_\nu - x)E_2(x)\,dx + 2\int_{\tau_\nu}^\infty B_\nu(\tau_\nu - x)E_2(x)\,dx, \tag{7}$$

the source function $B_\nu(\tau_\nu \pm x)$ is replaced by the first two terms of its development in a Taylor series:

$$B_\nu(\tau_\nu \pm x) = B_\nu(\tau_\nu) \pm x \frac{dB_\nu}{dx}. \tag{8}$$

Taking into account that

$$\frac{dB_\nu}{dx} = \frac{dB_\nu}{dT} \cdot \frac{dT}{dx} = \frac{dB_\nu}{dT} \cdot \frac{dT}{d\tau_{pr}} \cdot \frac{d\tau_{pr}}{dx} = \frac{dB_\nu}{dT} \frac{dT}{d\tau_{pr}} \cdot \frac{\kappa_{pr}}{\kappa_\nu},$$

where κ_{pr} is the radiation pressure mean and τ_{pr} the mean optical depth measured in terms of this mean, we obtain from equation (7):

$$F_\nu(\tau_\nu) = 2 \frac{dB_\nu}{dT} \cdot \frac{dT}{d\tau_{pr}} \cdot \frac{\kappa_{pr}}{\kappa_\nu} \left\{ \frac{2}{3} (1 - \tau_\nu E_3(\tau_\nu)) - \frac{1}{3} e^{-\tau_\nu} \right\} + 2B_\nu(\tau_\nu) E_3(\tau_\nu). \tag{9}$$

For large values of τ_{pr} (which implies also large values of τ_ν) equation (9) reduces to

$$F_\nu \simeq \frac{4}{3} \frac{dB_\nu}{dT} \cdot \frac{dT}{d\tau_{pr}} \cdot \frac{\kappa_{pr}}{\kappa_\nu},$$

since the other terms are negligible. Approximating F by

$$F \simeq \int_0^\infty F_\nu \, d\nu \simeq \tfrac{4}{3} \kappa_{pr} \frac{dT}{d\tau_{pr}} \int_0^\infty \frac{1}{\kappa_\nu} \frac{dB_\nu}{dT} \, d\nu,$$

we obtain from equation (2):

$$\frac{1}{\kappa_{pr}} \simeq \int_0^\infty \frac{1}{\kappa_\nu} \frac{dB_\nu}{dT} \, d\nu \Big/ \int_0^\infty \frac{dB_\nu}{dT} \, d\nu = \int_0^\infty \frac{1}{\kappa_\nu} \frac{dB_\nu}{dT} \, d\nu \Big/ \frac{dB}{dT}.$$

This approximation to the radiation mean is called Rosseland's mean κ_R; by introducing the Planck function

$$B_\nu(T) = \frac{2h\nu^3}{c^2} (e^{h\nu/kT} - 1)^{-1},$$

it can be reduced to

$$\frac{1}{\kappa_R} = \frac{15}{4\pi^4} \int_0^\infty \frac{1}{\kappa_\nu} \cdot \frac{u^4 e^{-u}}{(1 - e^{-u})^2} \, du, \tag{10}$$

where $u = h\nu/kT$. Rosseland's mean can be considered as a good approximation to the radiation pressure mean in the deep interior but it is less satisfactory for moderate optical depths since then the disregarded terms in equation (9) are not negligible. For $\tau = 0$ equation (9) gives

$$F_\nu \simeq \frac{2}{3} \frac{dB_\nu}{dT} \cdot \frac{dT}{d\bar{\tau}} \frac{\bar{\kappa}}{\kappa_\nu} + B_\nu(0),$$

and with the aid of this equation we obtain the following equation for the mean absorption coefficient $\bar{\kappa}$:

$$\bar{\kappa} = \left\{ \frac{2}{3} \frac{dT}{d\bar{\tau}} \bar{\kappa} \int_0^\infty \frac{dB_\nu}{dT} \, d\nu + \int_0^\infty \kappa_\nu B_\nu \, d\nu \right\} \Big/ \left\{ \frac{2}{3} \frac{dT}{d\bar{\tau}} \bar{\kappa} \int_0^\infty \frac{1}{\kappa_\nu} \frac{dB_\nu}{dT} \, d\nu + B(0) \right\}.$$

As this equation shows, we obtain for the mean absorption coefficient a value between the Rosseland and Planck means.

For intermediate (finite) values of $\tau \neq 0$ equation (9) can be written in the form

$$F_\nu(\tau_\nu) \simeq \frac{\bar{\kappa}}{\kappa_\nu} \Gamma_1 + \Gamma_2,$$

where the meaning of Γ_1 and Γ_2 can be found from the comparison of both equations. With these designations the mean absorption coefficient κ_u can be found from the equation

$$\kappa_u \int_0^\infty \left(\frac{\kappa_u}{\kappa_\nu}\Gamma_1+\Gamma_2\right) d\nu = \int_0^\infty \kappa_\nu \left(\frac{\kappa_u}{\kappa_\nu}\Gamma_1+\Gamma_2\right) d\nu.$$

This mean, introduced by Unsöld (**5**), is more general than the Rosseland or Chandrasekhar means but it can hardly be applied in practice for the same reason that the radiation pressure mean cannot be used: its numerical value is not known until the definitive structure of the atmosphere is known. With the aid of this mean, however, Unsöld was able to prove that generally Rosseland's mean is a better approximation to the radiation pressure mean than Chandrasekhar's mean. If, in a substantial part of the interval of integration, $\bar{\kappa}/\kappa_\nu\Gamma_1$ is larger than Γ_2, then approximately

$$\int_0^\infty \frac{1}{\kappa_\nu}\Gamma_1\, d\nu = \frac{1}{\bar{\kappa}}\int_0^\infty \Gamma_1\, d\nu,$$

which means that we obtain a reverse or harmonic mean of the Rosseland type. If, however, $\bar{\kappa}/\kappa_\nu\Gamma_1 \ll \Gamma_2$, then approximately

$$\bar{\kappa}\int_0^\infty \Gamma_2\, d\nu = \int_0^\infty \kappa_\nu\Gamma_2\, d\nu,$$

which means that we obtain a straight mean of the Chandrasekhar or Planck type. Unsöld's investigations show that Rosseland's mean is a better approximation to the radiation pressure mean if the variation of the absorption coefficient with the wave-length is small; if the variation is large the straight mean may be better than the harmonic mean but only in the outermost layers of the atmosphere. Since, however, for large optical depths Rosseland's mean approaches the radiation pressure mean asymptotically, the use of this mean in the computation of model stellar atmospheres promises better results than the use of any other mean—provided, of course, that the radiation pressure mean can be used with sufficient accuracy for the purpose of reducing the general case to the grey case.

3. *Michard's investigations*

The problem of the reduction of the non-grey model to the grey one was investigated by Michard (**1**), who considered two problems: the case where both the grey and the non-grey models should have the same temperature distribution and the same (constant) net flux, and the case where both models should have the same temperature distribution but without imposing the condition that their net fluxes should be equal.

In the first problem the condition that the fluxes of both models should be equal together with the approximation (8) leads to the equation

$$\int_0^\infty \left\{2\frac{dB_\nu}{dT}\frac{dT}{d\bar{\tau}}\frac{\bar{\kappa}}{\kappa_\nu}\left[\tfrac{3}{4}(1-\tau_\nu E_3(\tau_\nu))-\tfrac{1}{2}e^{-\tau_\nu}\right]+2B_\nu(\tau_\nu)E_3(\tau_\nu)\right\} d\nu$$
$$= 2\frac{dB}{dT}\frac{dT}{d\bar{\tau}}\left\{\tfrac{3}{4}(1-\bar{\tau}E_3(\bar{\tau}))-\tfrac{1}{2}e^{-\bar{\tau}}\right\}+2B(\bar{\tau})E_3(\bar{\tau}). \qquad (11)$$

For large values of $\bar{\tau}$ (and τ_ν) as well as for $\tau_\nu=\bar{\tau}=0$, we obtain from this equation:

$$\frac{1}{\bar{\kappa}}\frac{dB}{dT} = \int_0^\infty \frac{1}{\kappa_\nu}\frac{dB_\nu}{dT}\, d\nu,$$

which is the definition of the Rosseland mean. For finite values of $\bar{\tau} \neq 0$ the same result can be obtained if the variation of τ_ν, $E_3(\tau_\nu)$ and $e^{-\tau_\nu}$ with the frequency is disregarded and τ_ν is simply replaced in these functions by $\bar{\tau}$, which, of course, is not quite correct. Disregarding this difficulty we can use the Rosseland mean for an approximate reduction of a non-grey model to a grey one and since this mean is an approximation to the radiation pressure mean, this latter can also be used for that purpose. The same can be said of Unsöld's mean and, to a certain extent, of Chandrasekhar's mean which both have a common origin in equation (2). It should be stressed, however, that they can all secure only an approximate solution of the problem since it is impossible to reduce the non-grey case to the grey one in fully mathematical strictness.

The second problem discussed by Michard leads to the equation

$$\int_0^\infty \kappa_\nu (B_\nu - \bar{I}_\nu)\, d\nu = \bar{\kappa}(B - \bar{I}). \tag{12}$$

Remembering now that

$$\bar{I}_\nu = \Lambda_{\tau_\nu}(B_\nu) = \tfrac{1}{2}\int_{\tau_\nu}^\infty B_\nu(t) E_1(t-\tau_\nu)\, dt + \tfrac{1}{2}\int_0^{\tau_\nu} B_\nu(t) E_1(\tau_\nu - t)\, dt,$$

which remains valid for $\bar{I}$ after suppressing the subscripts ν, and replacing B_ν and B by the first two terms of their developments in a Taylor series, we obtain

$$\int_0^\infty \left\{ \kappa_\nu B_\nu(\tau_\nu) E_2(\tau_\nu) - \kappa_\nu [E_3(\tau_\nu) + \tau_\nu E_2(\tau_\nu)] \frac{dB_\nu}{d\tau_\nu} \right\} d\nu$$

$$= \bar{\kappa} B(\bar{\tau}) E_2(\bar{\tau}) - \bar{\kappa}[E_3(\bar{\tau}) + \bar{\tau} E_2(\bar{\tau})] \frac{dB}{d\bar{\tau}}. \tag{13}$$

Taking now into account that

$$\kappa_\nu \frac{dB_\nu}{d\tau_\nu} = \bar{\kappa} \frac{dB_\nu}{d\bar{\tau}},$$

and assuming that $E_2(\tau_\nu)$, $E_3(\tau_\nu)$ and τ_ν on the left-hand side of equation (13) can be replaced by their mean values $E_2(\bar{\tau})$, $E_3(\bar{\tau})$ and $\bar{\tau}$, we obtain

$$\bar{\kappa} = \int_0^\infty \kappa_\nu \frac{B_\nu}{B}\, d\nu,$$

which is the definition of the Planck mean. If, therefore, this mean is used in the computation of a grey model, the corresponding non-grey model should have an approximately constant flux, differing, however, from the flux of the grey model.

It is, however, doubtful whether this result is correct. Equation (12) is a strict one and the numerical value of both sides is equal to zero. If, therefore, the functions B_ν and B in this equation are replaced by the two first terms of their developments in a Taylor series, both sides differ from zero by small quantities of the same order but they can no longer be considered as equal unless it can be proved that they differ by a small quantity of a higher order. The sign of equality in equation (13) is therefore no longer justified since the left-hand side may be an unspecified multiple of the right-hand side. Consequently any results obtained from this equation may be wrong. This is very likely to be the case for large values of $\bar{\tau}$ when all terms of equation (13) become small.

A more promising approach in this case seems to be to assume that the net flux of the non-grey atmosphere F_{ng} is a multiple k of the flux of the grey model F_g:

$$F_{ng} = k \,.\, F_g.$$

In this case the right-hand side of equation (11) should be multiplied by k which leads to the result:

$$\frac{1}{\bar{\kappa}}\frac{dB}{dT} = \frac{1}{k}\int_0^\infty \frac{1}{\kappa_\nu}\frac{dB_\nu}{dT}\,d\nu,$$

which is valid for large values of $\bar{\tau}$. For the determination of the factor k it is necessary to know the boundary temperature of the non-grey model, which determines the flux of the grey atmosphere by means of equation (1). However, since this temperature is *a priori* unknown, it is not possible to apply the above result in practice. Putting $k=1$, we reduce the second problem investigated by Michard to the first one.

4. *Numerical approach*

Michard's theoretical investigations lead to the conclusion that the radiation pressure mean and all its approximations (the Unsöld, Rosseland and Chandrasekhar means) can be used for the purpose of reducing a non-grey model stellar atmosphere to a grey one, although a strict solution of this problem is impossible. They do not enable us, however, to find out which of these means is the best and of what order of magnitude are the deviations from the exact grey solution. The answers to these questions can be found from the results of numerical investigations of model stellar atmospheres, and the present paper is an attempt to solve this problem for a model solar atmosphere. The present investigations are based on a model published in my former paper (**6**) which will be referred to subsequently as Paper A. In this publication a model solar atmosphere was obtained with a practically constant net flux of energy. With one single exception the net flux computed for thirteen levels from $\tau=0$ to $\bar{\tau}=11{\cdot}522$ does not differ more than 2 per cent from its boundary value. The results of these investigations can, therefore, be used for the computation of the radiation pressure mean according to formula (2). I have already done this in another paper (**7**) in which the designation $\kappa^{(3)}$ was used for the computed value of the mean absorption coefficient. In the present investigation the other kinds of the mean absorption coefficient have been evaluated for seven values of the reciprocal temperature $\theta=5040/T$. The numerical procedure of the computation of the "absorption" mean κ_a according to formula (4) does not differ from the computation of $\kappa_{pr}=\kappa^{(3)}$ described in the previous papers (**6**, **7**). Extensive use of Reiz's tables (**8**) has been made in these computations.

The values of the monochromatic absorption coefficients which were used for the computation of the mean absorption coefficient are shown in Table I. They are referred to one heavy particle as defined by Vitense (**9**); this one heavy particle corresponds to 0·8437 atoms of hydrogen (in number). The monochromatic absorption coefficients were taken partly from Vitense's publication (for the ultra-violet region) and partly from my unpublished tables of absorption coefficients for neutral hydrogen and its negative ion (at larger wave-lengths). Corrections for Thomson and Rayleigh scattering were applied to values from the latter source. The entries of Table I are corrected for the stimulated emission.

Since it was intended to make the computation to four-figure accuracy, the values of the monochromatic absorption coefficients in Table I are given with the same accuracy, although the last digit at least has no real significance.

TABLE I

Monochromatic absorption coefficients

(The table gives the values of κ_ν/p_e in units of 10^{-26} cm^4 dyne^{-1})

λ in A	α \ θ	1·04	1·00	0·90	0·80	0·70	0·60	0·50
1100+	22·681	16410	6998·	1019	799·8	83·18	15·07	2·723
1242	20·088	8913	3698	663·7	135·5	20·99	3·404	0·6918
1424	17·495	12020	5188	922·6	140·3	19·95	2·786	0·7943
1674	14·902	3388	1585	380·2	70·31	11·14	2·163	0·9441
2027	12·309	402·7	219·8	62·37	16·22	3·758	1·380	1·216
2512−	9·9320	64·57	40·09	14·86	4·955	2·249	1·660	1·972
2512+	9·9320	45·50	28·71	12·30	4·385	2·042	1·641	1·928
2975	8·3868	13·87	11·09	5·689	3·006	2·249	2·213	3·090
3647−	6·8410	8·318	6·998	4·487	3·177	3·055	3·890	5·598
3647+	6·8410	8·279	6·966	4·188	2·333	1·462	0·8913	0·7031
4235	5·8908	6·926	5·822	3·795	2·419	1·519	0·9923	0·8355
5050	4·9407	8·231	6·958	4·545	2·906	1·842	1·249	1·168
6252	3·9906	9·822	8·328	5·448	3·499	2·256	1·632	1·769
8206−	3·0404	10·994	9·328	6·122	3·980	2·683	2·231	3·020
8206+	3·0404	10·991	9·325	6·105	3·905	2·463	1·649	1·569
9214	2·7079	10·790	9·168	6·020	3·875	2·485	1·750	1·873
10503	2·3754	9·826	8·371	5·545	3·623	2·401	1·844	2·309
12213	2·0427	7·673	6·590	4·480	3·047	2·174	1·950	2·985
14588−	1·7102	4·186	3·729	2·807	2·175	1·867	2·184	4·166
14588+	1·7102	4·185	3·727	2·798	2·130	1·717	1·740	2·924
16031	1·5564	3·183	2·931	2·392	1·975	1·739	1·946	3·538
17790	1·4024	3·083	2·909	2·501	2·163	1·992	2·346	4·435
19984	1·2485	3·745	3·544	3·069	2·674	2·491	2·990	5·746
22794−	1·0945	4·815	4·554	3·941	3·434	3·220	3·928	7·661
22794+	1·0945	4·814	4·553	3·933	3·394	3·079	3·486	6·375
30392	0·8209	8·302	7·853	6·793	5·887	5·411	6·313	11·91
45585	0·5473	18·10	17·15	14·83	12·82	11·58	12·96	23·55
91185	0·2736	70·42	66·74	57·87	50·06	45·26	50·57	91·64

5. *Comparison of mean absorption coefficients*

The results of the computations of different kinds of mean absorption coefficient are shown in Table II and in Fig. 1. They are referred to one heavy particle as defined by Vitense (**9**). For reasons explained in Paper A, the electron pressure is given together with the reciprocal temperature and the mean optical depth τ_{pr}. Chandrasekhar's mean could only be computed for four values of θ, since Chandrasekhar's weight function is given only to the optical depth $\tau=2{\cdot}0$. As Table II shows, there is little difference between the "absorption" mean κ_a and the "emission" mean κ_e, identical here with Planck mean κ_P; the greatest

TABLE II

Comparison of mean absorption coefficients

θ	$\log_{10}p_e$	Mean optical depth τ_{pr}	κ_{pr}	κ_a	$\kappa_P=\kappa_e$	κ_R	κ_{Ch}
1·04	0·149	0·0187	8·989	9·772	9·718	8·174	13·055
1·00	0·599	0·1291	7·524	8·442	8·346	7·100	10·363
0·9	1·074	0·5210	4·936	5·678	5·662	4·825	6·279
0·8	1·647	1·214	3·164	3·664	3·662	3·127	3·680
0·7	2·372	2·541	2·113	2·410	2·409	2·102	
0·6	3·137	5·369	1·547	1·901	1·902	1·545	
0·5	3·898	11·643	1·434	2·246	2·243	1·433	

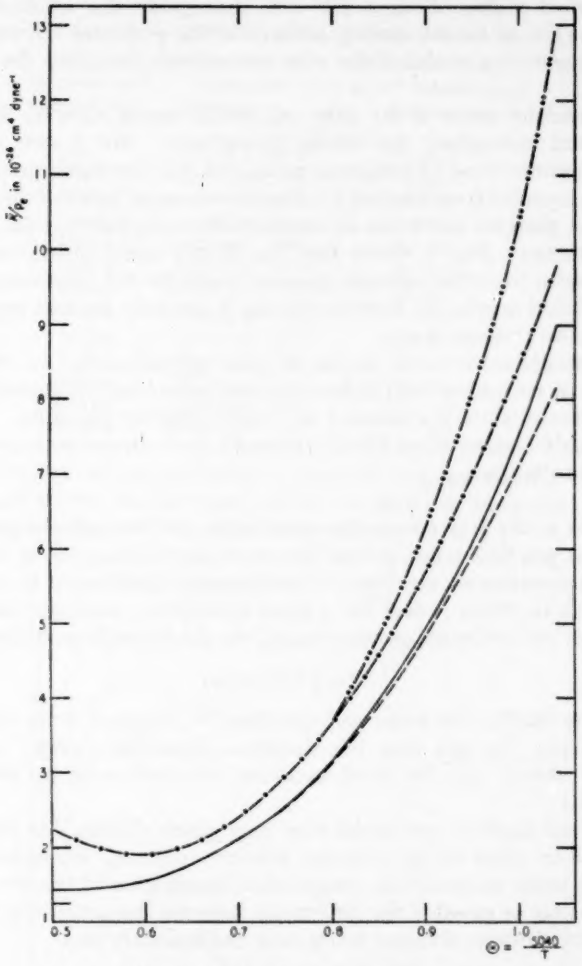

FIG. 1.—*Mean absorption coefficients.*

——— *radiation pressure;* - - - - - *Rosseland;*

- - - - *Planck;* - · - · - *Chandrasekhar.*

deviation for $\theta = 1{\cdot}00$ is about 1 per cent and for the last five values of θ it is of the same order of magnitude as the estimated accuracy of the numerical computations. In connection with the condition of radiative equilibrium written in the form

$$\int_0^\infty \kappa_\nu B_\nu \, d\nu = \int_0^\infty \kappa_\nu \bar{I}_\nu \, d\nu,$$

the approximate equality of the "absorption" mean κ_a and "emission" mean κ_e defined by equations (4) and (5) respectively, means that the equation

$$\int_0^\infty \bar{I}_\nu \, d\nu = \int_0^\infty B_\nu \, d\nu \qquad (14)$$

is also satisfied within about 1 per cent throughout the whole atmosphere. Equation (14) is, of course, strictly satisfied in the grey case. From this point of view our non-grey model of the solar atmosphere resembles the grey model very closely.

The Rosseland mean is the only one which comes close to the radiation pressure mean throughout the whole atmosphere. For $\theta=0{\cdot}6$ and $0{\cdot}5$ the agreement between these two means is perfect for well-known theoretical reasons. As could be expected from Section 2.3, for the outermost layers of the atmosphere the radiation pressure mean has an intermediate value between the Planck and Rosseland means. Fig. 1 shows that the Planck mean differs less than the Rosseland mean from the radiation pressure mean for the outermost layers, but for larger optical depths the Rosseland mean is certainly the best approximation to the radiation pressure mean.

The Chandrasekhar mean is not a good approximation to the radiation pressure mean and numerically it deviates even more from the correct value than the Planck mean which is evaluated on a quite different principle. The reason why the Chandrasekhar mean fails to represent the radiation pressure mean well is discussed in Section 9.

6. *Correction to the grey temperature distribution for the radiation pressure mean*

From the practical point of view the most convenient mean is the mean for which the correction to the "grey" temperature distribution is the smallest. It was shown in Paper A that for a mean absorption coefficient differing only slightly from our radiation pressure mean, the deviation from Milne's law

$$T^4=\tfrac{1}{2}T_e^4(1+\tfrac{3}{2}\tau)$$

is reasonably small; the same can therefore be expected from our radiation pressure mean. In this case the deviation from the "grey" temperature distribution should also be small and this was confirmed by the following investigations.

The optical depth of our model solar atmosphere (Table V in Paper A) was re-computed in terms of the radiation pressure mean κ_{pr} and subsequently an attempt was made to correct the temperature distribution of this model in order to remove as far as possible the differences between the actual net fluxes $F(\tau)$, computed for thirteen different levels, and the boundary flux

$$F(0)=62\,678\times 10^9\,\mathrm{erg\,cm^{-2}\,sec^{-1}/solid\ angle}\ 2\pi$$

(Table VI of Paper A). The variational method described in Paper A was applied for this purpose. The corrections to the source function $\Delta B(\tau)$ were represented by a linear combination of the eight following functions:

$$f_1(\tau)=1, \quad f_2(\tau)=\tau, \quad f_3(\tau)=\tau^2, \quad f_4(\tau)=\tau^3,$$
$$f_5(\tau)=e^{-\tau}, \quad f_6(\tau)=e^{-5\tau}, \quad f_7(\tau)=e^{-10\tau}, \quad f_8(\tau)=E_2(\tau).$$

The attempt to use an additional function $f_9(\tau)=E_3(\tau)$ led to an indeterminate system of equations, which means that eight functions are sufficient to find the corrections to the temperature distribution.

The corrected temperature together with its mean errors is shown in Table III for thirteen levels for which the net flux was found in Paper A. For intermediate values of τ the correction to the temperature can be found by graphical inter-

TABLE III

Temperature distribution of the solar model atmosphere

τ_{pr}	Uncorrected temperature	Corrected temperature	Deviation from "grey" temperature distribution	Residuals ΔF (per cent)
	°	°	°	
0	4811	4733·3 ± 246·9	+56·4	−0·17
0·0187	4846·1	4800·7 ± 170·6	+52·7	+0·19
0·1291	5040·0	4998·5 ± 26·8	−18·6	+0·20
0·3000	5305·3	5308·6 ± 16·8	− 7·0	−0·36
0·5210	5600·0	5627·0 ± 11·6	+ 8·4	−0·22
0·8157	5929·4	5948·0 ± 10·7	+ 0·6	+0·40
1·2142	6300·0	6300·7 ± 7·4	−12·1	+0·35
1·7600	6720·0	6712·9 ± 6·3	−11·3	−0·23
2·5414	7200·0	7201·1 ± 6·0	− 3·2	−0·53
3·6885	7753·8	7770·9 ± 5·7	+ 0·7	−0·01
5·3694	8400·0	8421·2 ± 5·9	− 3·9	+0·92
7·8419	9163·6	9163·4 ± 6·2	−11·9	−0·67
11·6431	10080·0	10050·5 ± 7·4	− 8·4	+0·14

polation. The last column of Table III gives the residual error in the net flux; as this column shows, the constancy of the net flux can be secured within less than 1 per cent throughout the whole atmosphere.

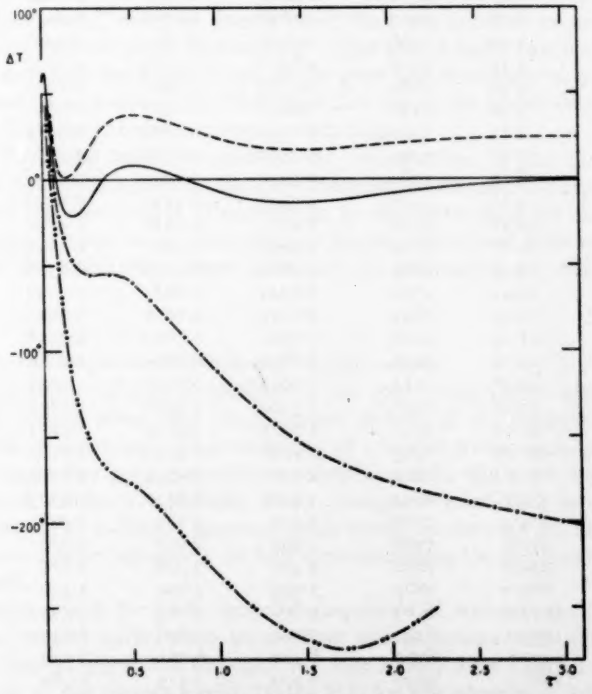

FIG. 2.—*Corrections to the grey temperature distribution.*
——— *radiation pressure mean;* – – – – – *Rosseland mean;*
- - - - - *Planck mean;* — · — · — *Chandrasekhar mean.*

The deviations of the derived temperatures from the "grey" temperature distribution shown in the third column of Table III and in Fig. 2 (continuous line) are reasonably small and not systematic, and are of the same order of magnitude as the possible mean errors. The largest deviations are obtained for the outermost layers of the solar atmosphere, but even there they are much smaller than the possible errors in the determination of the corrected temperatures. Unfortunately precise determination of the boundary temperature is not possible.

The above results show clearly that the radiation pressure mean can be used successfully in reducing the non-grey stellar atmosphere to a grey one, at least for solar type stars. Probably this applies also to early type stars. Therefore the general belief that the radiation pressure mean is the only correct one seems to be justified.

TABLE IV

Model solar atmosphere

(p indicates total pressure in dyne cm^{-2} due to hydrogen alone)

p	p_e	T	τ_{pr}	τ_R	τ_P	τ_{Ch}
0	0	4733·3	0	0	0	0
4000	0·56	4753	0·0030	0·0027	0·0032	0·0045
8000	1·06	4782	0·0112	0·0100	0·0120	0·0165
12000	1·51	4811	0·0237	0·0214	0·0255	0·0350
16000	2·00	4841	0·0401	0·0362	0·0432	0·0588
20000	2·48	4876	0·0608	0·0551	0·0656	0·0888
24000	2·98	4917	0·0846	0·0771	0·0917	0·1232
28000	3·49	4966	0·1126	0·1031	0·1223	0·1629
32000	4·11	5024	0·1428	0·1314	0·1557	0·2051
36000	4·72	5089	0·1773	0·1641	0·1941	0·2526
40000	5·44	5156	0·2133	0·1985	0·2343	0·3010
44000	6·23	5230	0·2544	0·2379	0·2803	0·3556
48000	7·08	5303	0·2966	0·2787	0·3280	0·4106
52000	8·04	5380	0·3442	0·3249	0·3816	0·4724
56000	9·12	5456	0·3930	0·3727	0·4373	0·5349
60000	10·37	5532	0·4474	0·4258	0·4992	0·6048
64000	11·87	5606	0·5042	0·4813	0·5644	0·6766
68000	13·43	5684	0·5682	0·5439	0·6378	0·7582
72000	15·45	5759	0·6343	0·6085	0·7140	0·8411
76000	18·03	5842	0·7113	0·6836	0·8022	0·9378
80000	21·14	5925	0·7925	0·7630	0·8958	1·0380
84000	25·24	6016	0·8870	0·8554	1·0045	1·1548
88000	30·38	6111	0·9910	0·9572	1·1244	1·2803
92000	37·48	6216	1·1126	1·0766	1·2641	1·4262
96000	47·09	6331	1·2515	1·2135	1·4251	1·5877
100000	61·05	6463	1·4186	1·3791	1·6181	1·7780
104000	81·71	6614	1·6207	1·5794	1·8514	1·9960
108000	114·5	6794	1·8780	1·8347	2·1473	2·2610
112000	170·1	7012	2·219	2·173	2·538	
116000	272·2	7288	2·699	2·650	3·086	
120000	484·8	7652	3·427	3·376	3·919	
122000	683·6	7885	3·954	3·902	4·530	
124000	1012·9	8169	4·668	4·614	5·375	
126000	1612·3	8532	5·701	5·646	6·639	
127000	2115·7	8760	6·421	6·365	7·549	
128000	2885	9036	7·370	7·313	8·782	
129000	4134	9380	8·683	8·624	10·552	
130000	6337	9828	10·608	10·548	13·312	
130500	8117	10113	11·944	11·881		

A model solar atmosphere with the temperature distribution obtained in Table III is shown in the first four columns of Table IV; the other columns are explained in the next section.

7. *Corrections to the grey temperature distribution for other mean absorption coefficients*

The method described in Section 6 could be used for the determination of the corrections to the grey temperature distribution if the optical depth were measured in terms of other mean absorption coefficients. Since, however, the definitive structure of the model solar atmosphere is known from the preceding section, another simpler procedure can be used for the same purpose.

The mean optical depth of the final model was re-computed in terms of the Rosseland, Chandrasekhar and Planck means; the results of these computations are shown in the last three columns of Table IV as τ_R, τ_{Ch} and τ_P. The differences between the true temperature (shown in the second column) and the "grey" temperature computed from equation (1) for the corresponding optical depths τ_R, τ_{Ch} or τ_P are plotted against the optical depth in Fig. 2.

The corrections for the Planck mean (equivalent to the "emission" mean κ_e) are quite large and show a systematic trend, which could be expected from the fact that this mean is always larger than the radiation pressure mean. They reach 200° for the optical depth $\tau_P = 3$ and over 400° for $\tau_P = 10$. The corrections for the "absorption" mean κ_a should be of the same order of magnitude since both means are almost equal numerically. The use of these two means for the purpose of reducing the general case to the grey one is, therefore, not justified. The same can be said also of the Chandrasekhar mean, for which the corrections to the grey temperature distribution are still larger.

If the Rosseland mean is used in the construction of the model stellar atmosphere, the deviations from the grey temperature distribution are reasonably small and of the same order of magnitude as the corrections for the radiation pressure mean. Apart from the outermost layers which have little effect on the structure of the atmosphere these deviations do not exceed 30° and vanish for $\tau_R = 9{\cdot}5$.

8. *Errors in the temperature distribution of grey models*

The application of any corrections to the grey temperature distribution is *a priori* impossible, since they are unknown as long as the definitive structure of the model is unknown. The computer of a model stellar atmosphere must, therefore, apply the grey temperature distribution in the hope that this law leads to good results if a suitable mean absorption coefficient is used in the computation. The radiation pressure mean would be the best for that purpose, but since it is *a priori* unknown, its best approximation, i.e. the Rosseland mean, must be used.

In order to check the likely order of magnitude of errors in the temperature distribution, a grey model solar atmosphere was computed with the Rosseland mean and the temperatures obtained for this model were compared with the temperatures of the correct model (Table III) for the same level defined by the same total pressure p. The differences between both models are shown in Fig. 3 (dashed line). They are all negative and somewhat larger than the corrections

found in Section 7 for the Rosseland mean. They reach 150° for the optical depth $\tau = 3{\cdot}1$ corresponding to the total pressure $p = 120\,000$ dyne/cm². Since all visible features of the stellar spectra are determined by the outer layers of the stellar atmosphere we can conclude that a grey model computed with the Rosseland mean is good enough for practical purposes. The cumulative effect of errors in the temperature distribution, however, causes large deviations for deep layers of the stellar atmosphere.

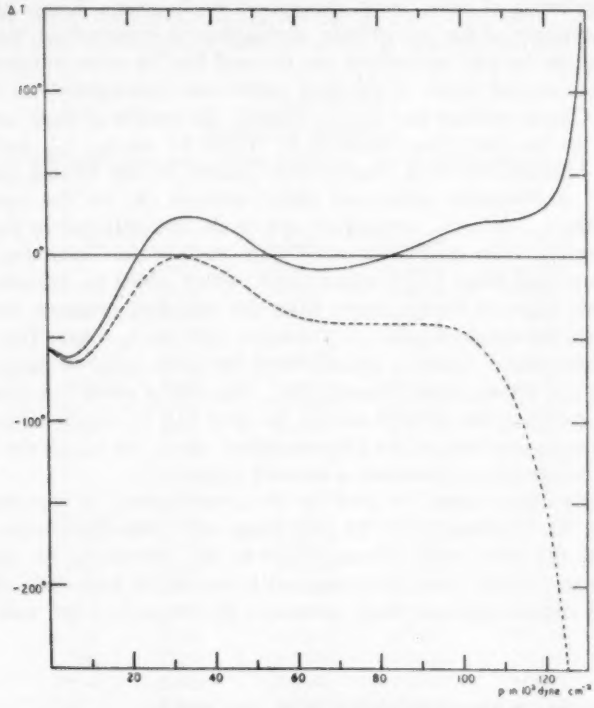

FIG. 3.—*Errors in the temperature distribution of grey model solar atmospheres.* ——— *radiation pressure mean;* – – – – – *Rosseland mean.*

A grey model computed in the same way by using the radiation pressure mean differs less from the correct model, as can be seen in Fig. 3 (continuous line). The deviations from the true temperatures do not exceed 30° up to the mean optical depth $\tau = 3{\cdot}0$ (total pressure $p = 118\,000$ dyne/cm²), if we disregard the upper layers, which have very little effect on the net flux. The deviations become more serious (over 100°) for the optical depth $\tau = 7{\cdot}5$ and the total pressure $p = 127\,750$ dyne/cm². There can be no doubt that the use of the radiation pressure mean for the computation of model stellar atmospheres would be the most advantageous if its numerical value were known. Since, however, this is not the case its best numerical approximation, i.e. the Rosseland mean, must be used.

9. *Comparison of weight functions*

In the preceding sections it was shown that numerically the Rosseland mean comes closer to the radiation pressure mean than do other means. This result is confirmed to an even higher degree by the comparison of weight functions used in the computation of different means.

The weight functions $W_P = B_\nu/B$ of the Planck mean and $W_{Ch} = F_a^{(1)}/F$ of the Chandrasekhar mean can be compared directly with the weight functions $W_{pr} = F_\nu/F$ of the radiation pressure mean and $W_a = \bar{I}_\nu/\bar{I}$ of the absorption mean which are known from the numerical computations of Paper A and the present paper. Since the Rosseland mean is not an arithmetical but a harmonic mean, its weight function

$$\frac{dB_\nu}{dT} \Big/ \frac{dB}{dT}$$

cannot be compared with the other weight functions. The identity

$$\int_0^\infty \kappa_\nu \left\{ \frac{\kappa_R}{\kappa_\nu} \frac{dB_\nu}{dT} \Big/ \frac{dB}{dT} \right\} d\nu = \kappa_R \left(\frac{dB}{dT} \right)^{-1} \int_0^\infty \frac{dB_\nu}{dT} d\nu = \kappa_R$$

shows, however, that the Rosseland mean can be transformed into an arithmetical mean with the weight function

$$W_R = \frac{\kappa_R}{\kappa_\nu} \frac{dB_\nu}{dT} \Big/ \frac{dB}{dT}, \tag{15}$$

which can be computed *a posteriori* when κ_R is known from formula (10).

The weight functions are shown in Figs. 4, 5 and 6 for $\theta = 1{\cdot}0$, $0{\cdot}8$ and 0.5 respectively. They are all referred to the same independent variable $\alpha = h\nu/kT_e$ introduced by Chandrasekhar (4).

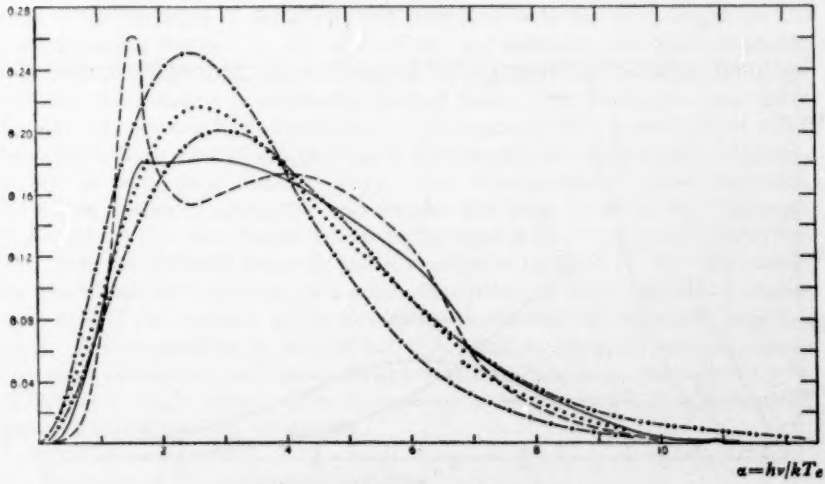

FIG. 4.—*Weight functions for* $\theta = 1{\cdot}0$.
——— *radiation pressure mean;* – · – · – · *Planck ("emission") mean;*
. . . . . *"absorption" mean;* – – – – – *Rosseland mean;*
– · – · – · *Chandrasekhar mean.*

The weight functions of the Rosseland mean and the "absorption" mean are not drawn on Fig. 6 (for $\theta=0{\cdot}5$), since they are practically identical with the weight function of the radiation pressure mean and the Planck mean respectively.

A comparison of weight functions for $\theta=1{\cdot}0$ shows that the weight functions for the Planck mean (or emission mean) and the absorption mean are similar but not identical, in spite of the fact that numerically these two means are almost equal; for this reason they must be considered as two different means. Of the two approximations to the radiation pressure mean neither the weight function of the Rosseland mean nor that of the Chandrasekhar mean comes close to the

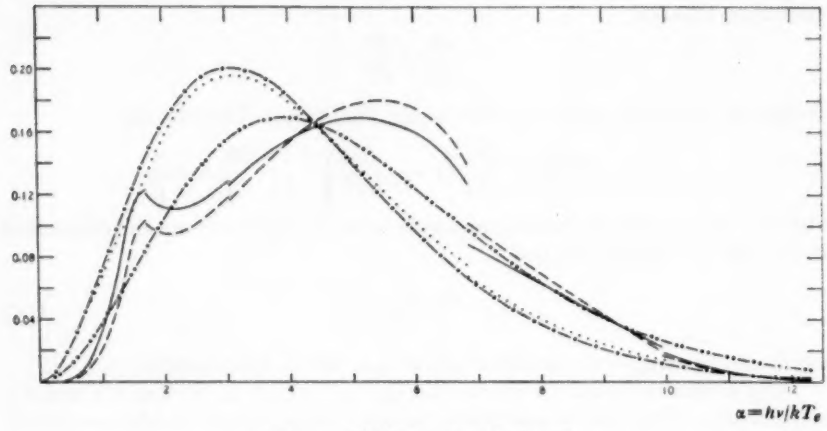

FIG. 5.—*Weight functions for* $\theta=0{\cdot}8$.
——— *radiation pressure mean;* - - - - - *Planck ("emission") mean;*
. . . . . *"absorption" mean;* – – – – – *Rosseland mean;*
– . – . – . *Chandrasekhar mean.*

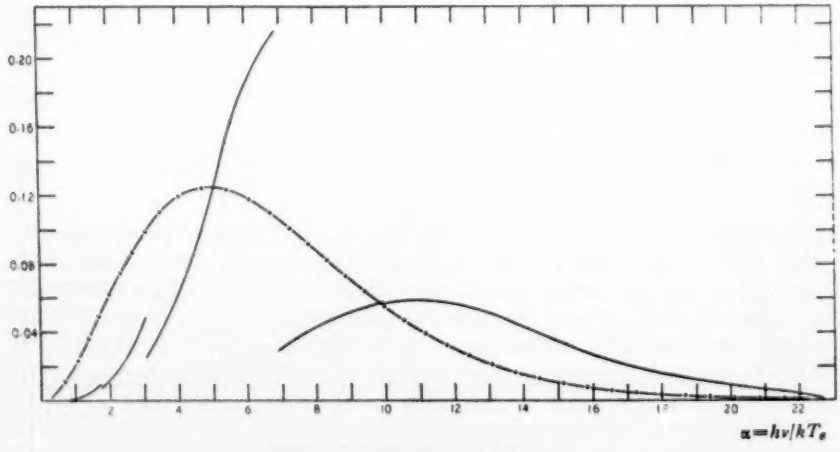

FIG. 6.—*Weight function for* $\theta=0{\cdot}5$.
——— *radiation pressure mean and Rosseland mean;*
– . – . – . *Planck mean and "emission" mean.*

weight function of the radiation pressure mean for all values of α. The Rosseland mean has, however, one advantage over the Chandrasekhar mean, in that its weight function is always of the same order of magnitude as the weight function of the radiation pressure mean; Chandrasekhar mean exaggerates the contribution of the ultra-violet to the mean absorption coefficient, since its weight function is for some wave-lengths more than a hundred times greater than that of the radiation pressure mean (for $\alpha \geqslant 15$).

For $\theta = 0{\cdot}8$ the weight function of the Rosseland mean resembles more closely that of the radiation pressure mean than it does for $\theta = 1{\cdot}0$. The same can be said of the Planck mean κ_p and the absorption mean κ_a, which both have very similar but not identical weight functions. For $\theta = 0{\cdot}5$ the corresponding differences between these two groups of mean absorption coefficients are so small that it is impossible to draw all four weight functions in Fig. 6, and, therefore, only that of the radiation pressure mean and that of the Planck mean are shown. The average deviations of the other two weight functions from the weight function of the radiation pressure mean or that of the Planck mean respectively are about 1 per cent. This result, of course, could be expected in view of the fact that for large optical depths the radiation field becomes isotropic.

The comparison of weight functions of different means leads to the conclusion that the Rosseland mean is the only one that can be considered as a good first approximation to the radiation pressure mean. It is the only mean with a weight function containing the monochromatic absorption coefficient, thus making possible the adjustment of the weight function to any deviation of the monochromatic absorption coefficient from the mean absorption coefficient. This adjustment of the weight function is well expressed by its discontinuity at every wave-length where the monochromatic absorption coefficient also shows a discontinuity. The failure of the Chandrasekhar mean to approximate well to the radiation pressure mean can be traced back to the fact that it disregards the effect of the variation of the absorption coefficient with the wave-length on the monochromatic fluxes. In the ultra-violet, for instance, the monochromatic absorption coefficient can be one hundred times greater than its mean value and therefore the radiation is practically blocked there. The Rosseland mean takes this fact into account by reducing the weight function there to the correct value through the large value of κ_ν appearing in the denominator of its weight functions, as can be seen from formula (15). The Chandrasekhar mean, however, disregards this effect altogether and weights the large values of the absorption coefficient in the ultra-violet with a factor appropriate to a small absorption coefficient not differing from the mean absorption coefficient. For this reason the Chandrasekhar mean can be a good approximation to the radiation pressure mean only if the variation of the absorption coefficient with the wave-length is small. If this condition is not fulfilled, it is better to disregard spectral regions with large absorption coefficients altogether than to take them into account with an incorrect weight factor. This is, however, a procedure which conscientious scientists can apply only reluctantly.

10. *Reddening of the photospheric radiation*

The net flux of energy of the model solar atmosphere used as a basis for the present investigations was computed for thirteen optical depths shown in Table III. The results of these computations give the weight function $W_{pr} = F_\nu/F$ for all

these levels. They are represented graphically in Fig. 7 with the omission of one level $\tau_{pr}=0{\cdot}0187$ corresponding to the reciprocal temperature $\theta=1{\cdot}04$; the weight function for this level approaches very closely to the weight function for $\tau=0$ and therefore cannot be drawn separately.

It should be stressed that the weight functions shown on Fig. 7 are valid only for the monochromatic absorption coefficient used in the computations of the monochromatic fluxes. These monochromatic absorption coefficients are shown in Table I for seven values of θ.

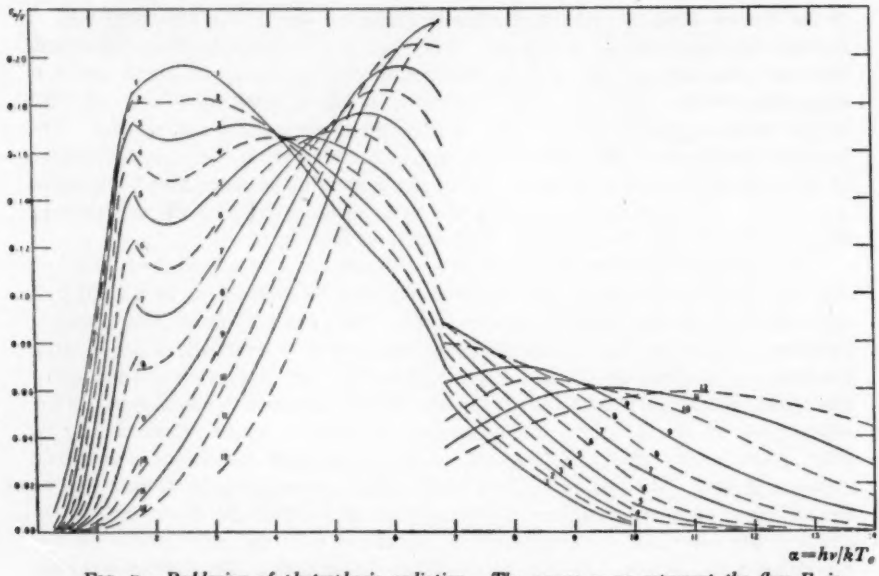

FIG. 7.—*Reddening of photospheric radiation. The curves* 1–12 *represent the flux* F_α *in units of the total flux F for* 12 *levels in the photosphere:* $\tau=0$ (*curve* 1); 0·1274, 0·2943, 0·5116, 0·8021, 1·195, 1·733, 2·505, 3·636, 5·291, 7·740, 11·528 (*curve* 12).

Fig. 7 can be considered as a graphical representation of the reddening of the photospheric radiation. A similar graph was published by Chandrasekhar (**4**), but its value is greatly affected by the fact that the absorption coefficient was assumed to be independent of wave-length and therefore his curves show no discontinuities. The discontinuities shown on Fig. 7 for $\alpha=1{\cdot}710$, 3·070, 6·871 correspond to the Brackett, Paschen and Balmer limits respectively and that for $\alpha=9{\cdot}932$ is due to magnesium.

Acknowledgments.—The present paper was read by Dr B. J. Bok and Dr W. Buscombe, who suggested some alterations and whose help is gratefully acknowledged. The author also wishes to express his thanks to Dr B. E. J. Pagel, whose constructive criticism of the first version helped to introduce some useful changes in the paper and thus enhanced its value.

Mt. Stromlo Observatory,
Australian National University,
Mt. Stromlo, Canberra, A.C.T.:
1959 *May* 5.

References

(1) R. Michard, *Ann. d'Ap.*, **12**, 291, 1949.
(2) E. Hopf, *M.N.*, **96**, 522, 1936.
(3) V. Kourganoff, *Basic Methods in Transfer Problems*, Ch. VII, Oxford 1952.
(4) S. Chandrasekhar, *Ap. J.*, **101**, 328, 1945.
(5) A. Unsöld, *Zs. f. Astrophys.*, **25**, 340, 1948.
(6) A. Przybylski, *M.N.*, **115**, 650, 1955 (referred to as Paper A).
(7) A. Przybylski, *M.N.*, **117**, 483, 1957.
(8) A. Reiz, *Medd. Lunds Obs.*, Ser. 1, No. 184, 1954.
(9) E. Vitense, *Zs. f. Astrophys.*, **28**, 81, 1951.

ON THE MAIN-SEQUENCE BAND AND THE HERTZSPRUNG GAP*

F. Hoyle

(Received 1959 May 7)

Summary

Stars evolve rapidly away from the main-sequence as soon as an inert helium core develops. Evolutionary sequences have been computed for the masses 30·1 ⊙, 8·94 ⊙, 3·89 ⊙, 1·52 ⊙. These integrations enable a band to be determined, the lower edge of the band being given by the zero-ago main-sequence and the upper edge by the moment of formation of an inert core. Stars near the main-sequence should lie within this band (apart from aspect effects introduced by rapid rotation).

A comparison is made with recent work by Blaauw on the Scorpio–Centaurus group. The stars of the nebular region within the group appear to have an age of about $12{\cdot}5 \times 10^6$ years, whereas the best theoretical age estimate for the whole group $\sim 26 \times 10^6$ years. The age determined by Blaauw from dynamical considerations $\sim 20 \times 10^6$ years.

---

1. *Introduction.*—A comparison of the colour–magnitude diagrams of a number of galactic and globular clusters has been made by Sandage (**1**). The observed sequences are continuous only for old clusters whose main-sequence stars are fainter than about $+3{\cdot}0$. The observed sequences in younger clusters show a gap in the H–R diagram, which widens with increasing luminosity.

In NGC 752, stars with $B-V < +0{\cdot}5$ are found near the main-sequence, but no stars are found as $B-V$ increases above about $+0{\cdot}5$ until subgiants appear at $B-V \cong +1{\cdot}0$, $M_v \cong +1{\cdot}5$. This cluster is one of the faintest (in absolute terms) in which such a gap is found. At high luminosities much wider gaps are observed. For example at $M_v = -7{\cdot}0$ in $h+\chi$ Persei the gap extends between $B-V \cong +0{\cdot}1$ and $B-V \cong +1{\cdot}6$.

This phenomenon, first discovered by Hertzsprung, has a simple explanation; namely that such gaps correspond to regions of very rapid evolution. Starting from the neighbourhood of the main-sequence, stars move rapidly to the right in the H–R diagram. The *bolometric* magnitude remains very nearly constant during this motion. The rapid evolution ceases when the subgiant, giant, or supergiant regions of the H–R diagram are reached—the particular case depending on M_v; for $M_v \cong +1{\cdot}0$ a subgiant region at $B-V \cong +1{\cdot}0$ is reached, for M_v in the range 0·0 to $-2{\cdot}0$, the giant region is reached at $B-V \cong +1{\cdot}2$, while for M_v brighter than $-5{\cdot}0$ a star takes up a position at $B-V \cong +1{\cdot}6$. Clearly in clusters of limited population, observed at a particular moment of time, it is unlikely that stars will be found in the regions of rapid evolution. These regions cover a roughly triangular area of the H–R diagram, determined by the following three points: $M_v = +2{\cdot}0$, $B-V = +0{\cdot}5$; $M_v = -7{\cdot}0$, $B-V = +0{\cdot}1$; $M_v = -6{\cdot}0$, $B-V = +1{\cdot}6$. The Cepheids lie within this region, which implies that the condition of cepheid instability is probably short-lived.

* The contents of the present paper were reported briefly at the IAU Moscow Meeting, 1958 (Symposium on the H–R diagram).

The cause of rapid evolution away from the neighbourhood of the main-sequence is also easily understood. Very rapid evolution occurs only for stars that in their main-sequence state possess convective cores. As evolution proceeds, the mass content of a convective core increases at first but then decreases steadily until convection ceases altogether, just before the hydrogen concentration declines to zero at the centre. It is emphasized, however, that convection does not cease until the central concentration of hydrogen is very close to zero indeed. For example in the integrations for the case of a star of mass $3{\cdot}89\odot$ it was found that strong convection still extended throughout the inner 5 per cent of the star's mass at the stage where the hydrogen concentration X had fallen as low as 1/3 per cent ($X=0{\cdot}0033$). Thus although it is true that X falls first to zero at the centre, the interval of time that elapses between this event and X also falling to zero throughout a substantial inner core (say 10 per cent of the total mass) is a very small fraction of the whole lifetime of the star. Indeed we may say, comparatively speaking, that the star develops a substantial helium core almost instantaneously. It is this sudden development that produces the rapid motion in the H–R diagram.

2. *Results.*—Integrations were performed to determine the evolutionary sequences for four different masses, viz. $M=30{\cdot}1\odot$, $8{\cdot}94\odot$, $3{\cdot}89\odot$, $1{\cdot}52\odot$. The initial value of X was taken to be 0·75, and the initial helium concentration Y was taken as 0·23. It may be remarked that the precise value of $1-X-Y$ is not of any great importance, since metals make little contribution to the internal opacity, nor is the effective surface temperature low enough in these stars for the metals to have an appreciable effect on the surface boundary condition. Indeed the value of $1-X-Y$ enters only in determining the carbon cycle rate, and the overall stellar structure is known to be extremely insensitive to the precise value of this rate. The integrations were performed in a manner that has already been described in detail in former papers (**2**, **3**, **4**).

Results are most complete for the case $M=3{\cdot}89\odot$ and these are given in Table I. A plot of the solutions in the (M_{Bol}, $\log T_e$) plane is shown in Fig. 1 (the first of the solutions with an inert helium core is specially marked in the figure). The development of the core produces an S-bend oscillation followed by a very rapid motion to the right. This S-bend oscillation was found in a former paper (**2**) and has also been obtained by Kushwaha (**5**). It appears to arise whenever the main-sequence state possesses a convective core. The motion of the star around the S-bend takes about 5 per cent of the time that preceded the development of the core. The subsequent motion to the right is almost "instantaneous", as can be seen from the age values given in Table I.

It will be seen that the central temperature T_c rises very rapidly at the last few solutions of the table. Indeed, at the next solution (not given here) T_c rose to the neighbourhood of 8×10^7 °K, at which stage energy production by helium-burning became important. Unfortunately the mathematical technique whereby the solutions were obtained turned out to be ill-adapted to follow through this "firing" of the helium, and perforce the integrations had to be discontinued at this highly interesting state (instabilities of a purely mathematical character were encountered).

It is worth noticing in this connection that $M_{Bol}=-2{\cdot}6$ at the last solution of Table I. Thus a continuation of the evolution (to the right in the H–R diagram) would carry the star through the region where the Cepheids of short period lie. ***Hence it seems certain that the central helium is already fired in the Cepheids.*** It is

TABLE I

Mass 3·89 ⊙; $X=0{\cdot}75$, $Y=0{\cdot}23$ initially. L = luminosity, R = radius, T_c = central temperature, P_c = central pressure, T_e = effective temperature. q = fraction of mass in the inert helium core.

L (10^{36} erg sec^{-1})	P_c (10^{16} dyne cm^{-2})	T_e (°K)	T_c (10^6 °K)	Age (10^{15} sec)	R (10^{11} cm)	q
1·1772	15·079	18,340	27·599	0	1·2097	0
1·3372	14·242	18,190	28·290	1·0880	1·3115	0
1·4792	13·581	17,960	28·930	1·8353	1·4139	0
1·6004	13·088	17,710	29·521	2·3620	1·5141	0
1·7072	12·734	17,440	30·081	2·7427	1·6112	0
1·8671	12·373	16,930	31·122	3·2305	1·7885	0
1·9745	12·384	16,510	32·086	3·5071	1·9344	0
2·0727	12·949	16,100	33·459	3·7253	2·0829	0
2·0952	13·259	16,030	33·902	3·7686	2·1135	0
2·1351	16·033	16,220	34·032	3·8027	2·0827	0·005
2·1703	18·621	16,390	33·930	3·8253	2·0566	0·010
2·2135	22·133	16,550	33·677	3·8461	2·0373	0·015
2·2722	27·510	16,700	33·474	3·8669	2·0271	0·020
2·3358	34·451	16,810	33·348	3·8870	2·0297	0·025
2·4010	43·274	16,860	33·277	3·9060	2·0449	0·030
2·4670	54·695	16,860	33·253	3·9240	2·0733	0·035
2·5325	69·682	16,800	33·288	3·9409	2·1159	0·040
2·5960	89·608	16,680	33·417	3·9568	2·1722	0·045
2·6633	120·46	16,490	33·744	3·9731	2·2511	0·050
2·7263	165·52	16,240	34·355	3·9879	2·3474	0·060
2·7844	234·75	15,930	35·425	4·0007	2·4653	0·070
2·8446	370·17	15,480	37·548	4·0127	2·6409	0·075
2·8933	608·73	14,910	40·756	4·0218	2·8702	0·080
2·9219	915·12	14,390	44·122	4·0282	3·0963	0·085
2·9157	2667·1	12,540	55·014	4·0331	4·0733	0·095

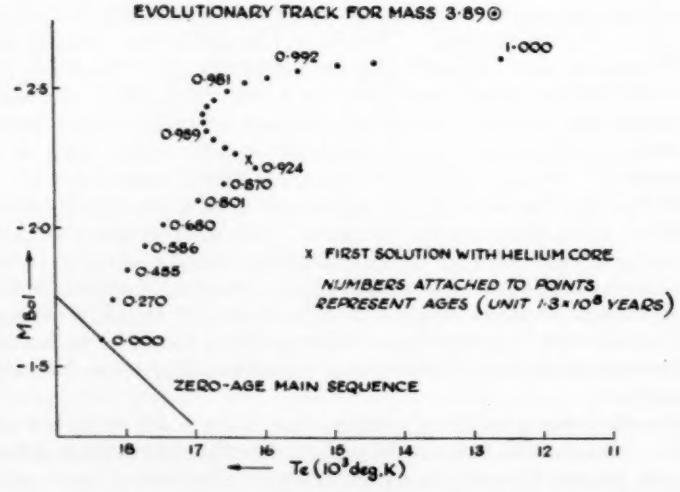

FIG. 1

also to be expected that evolution to the right will slow down, once the helium is burning sufficiently to contribute appreciably to the total energy generation. A plausible possibility is that the Cepheids are stars in which this slowing down has taken place.

Results for the other values of the mass are given in Tables II, III, IV. At the last solutions of Tables III, IV the central hydrogen concentration, X_c, had declined almost to zero. Rapid evolution round an S-bend, and then to the right, follows these last solutions. The value of X_c at the last solution of Table II was 0·23.

TABLE II

Mass 30·1 ⊙

L (10^{38} erg sec^{-1})	P_c (10^{16} dyne cm^{-2})	T_e (°K)	T_c (10^6 °K)	Age (10^{13} sec)	R (10^{11} cm)
4·6828	2·9770	44,100	40·016	0	4·1730
5·1274	2·9145	43,910	40·529	3·1766	4·4055
5·5607	2·8642	43·590	41·032	5·7816	4·7559
6·4606	2·8106	43,000	41·909	9·7581	5·1560
7·2374	2·7832	41,925	42·809	12·563	5·7407
7·9002	2·7889	40,720	43·676	14·540	6·3584
8·5732	2·8145	39,820	44·247	15·949	6·9265
9·1049	2·8636	38,610	45·041	17·081	7·5927

TABLE III

Mass 8·94 ⊙

L (10^{37} erg sec^{-1})	P_c (10^{16} dyne cm^{-2})	T_e (°K)	T_c (10^6 °K)	Age (10^{14} sec)	R (10^{11} cm)
1·7866	6·5868	28,050	33·382	0	2·0138
2·0688	6·1522	27,980	33·828	2·1312	2·1797
2·3230	5·8428	27,670	34·525	3·6875	2·3614
2·5627	5·6083	27,280	35·212	4·8308	2·5519
2·7808	5·4468	26,830	35·898	5·6730	2·7480
2·9742	5·3387	26,380	36·554	6·2923	2·9401
3·1420	5·2908	25,940	37·189	6·7534	3·1248
3·2850	5·2907	25,530	37·813	7·0996	3·2985
3·4041	5·3331	25,160	38·436	7·3607	3·4566
3·5039	5·4117	24,860	39·012	7·5579	3·5936
3·6529	5·6689	24,400	40·168	7·8262	3·8070
3·7521	6·0597	24,160	41·340	7·9859	3·9361
3·8171	6·5276	24,090	42·442	8·0815	3·9923

TABLE IV

Mass 1·52 ⊙

L (10^{34} erg sec^{-1})	P_c (10^{16} dyne cm^{-2})	T_e (°K)	T_c (10^6 °K)	Age (10^{16} sec)	R (10^{11} cm)
2·3219	25·877	8640	18·409	0	0·76555
2·7328	30·242	8845	19·804	1·6111	0·79234
3·2254	34·933	8935	21·685	3·2222	0·84371
3·4952	36·872	8885	22·776	3·9938	0·88820
3·7885	38·580	8755	23·983	4·7655	0·95248

It is of interest to compare the forms of the evolutionary tracks at different values of the total mass M. Write L_0, T_0 for the luminosity and effective surface

temperature at zero-age. Then for each evolutionary track the corresponding L_0, T_0 can be used as luminosity and temperature scale factors. This is done in Fig. 2. Because of the choice of scale factors (differing with each case of course) all the tracks start at the same point. The tracks for $M = 8{\cdot}94\odot$ and $30{\cdot}1\odot$ are so nearly the same that they have been drawn together. The case $M = 1{\cdot}09\odot$ has been drawn from data given formerly (**4**).

Stars of small mass move initially parallel to the main-sequence, whereas massive stars move almost perpendicularly to the main-sequence. The P–P chain is dominant in the energy production at $1{\cdot}09\odot$, whereas the carbon cycle is dominant in massive stars. This is the essential physical difference between the two cases. The relative tracks for massive stars are all very similar to each other.

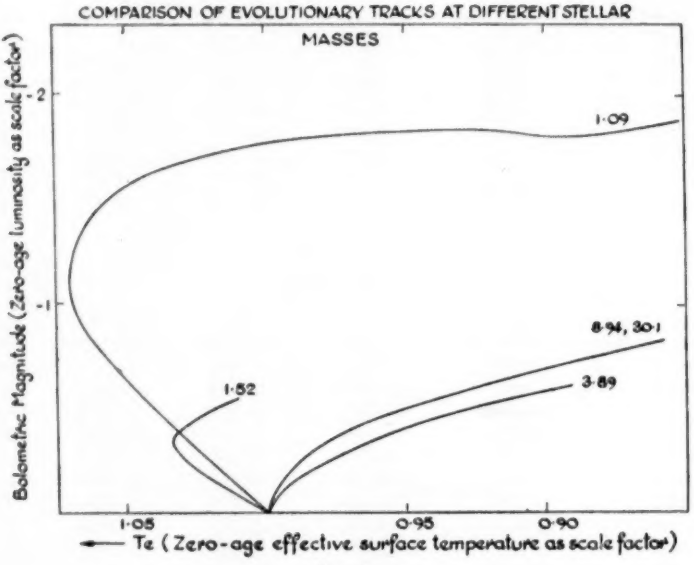

FIG. 2

3. *The main-sequence band.*—The essential information for determining the main-sequence band is assembled in Table V, where luminosities and effective temperatures are given both for the initial zero-age main-sequence and for the evolutionary stage at which X_c falls to zero at the centre of the star—i.e. just before the onset of rapid evolution to the right in the H–R diagram. The evolution time between these two states is also given in the table.

The zero-age values given in Table V lie of course on the zero-age main-sequence (**3**), which is plotted in Fig. 3. At the commencement of rapid evolution (M_{Bol}, $\log T_e$) always lies above the zero-age sequence. The values of (M_{Bol}, $\log T_e$) at this stage are also plotted in Fig. 3, and a curve has been drawn through the resulting points. This upper curve, together with the zero-age sequence, encloses a band in the (M_{Bol}, $\log T_e$) plane. This band determines a main-sequence neighbourhood. Apart from a special case to be discussed in a later section, and apart from stars at an advanced evolutionary stage (moving

to *left* in the diagram), stars near the main-sequence should always lie in this neighbourhood. Once an evolutionary track crosses the upper curve, an inert helium core is formed and evolution to the right takes place rapidly. (It is of course possible that a rapidly evolving star might occasionally be observed, but such cases must be rare.)

TABLE V

Mass (⊙)	30·1	8·94	3·89	1·52
At zero-age				
M_{Bol}	−8·1	−4·6	−1·6	+2·6
Log T_e	4·644	4·448	4·263	3·937
Fraction of mass in convective core	0·58	0·39	0·24	Nil
At the commencement of rapid evolution				
M_{Bol}	−9·0	−5·4	−2·2	+2·1
Log T_e	4·550	4·384	4·210	3·942
Age (10^6 years)	6·10	25·7	128	1390

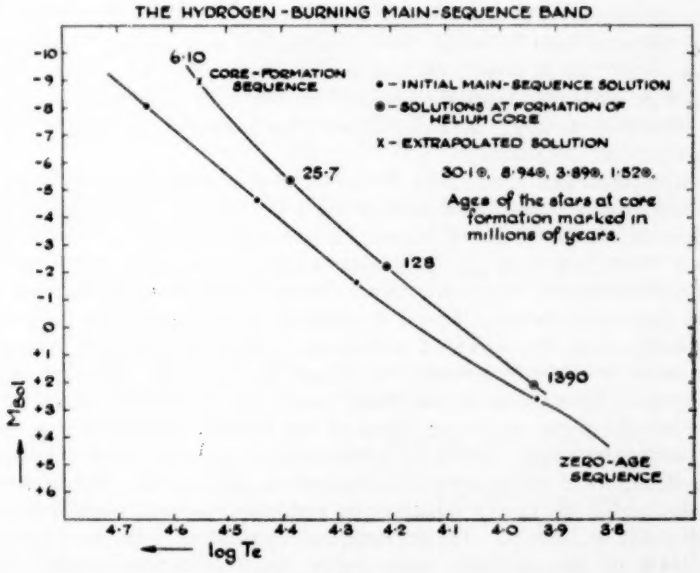

FIG. 3

Before continuing the discussion of this section it must be remarked that the point inserted in Fig. 3 for the case $M = 30{\cdot}1\odot$ does not correspond to the last solution of Table III; for the reason that $X_c = 0{\cdot}23$ at this last solution whereas we now require $(M_{Bol}, \log T_e)$ for $X_c = 0$. To deal with this situation, which arose from a machine copying error on to magnetic tape—tape flaw, we need only take account of the similarity between the evolutionary track for $M = 8{\cdot}94\odot$ and that for $M = 30{\cdot}1\odot$. The change of $(M_{Bol}, \log T_e)$ that occurs between $X_c = 0{\cdot}23$ and $X_c = 0$ can be estimated to very good accuracy simply by using the known change for the case $M = 8{\cdot}94\odot$; the required change is from

$(-8{\cdot}8, 4{\cdot}587)$ to $(-9{\cdot}0, 4{\cdot}550)$. There is a corresponding change in the evolution time from $5{\cdot}55 \times 10^6$ years to $6{\cdot}10 \times 10^6$ years. These are the values given in Table V.

4. *Comparison with the recent work of other authors.*—In a recent paper Schwarzschild and Härm (6) have considered the evolution of stars with masses $28{\cdot}2\odot$, $62{\cdot}7\odot$, $121{\cdot}1\odot$, $218{\cdot}3\odot$. By good fortune the first of these cases falls near $M = 30{\cdot}1\odot$, and a close comparison of results is therefore possible. This is given in Table VI.

TABLE VI

Mass ($\odot$)	28·2 (Schwarzschild–Härm)	30·1 (Hoyle)
Zero-age composition	$X=0{\cdot}75$, $Y=0{\cdot}22$	$X=0{\cdot}75$, $Y=0{\cdot}23$
$\log L/L_\odot$ at zero-age	5·035	5·093
$\log T_e$ at zero-age	4·630	4·644
$\log L/L_\odot$ at $X_c \cong 0$	5·403	5·450
$\log T_e$ at $X_c \cong 0$	4·520	4·550
Age at $X_c \cong 0$	$6{\cdot}07 \times 10^6$ years	$6{\cdot}10 \times 10^6$ years

The agreement is evidently very good indeed, particularly in view of the entirely different ways in which the computations were made. Remembering that $L \propto \sim M^{2{\cdot}5}$ at $M \sim 30\odot$ on the zero-age sequence, it is clear that the difference in $\log(L/L\odot)$, after correction for the mass difference, is extremely small. Probably the slight difference arises from a somewhat different use of the surface boundary condition.

Schwarzschild and Härm raise the interesting problem of the existence of a "semi-convection" zone. In massive stars the opacity arises almost wholly from electron scattering, in which case it is impossible for the convective core to end at a discontinuity of the molecular weight. (An outward discontinuous decrease of molecular weight requires a discontinuous outward decrease of the effective polytropic index. Hence, if material on the immediate inside of the discontinuity is at the verge of convective instability, material immediately outside must be violently unstable—a contradiction.) The apparent dilemma is resolved, as Schwarzschild and Härm point out, by dividing the convective region into two parts—an inner region of the normal convective type, and an outer "semi-convective" region. The material of the inner region is well-mixed and the transport of energy by convection can be appreciable. But in the semi-convective region the energy transport by convection is quite negligible and the material is not well-mixed. Yet the temperature gradient in the semi-convective region takes on the adiabatic value (to an excellent approximation) thereby allowing slow mixing to take place. The masses within the two regions and the variation of molecular weight throughout the semi-convective region are determined partly by the adiabatic condition and partly by the amount of helium that has been produced at any particular evolutionary stage. The molecular weight is everywhere continuous.

No special precautions were taken in the present work, apart from always employing the usual adiabatic condition for convection—it being argued that, if the machine could find solutions at all, the solutions could not contain physical contradictions. This somewhat naïve point of view turned out to be justified, as will be seen from the following discussion.

In changing the composition of a star during a time step, the star was divided into a number of zones—usually 1/60 of the mass of the star was placed in each zone. Except in almost impossibly rare cases, the surface of the well-mixed inner convective region does not fall at the exact beginning or end of one of the zones, but falls within a zone. The question therefore arises as to whether this particular zone is to be counted as belonging to the well-mixed convective region, or not. The question was decided by computing $(dT)_{\text{adiabatic}}/(dT)_{\text{radiative}}$ at the beginning and end of the particular zone. If the sum of these two quantities was $\leqslant 2$, the zone was counted as belonging to the inner region, but otherwise not. This procedure either underestimates or overestimates the extent of the inner region of strong convection.

In the early stages of the evolution of a massive star the region of strong convection tends to increase. Sooner or later then, the zone in which the surface of the region happens to lie comes to be counted as belonging to the region—i.e. the strong convection is overestimated and helium is mixed a little too far out from the centre. The immediate effect is to *reduce* the region of strong convection. Two further effects then arise. With continuing evolution, the region of strong convection may reassert itself and may extend outwards still further. But a new separate, quite shallow, convective shell can arise *outside* the main inner convective core. This convective shell mixes the helium carried outwards at the moment when the domain of the inner core was slightly exaggerated. It is just this latter effect that simulates the Schwarzschild–Härm semi-convection region.

The smooth curve 3 of Fig. 4 is drawn through the marked points, which represent the X values for the various zones at the last solution of Table III. The tendency of the points to fall into pairs ($0{\cdot}4 < X < 0{\cdot}7$) is a consequence of the procedure used for counting (or not counting) the zone in which the surface of the convective core lies.

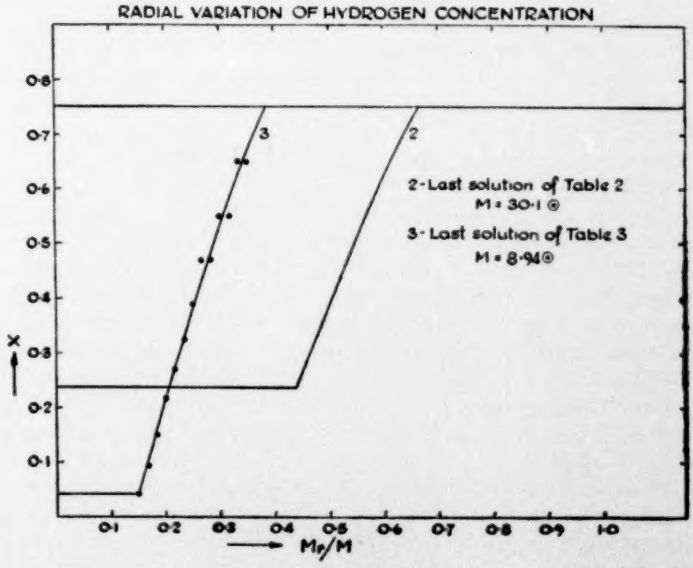

FIG. 4

The smooth curve 2 of Fig. 4 is the corresponding curve for the last solution of Table II. This may be compared with the corresponding solution of Schwarzschild and Härm (Fig. 2, $M = 28{\cdot}2\odot$, solution 4–3, p. 358 of their paper). The agreement is good.

Quite apart from this agreement two other circumstances give confidence in the results. In a purely automatic procedure (as in the present calculations) the machine very readily "loses" the solution if any serious random perturbation is introduced. Only by always working near to the actual physical structure of a star can a computer be used in a purely automatic fashion—at any rate without a very great increase of programming difficulty. Hence it is immediately clear, simply from an inspection of the behaviour of the machine, whether or not a discontinuous procedure (such as that outlined above) is introducing any serious change in the nature of the solutions. No difficulties of this kind were encountered—nothing in the least degree comparable with the difficulties that were mentioned above in connection with the "firing" of the helium core.

A less empirical check on the accuracy of the solutions was made by altering the zones from 1/60 of the total stellar mass to 1/200. If the procedure concerning the convective inner region introduced any appreciable error, then the error should be much less at a zone mass of 1/200 than at 1/60. In fact only very slight differences were found.

Results for stellar masses in the range $1{\cdot}5\odot$ to $30\odot$ have also recently been published (7) by Henyey, LeLevier and LeVee (HLL). Agreement is somewhat less satisfactory than with the Schwarzschild–Härm paper. The relative forms of the evolutionary tracks obtained by HLL are in reasonable agreement with those of Fig. 2, but the $(M_{Bol}, \log T_e)$ values appear to be systematically different. In part this may be due to the fact that HLL use an initial hydrogen concentration 0·68 as compared to the present 0·75. Also the energy generation rates employed by these authors do not incorporate the most recent estimates (cf. (3)). But it is difficult to see how the discrepancies in the age estimates—in one case by as much as a factor 1·5—can be explained in this way.

The differences between the present results and those obtained by Blackler (8) arise largely from the recent changes in the estimates of the nuclear energy generation rates.

5. *Comparison with observation.*—According to Fig. 3 the dispersion in luminosity of the main-sequence band, at fixed T_e, is about 2 mag. at high luminosities and about 1 mag. at low luminosities. If we accept a 1–1 correspondence between T_e and spectral type (ST) and between T_e and the colour index (CI) then the dispersion shown in Fig. 3 is certainly insufficient to explain the observational data. (Recently Sandage and Eggen have shown that such a correspondence does *not* exist for dwarf stars, where metallic lines can produce strong blanketing effects. There is no reason to expect such a complication for stars with $T_e > 10\,000$ °K however.) In the Pleiades, for example, there is a dispersion of about 3 mag. at $\log T_e = 4{\cdot}1$. The brightest stars of the cluster M11 are also about 3 mag. brighter than stars on the zero-age sequence at the same CI (although line blanketing might be important in this case).

The Pleiades are known to be in rapid rotation. In the case of Pleione, for example, the rotation is so rapid that the star appears to be at the verge of mechanical stability, implying (9) that the equatorial and polar radii are probably in a ratio of about 2/1. This effect has not been allowed for in the calculations,

which were carried out on the basis of spherical symmetry. Thus the calculations can only be thought of as an approximation to the average situation taken over the star's surface. The actual effective temperature would be expected to be higher than the calculated value in the polar regions and lower in the equatorial regions. Indeed a variation of T_e over the surface by as much as $2^{1/4}/1$ might well occur. Evidently then, it is of importance to the estimate of T_e to know whether the observer is looking predominantly at equatorial regions (as is probably the case for Pleione) or at the pole-on aspect of the star. Reference to Fig. 3 shows that an apparent luminosity dispersion of about 1·5 mag. may well be introduced by such an aspect effect (the observational $\log T_e$ might vary with aspect by as much as 0·075). Even so, a special problem still arises in the case of the Pleiades. This will be considered in a separate paper in which the strange case of the star Pleione is discussed.

At the Moscow Meeting of the IAU (Symposium on the H–R Diagram) Blaauw reported an investigation of the Scorpio–Centaurus group of B stars. In the nebular region of the group the five brightest stars have a moderate dispersion about a point $M_v = -4{\cdot}2$, Bo in the (M_v, ST) plane. (By taking the mean position of the five stars, rather than their individual positions, the dispersion due to any rotational aspect effect is compensated, at any rate in part.) The bolometric correction at Bo is about 3 mag. (**10**). Hence we are concerned with stars at $M_{Bol} \cong -7{\cdot}2$.

Now we expect the brightest stars to be found at the upper edge of the main-sequence band. Reference to Fig. 3 shows that on the upper edge of the band $\log T_e = 4{\cdot}477$ at $M_{Bol} = -7{\cdot}2$, from which it follows that the effective surface temperature at spectral type Bo must be near 30 000 °K, not to 25 000 °K, as given by Morgan and Keenan. This result is in agreement with the higher values found by Pecker (**11**) and by McDonald and Underhill (**10**).

Evolution times at four points are marked in Fig. 3 (in units of 10^6 years). It is seen that $M_{Bol} = -7{\cdot}2$ falls about midway between the two upper points, and hence that the appropriate age estimate must be close to the geometric mean (Fig. 3 is an essentially logarithmic plot!) between $6{\cdot}10 \times 10^6$ years and $25{\cdot}7 \times 10^6$ years—i.e. close to $12{\cdot}5 \times 10^6$ years. From dynamical considerations Blaauw estimates the whole Scorpio–Centaurus group to have an age of about 20×10^6 years. Since, however, the nebular region is much more compact than the main group it is possible, and even likely, that the ages of the stars in the nebular region are less than the age of the main group. The present estimate would therefore seem to be in reasonably satisfactory agreement with Blaauw's estimate.

Turning now to the main group, Blaauw finds two bright stars at $M_{Bol} = -7{\cdot}4$ ($M_v = -4{\cdot}6$, B.C. $= -2{\cdot}8$). A similar age estimate for these two stars also gives a value $\sim 12 \times 10^6$ years, which conflicts significantly with the dynamical age of 20×10^6 years. It seems somewhat unsafe, however, to place a heavy reliance on only two stars taken from a large group—for some special reason the two stars might be exceptionally late condensations. Rather does it seem safer to rely on a larger sample of stars. The next brightest stars occur at ST B2. Blaauw finds 7 of these stars clustered closely at $M_v = -2{\cdot}6$. A further 8 stars possess a considerable dispersion in luminosity, but their mean magnitude also falls near $M_v = -2{\cdot}6$.

The bolometric correction at B2 is about $-2{\cdot}6$; so that for this set of 15 stars we are concerned with $M_{Bol} \cong -5{\cdot}2$. Again taking the upper edge of the main-

sequence band, the value $M_{Bol} = -5{\cdot}2$ falls very close to one of the calculated points—yielding an age estimate $\sim 26 \times 10^6$ years. The agreement with the dynamical age is now quite satisfactory.

Acknowledgments.—It is a pleasure to acknowledge my gratitude to the Rockefeller Foundation and to the IBM Corporation for the support and facilities that were given to me during the course of this work.

St John's College,
Cambridge:
1959 *May.*

References

(1) Sandage, A. R., *Ap. J.*, **125**, 435, 1957.
(2) Haselgrove, C. B., and Hoyle F., *M.N.*, **116**, 515 and 527, 1956.
(3) Haselgrove, C. B., and Hoyle, F., *M.N.*, **119**, 112, 1959.
(4) Hoyle, F., *M.N.*, **119**, 124, 1959.
(5) Kushwaha, R. S., *Ap. J.*, **125**, 242, 1957.
(6) Schwarzschild, M., and Härm, R., *Ap. J.*, **128**, 348, 1958.
(7) Henyey, L. G., LeLevier, R., and LeVee, R. D., *Ap. J.*, **129**, 2, 1959.
(8) Blackler, J. M., *M.N.*, **118**, 37, 1958.
(9) Jeans, J. H., *Astronomy and Cosmogony*, Cambridge Press, p. 237.
(10) McDonald, J. K., and Underhill, A. B., *Ap. J.*, **115**, 577, 1952.
(11) Pecker, J. C., *Ann. d'Ap.*, **13**, 433, 1950.
(12) For the first investigation of the evolution of massive stars see:
Tayler, R. J., *Ap. J.*, **120**, 332, 1954.

PROBLEMS CONCERNING PLEIONE

J. Crampin and F. Hoyle

(Received 1959 May 7)

Summary

An evolutionary paradox arises in the case of the star Pleione. The implications of this paradox are discussed and several possibilities for overcoming it are investigated.

At first sight one would expect a star evolving from the main-sequence to become increasingly stable against rotation. It is shown, however, that increasing central condensation decreases the moment of inertia of the star sufficiently to produce two distinct epochs during which any initial tendency towards rotational instability is rendered more acute.

The mass of Pleione must be of order $4\odot$ and the radius of order 2×10^{11} cm. The calculated age depends on the evolutionary interpretation adopted, one interpretation gives an age as low as $4{\cdot}7 \times 10^7$ years, another gives an age as high as $1{\cdot}4 \times 10^8$ years.

Rotational instability causes the star to shed a disk of material, the disk probably being magnetically coupled to the star. The winding of the field, arising through rotation, may well be responsible for the ultimate instability of the disk. The process of disk formation and disruption can be repeated many times, the general order of the time required for disruption being 100 years.

---

1. *Introduction.*—The spectrum of Pleione has undergone unusual changes since this star was first observed in 1888 at the Harvard Observatory. Originally of type B8p with emission lines, in 1905 the lines disappeared and Pleione became a typical rapidly rotating star of normal B8 spectrum (**1**, **2**). The emission lines reappeared in 1938 however, and remained visible until 1951 when they again faded. During the period 1938 to 1951 observations of the spectrum were made by McLaughlin and Mohler (**3**), by Struve and Swings (**4**), by Underhill (**5**), and by Merrill (**6**).

These spectroscopic peculiarities have been explained in terms of the development, and disruption of, a disk or shell surrounding the main star. The following rotational velocities have been estimated by Underhill:

Star	292 km sec^{-1}
Disk (2·1 stellar radii)	140 km sec^{-1}
Disk (4·4 stellar radii)	67 km sec^{-1}

The rotational velocity of the star is so large as to suggest that the line of sight does not make any very great angle with the equatorial plane. Moreover the rapid rotation suggests that the star may be subject to incipient rotational instability, and that the instability manifests itself in the formation of an outlying disk.

2. *The evolutionary puzzle.*—According to the spectral classification and colour index given by Johnson and Morgan (**2**), the position of Pleione in the (M_{Bol}, $\log T_e$) plane is $\sim(-1{\cdot}94, 4{\cdot}107)$, corresponding to a visual absolute magnitude $-0{\cdot}80$ and an effective surface temperature of 12,800 °K at spectral type B8. The bolometric correction at this effective temperature is about $-1{\cdot}14$ mag.

Reference to the preceding paper (7) shows that this position for Pleione lies quite markedly outside the main-sequence band. The aspect effect discussed in the preceding paper could cause the observational estimate of T_e to be too low. It was seen that fluctuations by as much as 0·04 in log T_e (from the mean value) can arise according to aspect when the surface of a star is seriously disturbed by rapid rotation, as indeed the surface of Pleione must certainly be. Hence the effective mean position of Pleione can reasonably be taken at $\sim(-1{\cdot}94, 4{\cdot}15)$. This point still lies somewhat outside the main-sequence band shown in Fig. 3 of the preceding paper, indicating that Pleione has reached the phase of rapid evolution associated with the S-bend shown in Fig. 1 of the preceding paper.

The Pleiades contain blue stars that are considerably brighter than Pleione—the most luminous stars having $M_{Bol} = -4{\cdot}0$. The problem arises as to why these stars have not already completed the phase of rapid evolution. Why, if Pleione has evolved to the upper edge of the main-sequence band, have these brighter stars not already moved far to the right in the H–R diagram ?

A number of possible answers can be suggested :

(1) The Pleiades are not of uniform age. The brightest stars of the group are appreciably younger than Pleione.

(2) Owing to the shielding effect of diffuse material outside the star, the value of T_e given by observation is considerably below the true effective temperature.

(3) Pleione is not evolving from the main-sequence to the right in the H–R diagram, but is evolving to the left. That is to say, Pleione has already passed through the supergiant phase of its evolution. Starting originally perhaps at $M_{Bol} \sim -5$ on the zero-age main-sequence, Pleione was initially the brightest member of the group and hence was the first star to leave the main-sequence. It is now returning to the main-sequence at a lower luminosity, $M_{Bol} \sim -2$, because much mass was lost during the supergiant phase.

(4) Extensive mass loss has taken place near the main-sequence, in the sense advocated by the Russian school of astrophysicists.

The following discussion will be based on the possibilities (1) and (2). Too little is at present known of the advanced stages of evolution of stars for (3) to be considered in a quantitative way, while (4) seems inherently improbable in the case of Pleione. Mass loss reduces the mean angular momentum per unit mass, since material is ejected into space from the surface regions where the angular momentum per unit mass is greatest. For this reason it is difficult to see how Pleione can have lost a large fraction of its mass and still be rotationally unstable—as the spectrum peculiarities appear to require. (A similar objection applies to (3), but in this case the objection is not so strong, because the central condensation of the star may possibly increase very greatly at advanced evolutionary stages.) It is also difficult to see how mass loss could be significantly less important for the brighter stars with $M_{Bol} \sim -4$.

In case (2) we require the true effective temperature to be about 20,000 °K. Such a value has indeed been used by Struve (8). The position of Pleione in the (M_{Bol}, log T_e) plane then becomes $\sim(-3{\cdot}0, 4{\cdot}3)$, which now lies well within the main-sequence band. (The bolometric correction at $T_e = 20{,}000$ °K is $\sim 2{\cdot}2$ mag.) The starting point on the zero-age main-sequence would be close to $(-2{\cdot}5, 4{\cdot}32)$. In this case we may say that, whereas the brightest star of the Pleiades at $M_{Bol} \sim -4$ has reached, and perhaps has already crossed, the upper edge of the main-sequence band, Pleione has only moved about half-way across

the band. With M_{Bol} now at ~ -3 instead of ~ -2 this is an entirely reasonable resolution of the evolutionary difficulty, as will be seen from the age calculations given in Section 4.

3. *The rotation problem.*—At first sight it is curious that rotational instability can manifest itself at all in an evolving star. A star such as Pleione would seem to spend amply long enough close to the zero-age main-sequence to be able to rid itself of any excess angular momentum—indeed a star cannot accommodate excess angular momentum and must it seems get rid of it in a time no longer than the Kelvin–Helmholtz contraction time. And the likely presence of a magnetic field removes the possibility of more or less arbitrary changes in the distribution of angular momentum—the star should soon assume a condition approximating to uniform rotation.

The question now arises as to how evolution to the right of the main-sequence can promote rotational instability, on the reasonable assumption that the star is reduced to stability at the zero-age main-sequence. We shall examine this question on the further plausible assumption that a stellar magnetic field is effective in maintaining uniform angular velocity throughout the star at all stages of the evolution.

Write M, R for the mass and mean radius of the star. Let Ω be the angular velocity at any stage, and let kR be the radius of gyration about the polar axis. The angular momentum I is given by

$$I = Mk^2R^2\Omega, \tag{1}$$

and the mean density ρ is given by

$$\rho = \frac{3M}{4\pi R^3} \tag{2}$$

to a satisfactory approximation. (Taking the surface to be a spheroid $r = R(1+\epsilon P_2)$, in the approximation in which terms of order ϵ^2 are neglected the mean radius is R and the volume is $4\pi R^3/3$.)

The onset of rotational instability depends on the quantity

$$\Omega^2/2\pi G\rho, \tag{3}$$

where G is the gravitational constant. According to Jeans (9) instability arises when this quantity exceeds $\sim 1/3$. Jeans obtained 0·36075 for the onset of instability in the case of a Roche model of very great central condensation. For actual stars the value must be less than this—although actual stars do possess strong central condensation. Jeans's estimate of 0·31 for an adiabatic model of exponent 2·2 indicates that the present assumed value of 1/3 should be an excellent approximation for an actual star.

By using (1) and (2) to substitute for Ω and ρ in (3) we see that the onset of instability is governed by

$$\frac{2I^2}{3GM^3} \cdot \frac{1}{k^4R} \cdot \tag{4}$$

The quantity $(k^4R)^{-1}$ has been constructed from the detailed evolutionary solutions obtained for a star of mass 3·89$\odot$, which were reported in the preceding paper. The results are given in Table I, which also contains the luminosity L, the effective temperature T_e, and the mean radius R. These solutions, which have been numbered from 1 to 28, can readily be compared with those plotted in Fig. 1 of the preceding paper. The values of $(k^4R)^{-1}$ are plotted against solution number in the figure below.

TABLE I

Solution No.	Luminosity (10^{36} erg sec^{-1})	Radius (10^{11} cm)	Effective surface temperature (10^4 °K)	k	$k^{-4}R^{-1}$ (10^{-9}cm^{-1})
1	1·1773	1·2097	1·834	0·30302	0·9805
2	1·3372	1·3115	1·819	0·29549	1·0001
3	1·4792	1·4139	1·796	0·28930	1·0097
4	1·6025	1·5141	1·770	0·28419	1·0125
5	1·7073	1·6112	1·744	0·28000	1·0098
6	1·7929	1·7030	1·718	0·27656	1·0037
7	1·8671	1·7885	1·693	0·27378	0·9951
8	1·9263	1·8658	1·670	0·27152	0·9861
9	1·9745	1·9344	1·651	0·26969	0·9773
10	2·0137	1·9939	1·634	0·26820	0·9693
11	2·0459	2·0432	1·621	0·26701	0·9628
12	2·0726	2·0829	1·610	0·26606	0·9581
13	2·0950	2·1134	1·602	0·26531	0·9550
14	2·1351	2·0827	1·622	0·26477	0·9770
15	2·1702	2·0565	1·639	0·26431	0·9964
16	2·2135	2·0373	1·655	0·26362	1·0163
17	2·2722	2·0271	1·670	0·26257	1·0379
18	2·3358	2·0297	1·681	0·26134	1·0562
19	2·4010	2·0449	1·686	0·25999	1·0702
20	2·4670	2·0734	1·686	0·25857	1·0790
21	2·5324	2·1159	1·680	0·25704	1·0827
22	2·5960	2·1722	1·668	0·25549	1·0804
23	2·6633	2·2511	1·649	0·25376	1·0713
24	2·7263	2·3474	1·624	0·25203	1·0558
25	2·7844	2·4653	1·593	0·25030	1·0334
26	2·8446	2·6409	1·548	0·24828	0·9972
27	2·9219	3·0963	1·439	0·24455	0·9030
28	2·9157	4·0733	1·254	0·24046	0·7343

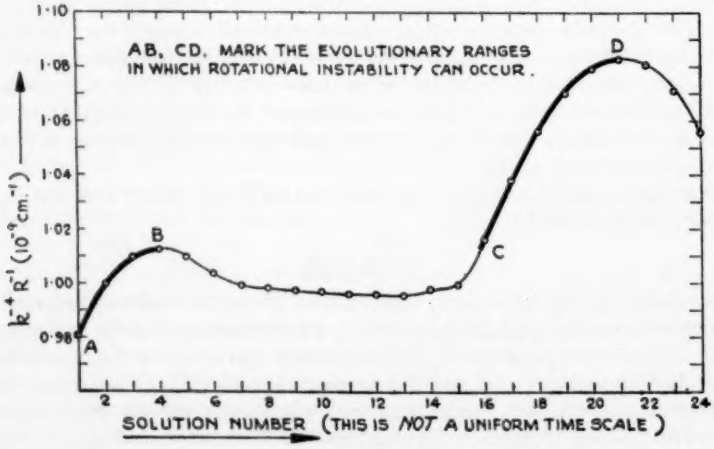

FIG. 1

The remarkable point now emerges that the maximum value of $(k^4R)^{-1}$ occurs, not at zero age, but at solution 21. The cause of this curious behaviour lies in the formation of a dense inert helium core, which decreases k sufficiently to more than offset the increase in R. There is also a subsidiary maximum at solution 4.

It is of course the case that the changing structure of the star also implies some change in the precise numerical criterion for instability. Increasing central concentration slightly increases the value that (4) must take in order that instability shall arise, since the approximation to the Roche model thereby becomes closer. But the effect of the formation of an inert inner core is not likely to be appreciable since the inner parts of the star must always approximate very closely to spherical symmetry, and no change of central condensation of these symmetrical regions can change appreciably the gravitational field in the outer parts of the star. For this reason the change of the instability criterion will be taken to be negligibly small.

Suppose now that the star becomes rotationally unstable during its initial condensation to the zero-age main-sequence. Then as a consequence of the loss of angular momentum (through disk formation) the value of (4) is reduced slightly below 1/3 at solution 1. But as the star evolves from solution 1 to solution 4 the value of (4) cannot be kept below 1/3 unless I is further reduced—i.e. unless the star loses angular momentum, presumably again through disk formation. Between solutions 4 and 15 there is stability, but from solution 15 to solution 21 the value of (4) would again rise above 1/3 unless I were again reduced. Thus a second phase of rotational instability is implied. The unstable parts of the evolution are indicated in Fig. 1 by the heavy portions of the curve. The star splutters continuously along these sections of the curve, as indeed Pleione is observed to do at the present time.

Unfortunately these considerations do not allow any decision to be made between the possibilities (1) and (2) of the previous section. In case (1) Pleione lies at

$$\sim(-1{\cdot}94,\ 4{\cdot}15) \tag{5}$$

in the $(M_{Bol}, \log T_e)$ plane. Since this point is somewhat to the right of the upper edge of the main-sequence band, Pleione would now be at the S-bend stage of the evolution which is just the stage that corresponds to solution 21 of the Table I above. In case (2) Pleione lies at

$$\sim(-3{\cdot}0,\ 4{\cdot}3). \tag{6}$$

Evolution from the zero-age main-sequence at $\sim(2{\cdot}5, 4{\cdot}32)$ would then correspond to evolution from solution 1 to solution 4. Thus the two rotationally unstable sections of the evolution correspond closely to these two evolutionary possibilities.

4. *The mass, mean radius, and age of Pleione.*—We consider first the case that Pleione is older than the brightest stars of the Pleiades—i.e. that Pleione is now at the S-bend stage of evolution and that it lies close to the point (5) of the $(M_{Bol}, \log T_e)$ plane.

The luminosity at solution 21 of Table I above is $2{\cdot}5324 \times 10^{36}$ erg sec^{-1}. This is for a star of mass $3{\cdot}89\odot$. A bolometric magnitude of $-1{\cdot}94$ for Pleione corresponds to a luminosity of $1{\cdot}592 \times 10^{36}$ erg sec^{-1} from which it follows that the mass of Pleione must fall somewhat below $3{\cdot}89\odot$ for this first case.

For small changes of mass the evolutionary track changes homologously to an excellent approximation (in fact the previous paper showed that the tracks are nearly homogolous over the whole mass range from $3{\cdot}89\odot$ to $30{\cdot}1\odot$). On the zero-age sequence L varies with the mass M as $\sim M^{3{\cdot}5}$, for mass values near $3{\cdot}5\odot$. The assumption of homology requires L to vary as $M^{3{\cdot}5}$ at all corresponding phases of evolution, in particular at the S-bend phase of the evolution. Using this condition, the mass of Pleione is seen to be close to

$$3{\cdot}89\left(\frac{1{\cdot}592}{2{\cdot}532}\right)^{2/7}\odot = 3{\cdot}41\odot, \tag{7}$$

a value very much less than that suggested by Struve (**8**).

The mean radius can be obtained by a similar argument. The radius for solution 21 at mass $3{\cdot}89\odot$ is $2{\cdot}1159\times10^{11}$ cm. At mass $3{\cdot}41\odot$ the corresponding radius must be close to $1{\cdot}936\times10^{11}$ cm, since the radius varies under homologous conditions as $\sim M^{2/3}$. It is important to remember that this is a mean value and that the equatorial radius of the star is greater by a considerable margin. According to Jeans (**9**), the shape of the surface is not greatly different from a spheroid, even at instability, and the ratio of the equatorial to the polar radius is then about 2/1. Such a surface may be represented by

$$R(1-0{\cdot}4P_2) \tag{8}$$

from which we see that with $R=1{\cdot}936\times10^{11}$ cm the equatorial radius is $\sim 2{\cdot}32\times10^{11}$ cm. (The approximation of using the mean radius for R in (8) and of employing (2) is still tolerable in spite of the large distortion—the second order terms amount to less than 10 per cent of the main terms.)

It may be added that the value of k is not altered by the homologous change from $3{\cdot}89\odot$ to $3{\cdot}41\odot$. At the solution corresponding to 21 of our table it remains equal to 0·257. An issue of some importance does arise, however, concerning the values of k given in the table. These have been determined from detailed solutions obtained under conditions of spherical symmetry. The question arises as to whether such estimates have any quantitative validity for a star so seriously distorted from sphericity as (8) implies. The answer is that the k values do possess validity. The essential point is that at uniform angular velocity the inner regions of the star do not depart seriously from spherical symmetry, and it is the inner regions where the main mass is located, and which makes the main contribution to the moment of inertia. At solution 21 only about 5 per cent of the total mass of the star lies in the outer 90 per cent of the volume. Reference to Jeans's diagram (*op. cit.* p. 245 for the Roche model) shows how closely the inner parts approximate to spherical symmetry.

In any case we are concerned not so much with determining actual values of k as with determining the variation of k during the evolution. Even if k were modified somewhat due to rotary distortion it is not to be expected that the relative change of k would be significantly changed.

The evolution time given by the calculations at $M=3{\cdot}89\odot$ is $1{\cdot}28\times10^8$ years. The evolution time at $M=3{\cdot}41\odot$ should be somewhat longer than this, since the evolution time varies as $\sim M/L$, which changes with mass according to $\sim M^{-5/7}$. With this dependence the age of Pleione is found to be $\sim 1{\cdot}4\times10^8$ years.

The present interpretation requires the brightest stars of the Pleiades to be younger than Pleione. It is of interest to consider the age of the brightest star, on the basis that the bolometric magnitude is $-4{\cdot}0$ and that the brightest star is

now crossing the upper edge of the main-sequence band. The age can then be determined (approximately) by an interpolation between the solutions for mass $3{\cdot}89\odot$ and those for $8{\cdot}92\odot$—as given in the preceding paper. The result is an age of $\sim 5{\cdot}2 \times 10^7$ years. Although the difference between this value and the above estimate of $1{\cdot}4 \times 10^8$ years for Pleione is very considerable, the possibility cannot be excluded that star formation in the Pleiades has been spread over a considerable interval of time.

We turn next to the possibility that the true effective surface temperature of Pleione $\sim 20{,}000$ °K, and that the position of Pleione, in the (M_{Bol}, log T_e) is given by (6). In this case we have no evolutionary integrations available that lie close to the track of Pleione, so that an interpolation between the cases $M = 3{\cdot}89\odot$ and $M = 8{\cdot}92\odot$ (as given in the preceding paper) must be used. On the zero-age main-sequence we have a bolometric magnitude $-1{\cdot}6$ for $M = 3{\cdot}89\odot$, $-4{\cdot}6$ for $M = 8{\cdot}92\odot$, and $\sim -2{\cdot}5$ for Pleione. A simple interpolation (remembering that the magnitude scale is essentially logarithmic) gives mass $5{\cdot}0\odot$ for Pleione. The radius follows directly from (6) by using the relation $L = \pi acR^2T_e^4$, and is $1{\cdot}935 \times 10^{11}$ cm. The time required for evolution across the *whole* main-sequence band can also be determined by interpolation between $25{\cdot}7 \times 10^6$ years at $M = 8{\cdot}92\odot$ and 128×10^6 years at $M = 3{\cdot}89\odot$. The result is 79×10^6 years. We are concerned here, not with evolution across the whole main-sequence band, however, but with an evolution that corresponds to the change from solution 1 to solution 4 of Table I. Reference to the preceding paper shows that this portion of the evolution requires ~ 60 per cent of the time for evolution across the whole main-sequence band. Hence the required age of Pleione is now $\sim 47 \times 10^6$ years.

It will be useful to collect the various results into a table:

TABLE II

Characteristics of Pleione

	Hypothesis that Pleione is at the S-bend stage of evolution	Hypothesis that the true effective temperature ~20 000 °K
Mass ($\odot$)	3·41	5·0
Radius (10^{11} cm)	1·936	1·935
Age (10^6 years)	140	47
Equatorial rotation speed (km sec^{-1})	340	410

The values given for the age may be compared with the above estimate of $5{\cdot}2 \times 10^7$ years for the age of the brightest star of the Pleiades. The brightest star has to be much younger than Pleione on the first hypothesis, but is closely the same on the second hypothesis. The latter agreement is therefore consistent with the view that the Pleiades are all of the same age—which would be the viewpoint on the second hypothesis. The existence of this agreement strongly supports the second hypothesis.

(There does not seem to be any definite physical reason for the close similarity between the two values for the radius. That the values must be roughly similar is of course clear, but the near identity appears to be no more than a coincidence.)

5. *The rotation speed of Pleione.*—We now put the expression (4) equal to 1/3, yielding the following criterion of rotational instability

$$I=\frac{1}{\sqrt{2}}k^2M^{3/2}(GR)^{1/2}. \tag{9}$$

Substitution in (1) gives

$$R\Omega=(GM/2R)^{1/2} \tag{10}$$

where $R\Omega$ is the rotation speed. Insertion of M and R from Table II yields the rotation speeds shown also in the table. Before these can be compared with the observed speed of 292 km sec^{-1} the theoretical values must be multiplied by sin i, where i is the angle of inclination of the line of sight to the polar axis of the star. To obtain agreement with observation we require $i\cong 60°$ for the first column of Table II and $i\cong 45°$ for the second column.

Were it not for this last result we should be inclined to favour the second of the hypotheses considered above—that the true effective temperature of Pleione is substantially higher than the observational estimate. But if the inclination is no greater than 45° it is difficult to see how this could be so, since the observer would not then be looking through the flattened disk-like outer system. It is of course possible that (10) overestimates the theoretical rotation speed required for the onset of instability. Such an error would moreover show itself rather sensitively in the estimation of the angle of inclination. For example, a 25 per cent reduction in (10) would raise i from 45° to 90°. Indeed, the determination is so sensitive that to have obtained reasonable values of i at all can be regarded as providing good support both to the theory and to the values of the mass and radius given in Table II.

6. *The instability of the outer disk.*—When material leaves a rotationally unstable star it is likely that a disk is formed in the equatorial plane, with the relatively diffuse material of the disk moving in circular orbits about the centre (**9**). The velocity in such circular orbits is less than the rotation speed of the star itself—as can be seen from the observational estimates mentioned above in the introduction to this paper. Hence the angular velocity is less in the disk than the angular velocity of the star, and hence any lines of force of a magnetic field that originally connected the material of the star with that of the disk must become twisted into a spiral structure.

Two cases arise. If the turns of the magnetic lines of force can mainly be stored inside the star, the disk can continue to move about the star for a long period of time. Indeed in this case the disk acquires considerable angular momentum at the expense of the star, and therefore moves markedly away from the centre—a process discussed by one of the present authors in connection with the problem of the origin of the solar system (**10**).

If, on the other hand, the turns of the magnetic field have to be mainly stored outside the star, the magnetic intensity (and consequently the magnetic pressure) increases steadily within the disk, and ultimately the whole structure becomes unstable—probably explosively so.

In the paper already referred to (**10**), it was suggested that the two cases can be distinguished according to whether or not the star possesses a deep outer convection zone. If it does we have the former case, otherwise the latter case. On this basis we have the first case in dwarf stars and the second case in early type stars like Pleione. This will be assumed in the following discussion. That is to say, we

assume that the turns produced by the rotary winding of the magnetic field are accumulated in the disk, not in the star.

The density of the material of the disk is not very well determined unfortunately. Underhill (5) suggests a value $\sim 10^{-10}$ gm cm^{-3}, and this value will be used in the following discussion. With this density, the kinetic energy per unit volume, T say, is given by

$$T \cong 10^4 \text{ ergs}, \tag{11}$$

since ~ 150 km sec^{-1} appears to be a typical velocity in the disk (5). Writing H for the magnetic intensity, the condition of stability is simply that $H^2/8\pi$ shall be less than a quantity of order T. Now $H \sim NH_0$, where H_0 is the initial field before any winding takes place and N is the number of turns. It is easy to see with this criterion that the disk becomes unstable when N becomes so large that

$$N > \sim H_0^{-1}\sqrt{8\pi T}. \tag{12}$$

The next step is to estimate H_0. An idea of the general order of H_0 is given by the following argument; it must be emphasised, however, that the precise value is quite uncertain.

Whichever of the evolutionary hypotheses we consider for Pleione, the mass and radius of the main star are given in order of magnitude by $M \sim 4\odot$, $R \sim 2 \times 10^{11}$ cm. Inserting these values in (2) gives a mean density $\sim 0{\cdot}24$ gm cm^{-3} within the star. A magnetic field expanded isotropically from this density down to the much lower density within the disk ($\sim 10^{-10}$ gm cm^{-3}) would be reduced in intensity by a factor equal to the two-thirds power of the density ratio; i.e. by $\sim 1{\cdot}8 \times 10^6$. Typically stellar fields appear always to be of order 10^4 gauss. If such a field were expanded isotropically, the field within the disk would thus be reduced to a value $\sim 5 \times 10^{-3}$ gauss. We shall therefore write

$$H_0 \cong 5 \times 10^{-3} \text{ gauss} \tag{13}$$

in the following discussion of the stability of the disk.

Inserting (11) and (13) into (12) shows that the disk becomes unstable when the number of turns N of the spirally wound magnetic field exceeds $\sim 10^5$.

The remaining step is to estimate the length of time required to produce $\sim 10^5$ turns. The observed rotational speed is 292 km sec^{-1}. Allowance for the angle of inclination of the system would probably raise the rotation speed to ~ 350 km sec^{-1}, as we have seen above. With a radius $\sim 2 \times 10^{11}$ cm the rotation period of Pleione is thus of order $3{\cdot}6 \times 10^4$ sec—i.e. about 10 hours. Hence in a time of t sec the number of rotations of the star $\sim (3{\cdot}6 \times 10^4)^{-1} t$.

This does not quite represent the number of turns of the field that are built up in time t, since only relative rotations between the star and the disk produce field winding. The angular velocity within the disk appears to be so very much less than that of the star, however, that no allowance for this effect is needed in an order of magnitude calculation (cf. the rotational speeds quoted above in the introductory section). It follows immediately that a time of $\sim 3{\cdot}6 \times 10^9$ sec is required to produce $\sim 10^5$ turns of the field—i.e. about 100 years. This may be taken as satisfactory agreement with the observed periods of instability, which seem to be of the general order of 30 years. Plainly, several of the quantities appearing in the calculation are too uncertainly known (H_0; the density within the disk) for it to be worthwhile attempting to push the agreement between theory and observation any closer than this.

We can say with some confidence, however, that a twisted magnetic field is capable of producing instability—probably a sudden instability—in a time interval of the same general order as that found by observation. Other suggestions—radiation pressure for example—fail to provide a satisfactory explanation by an enormous margin.

A further significant point is that, long before any actual instability arises, the magnetic forces acting on the material of the disk must become appreciable. The average radial component of the force must be directed outwards. Hence the orbital velocities within the disk should systematically be less than the Keplerian speeds. This indeed appears to be the case, as can be seen from the values given by Underhill (**5**, cf. introductory section above).

Acknowledgments.—The authors wish to thank the Rockefeller Foundation and the IBM Corporation for providing facilities for obtaining the stellar models on which certain of the computations of the present paper are based.

St John's College,
Cambridge:
1959 *May*.

References

(1) Eggen, O. J., *Ap. J.*, **113**, 81, 1950.
(2) Johnson, H. L. and Morgan, W. W., *Ap. J.*, **117**, 31, 1953.
(3) McLaughlin, D. B., *Ap. J.*, **88**, 622, 1938.
Mohler, O., *Ap. J.*, **88**, 623, 1938.
(4) Struve, O. and Swings, P., *Ap. J.*, **93**, 446, 1941.
Struve, O. and Swings, P., *Ap. J.*, **97**, 426, 1943.
(5) Underhill, A. B., *Ap. J.*, **110**, 166, 1949.
(6) Merrill, P. W., *Ap. J.*, **115**, 145, 1952.
(7) Hoyle, F., *M.N.*, **120**, 22, 1960.
(8) Struve, O., *Stellar Evolution*, Princeton, 133.
(9) Jeans, J. H., *Astronomy and Cosmogony*, Cambridge, 237.
(10) Hoyle, F., "On the origin of the solar nebula", to be published shortly.

THE RADIAL VELOCITIES OF FIVE STARS IN THE ζ PERSEI AGGREGATE

D. H. P. Jones
(Communicated by the Astronomer Royal)

(Received 1959 May 7)

Summary

New radial velocities are found for o Per, HD 22951, HD 24131, and HD 24640. Jordan's orbit for o Per is confirmed and HD 24640 is found to be a β-Cephei variable. The system reproduces the well-determined radial velocity of ζ Per.

Introduction.—Some years ago Ambartsumian (1952) demonstrated the existence of aggregates of O and B type stars. He showed that they were in general gravitationally unstable in the galactic field and a theory was developed in which the aggregates were identified as centres of star formation. More recently Blaauw and others have published detailed discussions of the proper motions of stars in these aggregates which can be interpreted in terms of linear expansion from a point. The scale of this expansion provides an estimate of the age of the aggregate and the stars in it. These ages have been made the basis of a large volume of theoretical work on Stellar Evolution. Thus Burbidge and Burbidge (1958) quote the following ages in support of their work.

Aggregate	Age	Analysed by
ζ Persei	$1{\cdot}3 \times 10^6$ years	Blaauw (1944, 1952 and 1953 with J. Delhaye)
Lacerta	4·2 ,,	Blaauw and Morgan (1953)
Cepheus II	4·5 ,,	Markarian (1953)
Cassiopeia–Taurus	~50 ,,	Blaauw (1956)

But Petrie in a recent paper (1958) has shown that the expansion of Cassiopeiae–Taurus is fictitious and has thrown much doubt on the aggregate's physical existence. Moreover Woolley and Eggen (1958) have shown that the expansion of the Lacerta aggregate is doubtful, although the aggregate probably exists physically.

The physical existence of a cluster of early type stars around ζ Persei is indisputable, and the evidence of expansion, derived from proper motions, is good (Delhaye and Blaauw 1953). However, the radial velocities are not in general well determined and the evidence of expansion from radial velocities is slim (Blaauw 1952). The object of this and subsequent papers is to improve the radial velocity data for the aggregate. It is hoped in a later paper to publish absolute magnitudes for the members, based on the MK type and also on the equivalent width of Hγ. The effect of interstellar absorption can be calculated indirectly from the colour excesses published by Stebbins, Huffer and Whitford (1939). Improved radial

velocity measures combined with individual distance moduli may make it possible to arrive at a completely independent value of the expansion. Blaauw's latest value for the expansion (Delhaye and Blaauw 1953) is

$$+0''\cdot00236 \text{ per year per degree}$$
$$\pm 0''\cdot00025 \text{ p.e.}$$

which corresponds to an expansion-age of $1\cdot5 \times 10^8$ years. Assuming spherical symmetry the aggregate has a diameter of 30 parsecs so that there should be a difference in radial velocity of 20 km/sec between front and back. Radial velocities can be measured to a far higher accuracy than this—the inherent difficulty is to measure individual distances sufficiently accurately.

Method of observation and reduction.—The spectrograph at the Cassegrain focus of the 36-in. Yapp reflector has an optical train highly transparent to the ultra-violet. It may be used in the 'one-prism' or 'three-prism' form; the former was used for these observations. The dispersion is then 122 A/mm at Hγ rising to 87 A/mm at H12 (3750A), which is easily seen on a good plate. The collimator : camera ratio is 2·5 : 1 so that the slit-width of 30 μ which was habitually used projects to 12 μ on the plate. The spectra were broadened to 0·3 mm by trailing the star along the slit in hour angle, using a modified speed of telescope drive. The exposures were all made at zenith distances of less than fifty degrees, so no attempt was made to compensate for atmospheric dispersion, which was much smaller than the seeing disk (about 2″).

A fifth-magnitude star requires an exposure of 7 minutes with Oa–O emulsion or 24 with baked IIa–O (U.K. Kodak). For B stars such spectra are measurable from 4471A He I to 3750A H12; Hβ can be seen with Oa–O emulsion but adds no weight to the radial velocity determinations. Each plate was measured in both directions against a comparison iron arc exposed for equal periods before and after each stellar exposure. The lines used with their adopted wavelengths are shown in Table I.

TABLE I

Adopted wave-lengths

Element	Laboratory wavelength	Adopted wavelength
He I	4471·48	same
Hγ	4340·47	same
Hδ	4101·74	same
He I	4026·19	same
Hε	3970·08	same
He I	3964·73	same
H8	3889·05	same
H9	3835·39	3835·64
He I	3819·61	same
H10	3797·90	3797·80
H11	3770·63	same
H12	3750·15	same

The wavelengths were arrived at empirically from the plates of ζ Persei (a standard-velocity supergiant). With the accuracy obtainable it was found possible to use the laboratory wavelength for all but two of the lines, viz. H9 and H10.

These were adjusted to agree with the mean of the remaining lines. The lines He 4471 and 4026 require careful attention. In the Victoria system they have different wavelengths for supergiants and for main-sequence stars because of differing strengths of the forbidden absorptions (Petrie 1953b). However it is difficult to extrapolate these results to the low dispersion used here. Instead it is proposed to use the system as it stands and calibrate it against further standard-velocity stars of different luminosities and spectral types. This work is at present in hand at the Royal Greenwich Observatory.

No attention was paid to interstellar lines. The K line of Ca II is barely visible on a typical plate of these five stars and is only measurable on a few. The intensity of the H line is considerably less than the K line, so its possible effect on Hε or He 3964 was disregarded.

The mean of the velocities of the lines was taken as the velocity of the star, rejecting lines which appeared doubtful during measurement and deviated widely. Each measure was corrected for the solar motion in the usual way. The internal probable error of a good plate was of the order of ± 5 km/sec. There was some evidence of short exposures producing incorrect results because of uneven illumination of the slit, so all exposures of two minutes or less were rejected. At a declination of + 30° a star requires 1½ minutes to trail down the slit.

Stars with constant velocities.—The first three columns of Table II contain the Henry Draper number, name and visual magnitudes of the stars. Columns four and five are the spectral types on the Henry Draper and Morgan-Keenan systems (Johnson and Morgan 1953, Slettebak and Howard 1955). The sixth column is the radial velocity in km/sec which is the weighted mean of the individual spectra. The weights are calculated from the internal probable errors of the plates, by the usual method of least squares. Column seven is the probable error of the weighted mean and column eight contains the number of spectra measured. The velocities from Wilson's general catalogue (1953) are given in column nine together with their qualities.

TABLE II

Stars with constant velocities

HD	Star	m_v	Sp. HD	Sp. MK	RV	p.e.	n	Wilson	p.e. of unit wt.
22951	40 Per	5·04	B2	Bo·5 V	+20	±1	33	+19c	±7
24131	GC 4649	5·73	B3	B1 V	+10	±1	17	+17·8a	±5
24398	ζ Per	2·91	B1	B1 Ib	+19	±1	11	+20·6a	±4

A typical plate has an internal probable error of ± 5 km/sec, and this was taken as the unit of weight. However, intercomparison of the individual plate measures gives an external value of the probable error of unit weight, and this quantity is shown in the last column. For a star with constant velocity it should be ~ ± 5 km/sec but where the velocity is variable it is greater. Thus the constant velocities of HD 24131 and ζ Persei are confirmed. There is evidence of real variation in HD 22951 but the amplitude is too small for it to be investigated with this accuracy.

Stars with variable velocity.—Table III gives essentially the same quantities for the variable stars as Table II for the constant stars. However, the radial

TABLE III

Stars with variable velocities

HD	Star	m_v	Sp. HD	Sp. MK	RV	p.e.	n	Wilson
23180	o Per	3·94	B1	B1 III	+14	±3	42	+18·5a
24640	GC 4734	5·48	B3	B2 V	+ 7	±2	33	+17c

TABLE IV

Measures of individual spectra of stars with variable velocity

o Per

Plate	Date	RV	p.e.	Ph.
Y1p				d
30a	1958 Oct. 13·069	− 43	± 5	0·675
b	13·075	− 6	8	0·681
45d	31·838	+ 84	6	1·767
e	31·845	+ 88	7	1·774
72a	1958 Nov. 19·880	+ 33	10	3·132
d	19·966	+ 4	16	3·218
73b	19·853	+ 55	7	3·105
78d	1958 Dec. 1·883	+108	5	1·817
e	1·889	+ 72	7	1·823
f	1·898	+ 97	7	1·833
79c	2·135	+ 81	7	2·068
d	2·142	+122	5	2·075
e	2·149	+118	7	2·083
81c	2·925	+ 52	6	2·854
e	2·980	+ 49	5	2·913
83f	4·130	− 70	6	4·063
97c	31·936	− 1	5	0·936
g	1959 Jan. 1·008	+ 12	4	1·008
98b	1·012	+ 4	4	1·012
111e	10·075	+ 14	9	1·237
114b	10·960	+127	6	2·122
140b	27·899	+ 29	5	1·384
156b	1959 Feb. 3·847	− 70	5	3·913
c	3·851	− 46	5	3·917
164b	15·769	+ 66	8	2·577
c	15·778	+ 88	8	2·585
165a	15·797	+ 93	7	2·605
173c	25·834	− 31	6	3·804
175b	26·797	− 70	9	0·344
c	26·802	− 79	6	0·347
d	26·809	− 85	4	0·353
181b	27·826	+ 31	7	1·385
188a	1959 Mar. 10·834	+ 4	8	3·447
b	10·837	− 10	5	3·550
c	10·844	− 3	5	3·557
d	10·851	− 5	3	3·564
e	10·856	− 28	8	3·569
198b	13·857	+117	4	2·150
211b	25·856	− 21	4	0·892
c	25·863	− 14	5	0·899
d	25·870	+ 7	4	0·906
e	25·877	− 44	±14	0·913

HD 24640

Plate	Date	RV	p.e.	Ph.
Y1p				d
48c	1958 Nov. 1·014	− 8	±4	0·092
71a	19·069	−12	7	0·106
c	19·141	− 1	6	0·047
72b	19·900	− 6	4	0·015
75a	1958 Dec. 1·065	+32	4	0·118
76a	1·159	+18	6	0·080
b	1·178	+24	9	0·099
d	1·215	+25	11	0·004
79a	2·087	+26	3	0·086
b	2·113	+32	6	0·112
81a	2·851	−16	4	0·060
b	2·899	+27	4	0·108
d	2·955	+ 3	8	0·033
88a	14·883	− 3	5	0·108
c	14·908	+21	4	0·002
d	14·923	− 1	4	0·017
94a	22·013	+ 1	5	0·127
96b	31·858	+11	4	0·095
97a	31·894	− 1	5	0·000
b	31·917	− 1	4	0·023
d	31·952	−19	4	0·058
f	31·991	+10	7	0·097
98a	1959 Jan. 1·039	+10	6	0·013
d	1·071	+ 1	5	0·045
f	1·113	+11	4	0·087
100a	1·942	+15	5	0·126
c	1·994	−12	5	0·046
103a	3·947	−30	6	0·024
111a	9·898	+14	6	0·049
b	9·984	− 2	5	0·003
c	10·040	+31	4	0·059
122a	12·944	+ 5	7	0·066
b	12·974	+29	±4	0·096

velocity and its probable error are not the weighted means but the values adopted for the reasons given in the subsequent discussion. Table IV gives the individual measures with their dates. It also gives the phase of each observation with respect to the period finally adopted for each star, viz $4^d{\cdot}41916$ for *o* Per and $0^d{\cdot}13169$ for HD 24640.

(i) *o* Persei HD 23180. This star is a spectroscopic binary whose orbit was calculated by Jordan (1910) and confirmed by Muller, Walraven and Woltjer (1956). The orbit has $e=0{\cdot}0$ and $P=4^d{\cdot}41916$. Jordan also observed the spectrum of the secondary but this cannot be seen on the Yapp plates, and its presence has not been confirmed by investigation subsequent to Jordan's discovery. Using the above period and eccentricity the observations were fitted to the best sine-curve by the method of least squares (Fig. 1). The solution gave the following results.

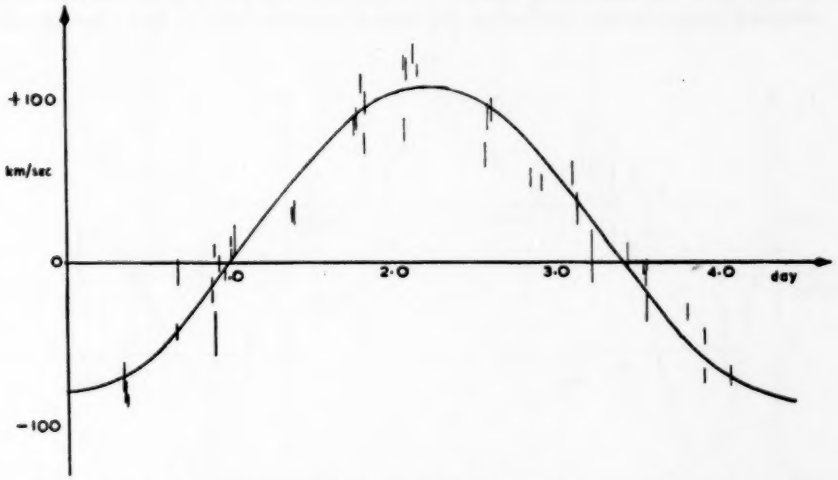

FIG. 1.—*o Persei: comparisons of least squares solution with observation. (Length of vertical line twice p.e. of observation.)*

$$v=+14\ \pm 3\text{ p.e.} \qquad +93\sin\theta\ \pm 4\text{ p.e.} \qquad \theta=81^\circ{\cdot}4634\ (t^d\text{—Jan. }1{\cdot}114\pm 0{\cdot}027)$$

(p.e. of unit weight ±15).

Jordan found

$$v=+18{\cdot}5\pm 0{\cdot}7 \qquad +111{\cdot}9\sin\theta\pm 1{\cdot}0$$

from 70 plates, p.e. of a plate ±7·0 at 40 A/mm at Hγ. Muller, Walraven and Woltjer derived

$$v=+14{\cdot}0\pm 3{\cdot}0 \qquad +112{\cdot}0\sin\theta\pm 1{\cdot}0$$

from 27 plates, p.e. of a plate ±10 at 25 A/mm at Hγ, and by harmonizing their phase with Jordan derived the improved period

$$4^d{\cdot}419175\pm 0{\cdot}000013\text{ p.e.}$$

Similarly this discussion gives

$$4^d{\cdot}4191666\pm 0{\cdot}000006\text{ p.e.}$$

in excellent agreement. More disturbing is the high probable error of unit weight, viz. ±15 km/sec. This cannot be lowered significantly by introducing eccentricity into the spectroscopic orbit. It is impossible to tell whether this is due to a superimposed variation of, perhaps, the β Cephei type with period ~$0^d.25$, because of the distribution of the plates. The star has been suspected of light variation by Walker (1952) and has the same spectral type as stars known to be β Cephei variables. The high probable errors found by other investigators, who only took one plate a night in general, might also be symptomatic of this effect.

(ii) HD 24640. The weighted mean of all the plates is +8 ± 2 p.e. km/sec. However the probable error of unit weight is ±12 compared to ±5 for constant velocity stars. A few trials show that there is no simple sine-curve which fits the observations—the motion is periodic in about $0^d.13$ but there appear to be large variations in amplitude. Fortunately 9 spectra (75a to 81d) fall in a compact group around December 2·0 and 10 spectra (96b to 100c) are closely

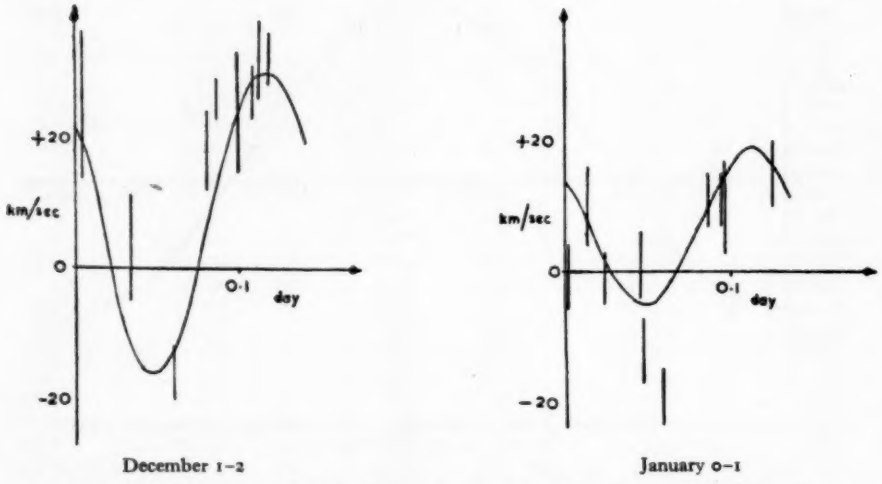

FIG. 2.—*Velocity curves of HD 24640 reduced to a single cycle,* $0^d.13169$. (*Length of vertical line twice p.e. of observation.*)

grouped around January 1·0. Each of these groups was reduced to a single cycle using the period $0^d.13169$. A sine curve was then fitted to each group with constant mean velocity throughout but different amplitudes. The solutions were

$$v = 6{\cdot}7 + 23{\cdot}0 \sin\theta \qquad \theta = 2734° (t\text{—Dec. } 1{\cdot}028)$$

$$v = 6{\cdot}7 + 11{\cdot}7 \sin\theta \qquad \theta = 2734° (t\text{—Jan. } 0{\cdot}844)$$

The agreement of these curves with the observations is shown in Fig. 2. However when all the observations are reduced to a single cycle with period $0^d.13169$ the sinusoidal variation is largely obscured. Several other periods were tried without success. Using $0^d.13169$ a sine curve (Fig. 3) was forced through the observations by least squares with the following result

$$v = 6{\cdot}3 + 8{\cdot}3 \sin\theta \qquad \theta = 2734° (t\text{—Nov. } 0{\cdot}065)$$

This reduces the probable error of unit weight from ±12 to ±10. Because the periods are arbitrary no probable errors can be assigned to the parameters in these solutions. However, the different assumptions (including that of constant velocity) agree very closely on the mean velocity. *A priori* the value adopted is more likely than the weighted mean itself and so we can transfer the p.e. of the weighted mean to it. Thus we adopt.

Mean velocity = +7 ± 2 p.e. km/sec.

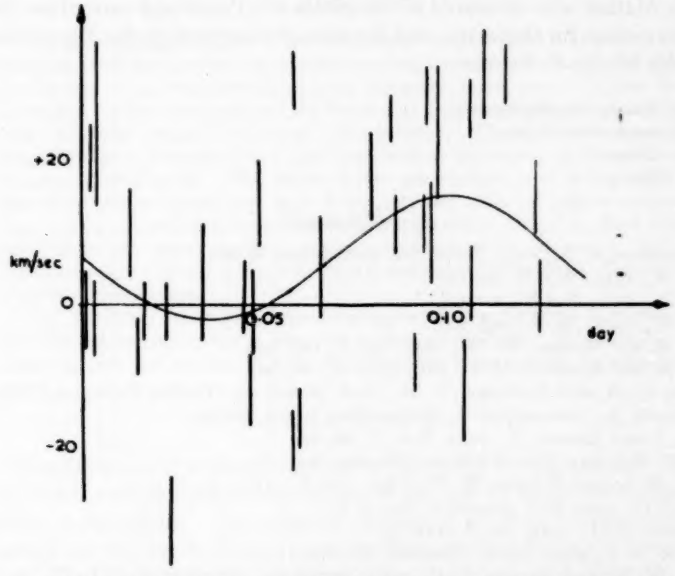

FIG. 3.—*HD* 24640. *All observations reduced to a single cycle,* $0^d{\cdot}13169$, *and least squares solution. (Length of vertical line twice p.e. of observation.)*

The unsatisfactory nature of these results is clearly caused in part by variations in amplitude. However variations in the mean velocity and period cannot be ruled out. This radial velocity behaviour is typical of that of a β Cephei variable. Moreover its light is slightly variable—it was discarded as a standard by Huffer (1931) when observing the eclipsing variable AG Persei but has never been further investigated. There are two current period-luminosity relationships for β Cephei stars (Blaauw and Savedoff 1953, Petrie 1954). For a period of $0^d{\cdot}13169$ the former predicts an absolute magnitude of −2·1 and the latter −2·0. However Petrie's relation refers to the Victoria absolute magnitude system (Petrie 1953 a) which is 0·4 magnitudes faint on that generally adopted. The MK spectral type of this star, B2V, implies an absolute magnitude of −2·6 (Morgan and Keenan 1951). In his discussion of the ζ Persei aggregate, Blaauw (1944) estimated it at −2·3. It is clear that HD 24640 fits the period-luminosity relationship very well in spite of the fact that its period is shorter than any previously known β-Cephei variable and it is luminosity class V where the others are mostly II-IV. In fact, the luminosity classification of V might be expected from the run of period with

position in the M_v, $U-B$ diagram for the known β-Cephei variables listed by Struve (1955). Struve's results indicate that a star with $P \sim 2$–3 hours would lie on the unevolved main sequence.

Acknowledgments.—This investigation forms part of a spectroscopic programme for the improvement of data on stellar dynamics which was initiated by the Astronomer Royal and is under the direction of Dr B. E. J. Pagel, to both of whom the author is grateful for much help and advice. In this context he would also like to thank Dr O. J. Eggen for advice on a number of points and all those present at the Herstmonceux conference in 1959 April when the matter was discussed; Miss L. Mather who measured all the plates of *o* Persei and carried out the least-squares solution for that star; and the team of observers on the Yapp telescope—especially Mr D. R. Palmer.

Royal Greenwich Observatory,
Herstmonceux Castle,
Sussex :
1959 *May* 4.

References

Ambartsumian, V. A., 1952, *Trans. Int. Astr. Union*, **8**, 665.
Blauuw, A., 1944, *B.A.N.*, **10**, 29.
Blaauw, A., 1952, *B.A.N.*, **11**, 405.
Blaauw, A., 1956, *Ap. J.*, **123**, 408.
Blaauw, A. and Morgan, W. W., 1953, *Ap. J.*, **117**, 256.
Blaauw, A. and Savedoff, M. P., 1953, *B.A.N.*, **12**, 69.
Burbidge, G. R. and Burbidge, E. M., 1958, Article on " Stellar Evolution ", Handbuch der Physik, **51**, Astrophysik II, Sternaufbau, p. 134, Berlin.
Delhaye, J. and Blaauw, A., 1953, *B.A.N.*, **12**, 72.
Huffer, C. M., 1931, *Pub. Washburn Obs.*, **15**, 192.
Johnson, H. L. and Morgan, W. W., 1953, *Ap. J.*, **117**, 313.
Jordan, F. C., 1910, *Pub. Allegheny Obs.*, **2**, 63.
McNamara, D. H., 1955, *Ap. J.*, **122**, 95.
Markarian, B. E., 1953, *Soobs. Bjurakan Obs.*, No. 11.
Morgan, W. W. and Keenan, P. C., 1951, Article in " Astrophysics " (ed. J. A. Hynek), p. 23.
Muller, A. B., Walraven, Th. and Woltjer, L., 1956, *B.A.N.*, **13**, 51.
Petrie, R. M., 1953a, *Pub. D.A.O.*, **9**, 251.
Petrie, R. M., 1953b, *Pub. D.A.O.*, **9**, 297.
Petrie, R. M., 1954, *Contr. D.A.O.*, No. 38; also *J.R.A.S. Canada*, **48**, 185.
Petrie, R. M., 1958, *M.N.*, **118**, 80.
Slettebak, A. and Howard, R. F., 1955, *Ap. J.*, **121**, 102.
Stebbins, J., Huffer, C. M. and Whitford, A. E., 1939, *Ap. J.*, **91**, 20.
Struve, O., 1955, *P.A.S.P.*, **67**, 135.
Walker, M. F., 1952, *A.J.*, **57**, 227.
Wilson, R. E., 1953, *Pub. Carnegie Inst. Washington*, No. 601.
Woolley, R. v. d. R. and Eggen, O. J., 1958, *The Observatory*, **78**, 149.

THE RELATION BETWEEN INTERSTELLAR EXTINCTION AND POLARIZATION*

R. Wilson†

(Received 1959 May 5)

Summary

An approximate solution of the problem of scattering by a long dielectric cylinder, with axis inclined at an arbitrary angle to the line of sight, is given (in Section 2) for the limiting case of refractive index $m \to 1$. Using this, extinction curves are computed (in Section 3) for a fixed sample of particles with different angular frequency distributions. These distributions are chosen to give maximum and zero polarization according to the different theories of alignment. The curves differ substantially and it is predicted that the colour excess per unit mass and the ratio of colour excesses $E_{(U-B)}/E_{(B-V)}$ are both functions of the polarizability $p/E_{(B-V)}$. Both these predictions are tested against existing observations in Section 4, with a positive result in favour of the distribution predicted by the Davis–Greenstein alignment mechanism.

An important corollary of the investigation is that the ratio R of total to selective extinction is also a function of the polarizability, R increasing by about 60 per cent as the polarizability increases from zero to its maximum value.

---

1. *Introduction.*—Our knowledge of the physics of the interstellar dust grains has developed mainly from observations of the law of space reddening and of interstellar polarization. The classical analysis of the observed extinction curve was carried out by van de Hulst (**1**) using the scattering theory of homogeneous spheres. He concluded that the interstellar particles were dielectric with an effective size of $0{\cdot}8\,\mu$. The pronounced "toe" of the extinction curve, shown by Whitford's (**2**) extension of the measures to the infra-red, seemed a strong argument against the hypothesis of metallic particles, which were expected to show a $1/\lambda$ law at long wave-lengths. This hypothesis was revived, however, by the work of Güttler (**3**), who took account of the variation with wave-length of the optical properties of metals in the visible and infra-red. Following up the earlier work of Schalén (**4, 5**), he concluded that the extinction by a mixture of iron particles, with an effective size of $0{\cdot}08\,\mu$, could explain the observed curve.

It would therefore appear that an analysis of the extinction curve itself is insufficient to decide between the two hypotheses. However, the scattering properties of dielectric and metallic particles are quite different and observations of the intensity of the diffuse light in the Galaxy should be particularly pertinent to this problem. Such observations were carried out by Henyey and Greenstein (**6**) who showed that the particles had an albedo greater than 0·3 with a strongly forward-directed phase function. They pointed out that this was to be expected if the

* *Contributions from the Dominion Astrophysical Observatory*, No. 64. Published by permission of the Deputy Minister, Department of Mines and Technical Surveys, Ottawa, Canada.

† Fellow of National Research Council, Ottawa, 1957–58, on leave from Royal Observatory, Edinburgh. Now at Atomic Energy Research Establishment, Harwell.

particles are dielectric, but Güttler (**3**) has since argued that metallic particles can also have a high albedo and that their results are consistent with this hypothesis. However, the presentation of the observations of Henyey and Greenstein by van de Hulst (**7**) would seem to be a very strong argument in favour of the dielectric particle hypothesis.

The discovery of interstellar polarization by Hall (**8**) and Hiltner (**9**) indicated that the dust particles are asymmetric in shape, probably in the form of long needles. Extensive observations of polarization have since been made by Hall and Mikesell (**10**) and Hiltner (**11, 12, 13**). These show a definite dependence on galactic longitude, which is best illustrated by the observations of the outer part of the Galaxy. In the region of Perseus near galactic longitude $l = 100°$, where the spiral arm is observed normal to its axis, the intensity of polarization is high and the plane of vibration (i.e. the plane for which the electric vector is a maximum) shows a marked preference for the galactic plane. As we move along the Milky Way in decreasing longitude, the polarization decreases until when we reach Cygnus at $l = 40°$, where the spiral arm is observed nearly parallel to its axis, the intensity of polarization is generally small and the planes of vibration show no preferential direction.

The preference of the plane of vibration for the galactic plane means that the long axes of the interstellar particles must lie in a direction perpendicular to the galactic plane, and to explain the observed intensity of polarization, a considerable degree of alignment is required. Three theories have been proposed to explain this alignment. One of these, by Gold (**14**), proposes an alignment mechanism based on the relative streaming of gas and dust clouds, but this would seem to fail under quantitative examination (**15**). The two remaining theories use the concept of a general galactic magnetic field as the aligning force. Spitzer and Tukey (**16**) assume each particle to contain a highly magnetized ferromagnetic domain with a magnetization parallel to the long axis. They adopted van de Hulst's (**1**) proposed constitution for the interstellar particles as being mainly dielectric with metallic impurities, and devised a mechanism due to collisions whereby the impurities could be formed into ferromagnetic grains, which would then act as condensation nuclei and grow a dielectric "skin". The required magnetic field has a direction perpendicular to the galactic plane and a field strength of 2×10^{-3} to 10^{-4} gauss. The small values of polarization observed in Cygnus need to be explained by some depolarization effect.

Davis and Greenstein (**17**) make the very plausible assumption that the grains are paramagnetic. In the absence of a magnetic field, elongated particles will spin at random about their short axes due to equipartition between the kinetic energy of rotation and the kinetic energy of the interstellar gas molecules. In the presence of a field, the magnetization lags behind the field and this causes a dissipative torque due to paramagnetic relaxation which tends to bring the axis of spin in line with the magnetic lines of force. The direction of the magnetic field is required to be in the galactic plane, along the spiral arms, and its strength about 10^{-4} to 10^{-5} gauss. This is a much more plausible field than required by the theory of Spitzer and Tukey, and is of the same strength and direction as obtained by Chandrasekhar and Fermi (**18**) on theoretical grounds. Further, there is a natural explanation of the variation of polarization with galactic longitude. In the region of Perseus, where we view the spiral arm perpendicular to its axis, we see the spinning particles edge on and therefore observe maximum polarization. In

Cygnus, where we view the arm almost parallel to its axis, we see the spinning particles full face on and therefore observe zero polarization.

To summarize the relative merits of the different theories proposed to explain the observable characteristics of the interstellar dust, we can say that the balance of evidence is in favour of the particles being dielectric and in the form of elongated needles oriented in a magnetic field by the Davis-Greenstein mechanism. The conclusions of this paper strongly support this view.

2. *Solution of the problem of scattering by a long dielectric cylinder for arbitrary incidence in the limiting case* $m \to 1$.—The interpretations of the observed extinction curve were made using theoretical curves computed from the formal solution derived by Mie (**19**) for the scattering by homogeneous spheres. The theories of polarization were based on the solution by Gans (**20**) for the case of spheroids small compared with the wave-length of incident radiation. Obviously a great advance could be made and a comprehensive theory introduced if we could calculate the scattering properties of long cylinders for arbitrary size, refractive index and angular incidence. Such calculations are not available (the state of scattering theory in this connection has been reviewed by van de Hulst (**21**)), but an approach can be made by considering the problem in the limiting case of the refractive index $m \to 1$. This follows the lead of van de Hulst who calculated the extinction curves in the limiting case $m \to 1$, for spheres (**1**) and long cylinders undergoing perpendicular incidence (**22**). He showed that these curves were closely similar to those obtained by rigorous computation for normal, real values of m if expressed in terms of the parameter

$$\rho = 4\pi r(m-1)/\lambda, \tag{1}$$

where r is the radius of the sphere or cylinder and λ the wave-length of the incident light.

We will follow van de Hulst's derivation for a sphere (**23**) using the theory of anomalous diffraction. We take a cylinder of length l and radius r with the conditions

$$l \gg r, \quad m \to 1, \quad r/\lambda \gg 1.$$

Using Cartesian co-ordinates, we place the cylinder in the yz plane with its long axis making an angle θ with the y-axis, which is also the direction of incidence.

We will express the extinction factor of the particle in units of the monochromatic intensity which would be geometrically incident on the cylinder for *perpendicular* incidence. Then this is given by

$$E(\rho, \theta) = \frac{2\pi}{k^2 lr} \text{Real}\,[S(0)], \tag{2}$$

where the wave-number $k = 2\pi/\lambda$, and $S(0)$ is the complex amplitude function.

A ray of light traversing the cylinder in the volume element $2y\,dx\,dz$, suffers a phase lag of $\rho y/r$. The amplitude function is therefore given by

$$S(0) = \frac{k^2}{2\pi} \int_0^{l \sin\theta} \int_{-r}^{+r} [1 - \exp(-i\rho y/r)]\,dx\,dz, \tag{3}$$

where x and y are related by the expression

$$x^2 + y^2 \sin^2\theta = r^2. \tag{4}$$

We can therefore make the substitutions $x = r \sin\tau$, $y = r\cos\tau/\sin\theta$ and this gives the extinction factor to be

$$E(\rho, \theta) = 2\sin\theta\, \text{Real} \int_0^{\pi/2} [1 - \exp(-i\rho\cos\tau/\sin\theta)]\cos\tau\, d\tau. \tag{5}$$

Taking out the real part and after some manipulation, this reduces to

$$E(\rho,\theta)=2\rho\int_0^{\pi/2}\sin\left(\frac{\rho}{\sin\theta}\cos\tau\right)\sin^2\tau\,d\tau$$
$$=\pi\sin\theta\,\mathscr{S}_1(\rho/\sin\theta), \tag{6}$$

where $\mathscr{S}_1(\rho/\sin\theta)$ is the first-order Struve function and is tabulated by Jahnke and Emde (**24**). For perpendicular incidence ($\theta=\pi/2$), the expression reduces to that derived by van de Hulst (**22**).

3. *Computation of extinction curves.*—No polarization results in the limiting case discussed in the preceding section. However, it is possible, from equation (6), to compute extinction curves for different degrees of polarization, according to the different theories.

Equation (6) refers to a single particle inclined at an angle θ to the direction of incidence. In practice we will observe several particles at varying angles of θ. Let the frequency distribution of the number of particles with θ be $f(\theta)$, where θ varies from 0 to $\pi/2$. Then the mean extinction factor per particle is given by

$$E_\theta(\rho)=\frac{\pi\int_0^{\pi/2}\sin\theta\,\mathscr{S}_1(\rho/\sin\theta)f(\theta)\,d\theta}{\int_0^{\pi/2}f(\theta)\,d\theta}. \tag{7}$$

This equation refers to a system of particles of identical sizes, and although it is not absolutely essential, for the purposes of this paper, it is nevertheless convenient to introduce a size dispersion. We will assume that the cloud of particles is a system of similar cylinders. The frequency distribution in size can then be expressed in terms of a single parameter $u=r/r'=l/l'$, where r' and l' are the dimensions of an arbitrary cylinder. The extinction can then be expressed as a function of ρ', where ρ' is related to r' in the same manner as ρ and r in equation (1). If the size distribution is expressed as $g(u)$, then the mean extinction factor for the cloud, averaged over all θ and all u, is given by

$$E_{\theta,u}(\rho')=\frac{\int_0^\infty E_\theta(u\rho')g(u)u^2\,du}{\int_0^\infty g(u)u^2\,du}, \tag{8}$$

where $E_{\theta,u}(\rho')$ is expressed in units of the total monochromatic intensity which would be geometrically incident on all particles for perpendicular incidence ($\theta=\pi/2$).

From equations (7) and (8) it is possible to compute extinction curves for any size or angular distribution of the particles. The calculations were made for the size distribution determined theoretically by Oort and van de Hulst (**25**) on the assumption that the particles were formed by condensation out of the interstellar gas. The actual numerical values are those tabulated by van de Hulst (**26**). It should be mentioned here that the fact that the interstellar particles are elongated means that some other factor, not considered by Oort and van de Hulst, must influence the growth of the particles and therefore, presumably, their ultimate size distribution (a mechanism for the growth of ice needles has been proposed by Kahn (**27**)). However, any difference between the assumed and actual size distributions will not affect the conclusions of this paper, since these are based on a

comparison of extinction curves for different functions $f(\theta)$, but with a common size distribution $g(u)$ whose effect will tend to cancel. In any case, the computed extinction curve is not very sensitive to changes in $g(u)$.

For the adopted size distribution, we can now compute the extinction curves for different values of the polarizability P (defined as the polarization per unit colour excess) according to the different theories. Throughout this paper we use the polarization p in magnitudes as defined by Hiltner (**28**) and the colour excess $E_{(B-V)}$ on the U, B, V system. The polarizability is therefore given by

$$P = p/E_{(B-V)}. \tag{9}$$

With the approximate scattering theory used here, we cannot compute values of p, but we can set up expressions for $f(\theta)$ for the extreme cases P = zero, and P = maximum (= 0·18 as measured by Hiltner (**13**)), according to the two theories of polarization:—

$$\text{Spitzer and Tukey} \left\{ \begin{array}{ll} P_0: & f(\theta) = \sin\theta \\ P_{max}: & f(\theta)\,d\theta = 1 \text{ for } \theta = \pi/2, = 0 \text{ for other } \theta \end{array} \right\} \tag{10}$$

$$\text{Davis and Greenstein} \left\{ \begin{array}{ll} P_0: & f(\theta)\,d\theta = 1 \text{ for } \theta = \pi/2, = 0 \text{ for other } \theta \\ P_{max}: & f(\theta) = 2/\pi \text{ for all } \theta \end{array} \right\} \tag{11}$$

The value of $\int_0^{\pi/2} f(\theta)\,d\theta$ is reduced to one and it is assumed that the alignment is perfect except for zero polarizability in the theory of Spitzer and Tukey, which can be explained only by some depolarization effect, and the spatial distribution of the axes is assumed to be random.

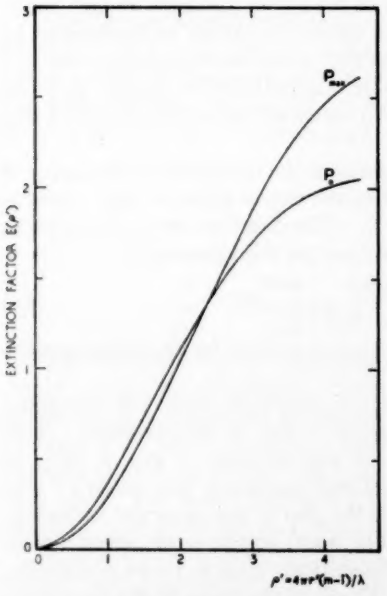

FIG. 1.—*Theoretical extinction curves computed for zero and maximum of values the polarizability $P = p/E_{(B-V)}$ according to the Spitzer–Tukey alignment mechanism.*

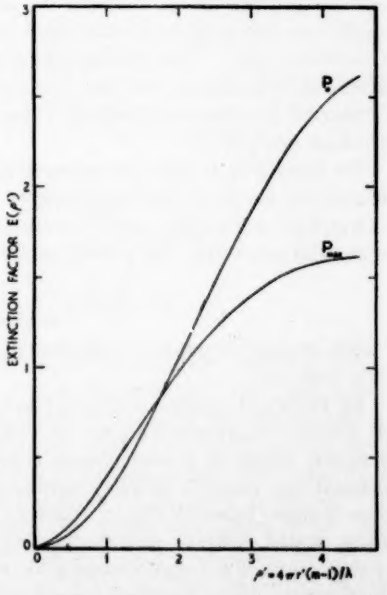

FIG. 2.—*Theoretical extinction curves computed for zero and maximum values of the polarizability $P = p/E_{(B-V)}$ according to the Davis–Greenstein alignment mechanism.*

The corresponding extinction curves, computed by means of equations (7) and (8) for the different functions $f(\theta)$, are given in Figs. 1 and 2. It will be noticed that two of these curves are identical; the curve for maximum polarizability according to the Spitzer–Tukey theory being the same as that for zero polarizability according to the Davis–Greenstein theory. Each theory predicts changes in the observed extinction curve which are of the opposite sense with respect to polarization, and which are greater in magnitude in the Davis–Greenstein case.

4. *Comparison with observation.*—By means of the computed extinction curves given in Figs. 1 and 2, we can now make specific predictions which can be tested by observation. Since these observations are made in different parts of the sky, and the extinction curves have all been computed for a specific sample of particles, we are making the implicit assumption that the composition, shape and size distribution are the same in all regions of space.

In this section two predictions will be made which can be tested by existing observations. Both of these are borne out by the Davis–Greenstein theory, i.e. by using the curves in Fig. 2, and for convenience of presentation we shall confine ourselves to this case, bearing in mind that the Spitzer-Tukey theory would predict effects in the opposite sense but of smaller magnitude. To give numerical values it is necessary to establish the scale of ρ' in terms of $1/\lambda$ and we do this by obtaining a fit between the observed and theoretical extinction curves.

The fit of the observed and theoretical extinction curves

The observed extinction curve is obtained from Whitford's extension (**2**) of the six-colour photometry of Stebbins and Whitford (**29**). Only four stars are involved and the values used are the mean of the actual measures at each wavelength but with a correction applied to the ultraviolet points as determined by Miss Divan (**30**). The theoretical curves in Fig. 2 refer to the extreme values of polarizability and since the observed stars were selected quite arbitrarily, they will correspond to some intermediate value. An intermediate extinction curve was therefore computed.

We introduce an angle in azimuth ϕ, defined as the inclination of the plane of the rotating needle to the line of sight. Then the curves given in Fig. 2 refer to $\phi=0$ and $\phi=\pi/2$ for P_{max} and P_0 respectively. The distribution function $f(\theta, \phi)$ for an arbitrary value of ϕ is easily calculated from the solid geometry:

$$f(\theta,\phi)\,d\theta=\frac{2}{\pi}\left(\frac{\sin^2\theta}{\cos^2\phi-\cos^2\theta}\right)^{1/2}d\theta. \qquad (12)$$

This general expression reduces to those given in (11) for the limiting cases $\phi=0$ and $\pi/2$.

By means of equations (7), (8) and (12), an extinction curve was computed for $\phi=30°$, corresponding to an intermediate value of polarizability. This particular value of ϕ was chosen because it was believed to give a value of polarizability roughly halfway between zero and maximum (see below). The curve is reproduced in Fig. 3, together with the plot of the observed extinction values, scaled down to give the best fit. The mean square error, derived from the deviations of the observations from the theoretical curve, is $\pm 0{\cdot}02$ magnitude, which represents an excellent agreement. The fit of the scales of abscissae gives

$$\rho'=1{\cdot}05/\lambda, \qquad (13)$$

where λ is expressed in microns.

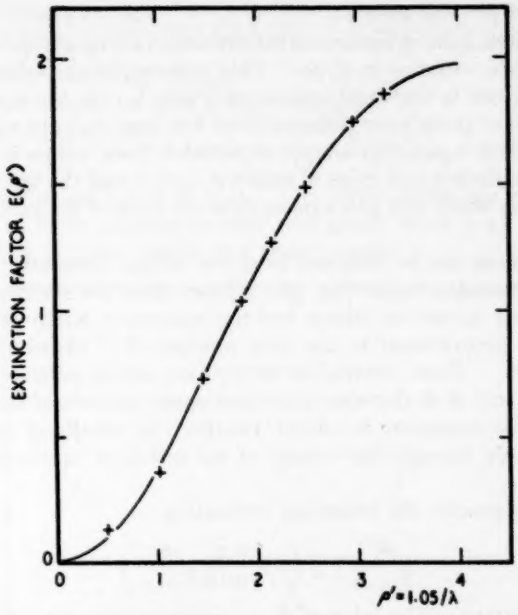

FIG. 3.—*The fit of the extinction measures of Stebbins and Whitford with the theoretical curve computed for an intermediate value of polarizability according to the Davis–Greenstein mechanism.*

Having now established the $1/\lambda$ scale of the theoretical extinction curves given in Figs. 2 and 3 for $\phi = 0°$, $30°$ and $90°$, we can proceed to read off the numerical values on which the subsequent conclusions are based. All the quantities used. are obtained from the extinction factors corresponding to the effective wavelengths of the *U*, *B*, *V*, system (**31**), and are assembled in Table I.

TABLE I

ϕ	$\frac{p}{E_{(B-V)}}$	$E_{(B-V)}$	$\frac{E_{(U-B)}}{E_{(B-V)}}$	$\frac{A_V}{E_{(B-V)}}$
0°	0·18	1·0	0·78	3·4
30°	(0·1)	1·4	0·76	2·9
90°	0·00	1·7	1·02	2·1

The curve for $\phi = 30°$ corresponds to some intermediate value of $p/E_{(B-V)}$ which cannot be calculated. However, since the magnetic field lies along a spiral arm, ϕ is simply the complement of the angle between the line of sight and the axis of the arm. Using the spiral structure of the Galaxy as determined by Morgan *et al.* (**32**), then $\phi = 30°$ corresponds to galactic longitudes at about 80° and 140°. For these longitudes, Hiltner's measures (**13**) give an average value of $p/E_{(B-V)}$ of about 0·1, and this value has been entered in brackets in the table.

The last three columns of Table I give certain quantities which can be seen to vary with polarizability. We will deal with each of these quantities in turn, but first it should be pointed out that their values, being ratios, are not particularly sensitive to errors in the scale factor (1·05) which itself depends on the choice of $\phi(30°)$ in the theoretical curve being matched.

The colour excess per unit mass

One of the most striking features of the extinction curves computed for different values of ϕ, is their variation in slope. This is shown by the values of the colour excess $E_{(B-V)}$, given in the third column of Table I. As the scale is arbitrary, the value for $\phi = 0°$ (maximum polarizability) has been reduced to unity. Since we are dealing with a common sample of particles, these values are proportional to the colour excess per unit mass of material, and to test the figures, we require some observation which will give a measure of the mass of the particles in the line of sight.

Such a measure can be obtained from the diffuse interstellar lines (**33**, **34**) or the broad interstellar bands (**35**, **36**). Since these are shallow, they will not be subject to any saturation effects and the equivalent width W of any single feature will be proportional to the total number of " absorbing centres " in the line of sight. These interstellar features are almost certainly produced by the dust grains and W is therefore a proportionate measure of the total mass of the grains. This statement is correct whether the absorbing centres are distributed uniformly through the volume of the grains or confined to a " skin " at their surfaces.

We can now predict the following correlation:—

$$\frac{W}{E_{(B-V)}} = C\left(1 + \frac{0{\cdot}7}{0{\cdot}18}\frac{p}{E_{(B-V)}}\right) \qquad (14)$$

where C is a constant. The value of $E_{(B-V)}$ given in Table I for the intermediate case shows that there is no gross departure from linearity, and the relation has therefore been expressed in a linear form.

This prediction can be tested by existing observations and the results are displayed in Fig. 4. The values of W are the sum of the equivalent widths of the two strongest diffuse lines ($\lambda 6284 + \lambda 5780$) as measured by Merrill *et al.* (**37**). All stars were used for which polarization measures were available except a few whose measures were given very low weight by the authors. Polarization measures were taken mostly from Hiltner's catalogue (**13**) supplemented by some by Hall and Mikesell (**10**). Where no U, B, V colours were available, the C_1 colours of Stebbins, Huffer and Whitford (**38**) were used and converted to the U, B, V system by means of the transform given by Morgan *et al.* (**39**). All stars occur in low galactic latitudes between $\pm 7°$.

The scatter of the points in Fig. 4 is due to two causes. First, a random scatter due to errors of measurement and, secondly, a systematic scatter due to any large-scale depolarization, e.g. when the axes of polarized clouds are " crossed " in the line of sight. In this latter case, the observed polarization will be reduced but all other parameters will correspond to high polarization; the result will be to move the points horizontally from right to left in the diagram.

The plot of the observations in Fig. 4 shows the correlation predicted by equation (14). The scatter of the points is of the order expected due to errors of measurement with two exceptions, which are marked by crosses in the diagram. These points lie well above the general scatter shown by the others. Their measured polarizations are rather low although the stars occur in a region of the sky (near Perseus) associated with heavy polarization. It therefore seems very possible that these points are affected by large-scale depolarization. Neglecting these two points, the line of best fit is given by

$$\frac{W(6284+5780)}{E_{(B-V)}} = (1{\cdot}1 \pm 0{\cdot}1)\left(1 + \frac{1{\cdot}0 \pm 0{\cdot}2}{0{\cdot}18}\frac{p}{E_{(B-V)}}\right), \qquad (15)$$

and the correlation coefficient is 0·58.

For all observations, the line of best fit is given by

$$\frac{W(6284+5780)}{E_{(B-V)}} = (1{\cdot}2 \pm 0{\cdot}1)\left(1 + \frac{0{\cdot}8 \pm 0{\cdot}2}{0{\cdot}18}\frac{p}{E_{(B-V)}}\right), \qquad (16)$$

and the correlation coefficient is 0·49. The errors given are standard errors. A comparison of these expressions with that given above (14) shows that the predicted relation is borne out by the observations.

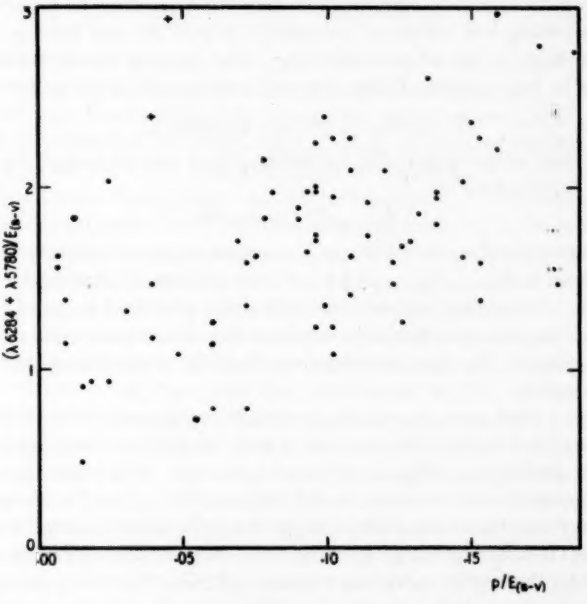

FIG. 4.—*The plot of the strength of the interstellar diffuse lines per unit colour excess against the polarizability. The correlation is as predicted by equation* (14) *in the text.*

The same effect should be shown by measures of the broad interstellar bands. Several observations of the strongest of these, at λ4430, are available (**35**, **40**, **41**, **42**) and a plot similar to Fig. 4 was constructed, but the scatter of the points was so large as to mask completely the predicted correlation, if this existed. This is caused by the very high inaccuracy involved in the measurement of such a broad shallow feature by "conventional" means. It will be necessary to obtain more accurate measures of the λ4430 band by the kind of technique developed at Edinburgh (**43**, **44**) before the predicted relation can be tested in this case.

The ratio of ultraviolet to visual colour excess

The fourth column of Table I gives the ratio of colour excesses $E_{(U-B)}/E_{(B-V)}$, which is essentially a measure of the shape of the extinction curve over the range of wave-length covered by the *U*, *B*, *V* system. The values indicate that the ratio is constant for high and medium values of polarizability and shows a sharp increase by about 30 per cent as the polarizability approaches zero.

This prediction cannot be tested directly with observation since, with wide-band photometry, the observed ratio $E_{(U-B)}/E_{(B-V)}$ depends on the amount of reddening and the shape of the extinction curve (**45**). However, the result explains the effect discovered by Hiltner and Johnson (**46**) who found that the law of reddening (over the *U*, *B*, *V* wave-length range) was different for the Great Rift in Cygnus as compared with the rest of the sky. They suggest that this may be due to a difference in particle size in this region, perhaps caused by the large density of O stars, but the result follows naturally from the present treatment.

Hiltner and Johnson confine their attention to O stars and their division of the stars according to region is essentially a division according to polarization, the Cygnus stars having low values of polarizability and the rest having, in general, moderate and high values of polarizability. For most of the sky, and therefore for moderate to high polarizability, the reddening path is given by

$$E_{(U-B)}/E_{(B-V)}=0{\cdot}72+0{\cdot}05E_{(B-V)}. \tag{17}$$

For Cygnus, their observations did not indicate any curvature and the reddening path can be represented by

$$E_{(U-B)}/E_{(B-V)}=0{\cdot}86. \tag{18}$$

To compare with the predicted result, we ignore the curvature term, and this gives an increase in $E_{(U-B)}/E_{(B-V)}$ of 20 per cent in Cygnus as compared with the rest of the sky. This is appreciably lower than the predicted value of 30 per cent, but this refers to zero polarizability whereas the observation refers to a higher value (about 0·03). We can therefore say that the observations are consistent with the prediction.

To test this a little more rigorously, a similar treatment to that of Hiltner and Johnson was carried out by dividing the O stars in Hiltner's catalogue (**13**) into two groups according to $p/E_{(B-V)}>0{\cdot}09$ and $<0{\cdot}03$. The resulting reddening paths were essentially the same as given by equations (17) and (18) respectively, but in the latter case there was a slight suggestion of a small amount of curvature. This agreement is not surprising, since the difference between the reddening paths is established by the highly reddened O stars and these, for low polarizability, lie exclusively in the Great Rift. Strictly speaking, therefore, it is not possible from these results alone, to decide whether the variation in reddening path is a regional effect or due to a variation in polarizability. This is not the case, however, with the previous prediction, expressed by the correlation shown in Fig. 4, which would still exist if the Great Rift stars were removed. Taking into account the observational support for both predictions it is reasonable to say that the analysis presented here, based on the Davis–Greenstein alignment mechanism, is confirmed.

The ratio of total to selective extinction

The determination of the ratio *R* of total to selective extinction is of fundamental importance. Its value, on the *U*, *B*, *V* system, is tabulated in Table I for the three theoretical extinction curves corresponding to different values of polarizability, and there is obviously a considerable variation.

Hitherto, it has been generally accepted that *R* is constant with a value 3·0. The reason for this is apparent from the previous subsection. Attempts to detect a variation in the law of extinction have been confined to a limited range of

wave-length in the visible and ultra-violet, where the shape of the extinction curve varies little except at very small values of polarizability. It was thought for a while that the law of reddening and therefore R, was different for the trapezium stars in Orion (**29**) but this has been proved incorrect by Miss Divan (**47**). It is apparent that any further work in this direction must cover the whole range of accessible wave-length.

The values of R read from the theoretical curves indicate a variation with polarizability which, to a first approximation, we can take to be linear. The values are consistent with the following expression

$$R = \frac{A_v}{E_{(B-V)}} = 2{\cdot}1(1 + 3{\cdot}4p/E_{(B-V)}). \qquad (19)$$

This expression can be used to calculate R for individual stars or for different regions of the sky according to the average value of $p/E_{(B-V)}$.

The variation in R is considerable. For a fixed colour excess, say $E_{(B-V)} = +1{\cdot}0$, the total visual extinction will differ by 1·3 magnitudes over the whole range of polarizability (0·00 to 0·18). Regions of low polarizability are more transparent per unit colour excess than regions of high polarizability. Previously, therefore, stars with low polarizability will have had their distance moduli underestimated and/or their intrinsic luminosities overestimated. As an example let us take the heavily obscured O-association VI Cygni, which has been observed by Johnson and Morgan (**48**) who determine the distance modulus to be 10·9 mag. Star No. 12 in this association is the most heavily reddened star yet observed (**49**) and Sharpless (**50**) finds it to be superluminous with an absolute magnitude $M_v = -9{\cdot}5$. Hiltner has measured the polarization of five of the stars in the association and for the average of these, equation (19) gives $R = 2{\cdot}3$. Reworking the above material with this value of R instead of 3·0 gives the distance modulus to be 12·1 mag. instead of 10·9 mag., and the absolute magnitude of No. 12 to be $-8{\cdot}3$ instead of $-9{\cdot}5$. The total obscuration of No. 12 is reduced from 10·1 mag. to 7·7 mag. but the effect on M_v is partially counteracted by the increase in distance modulus. This star had hitherto been thought to be the most luminous known in our own Galaxy and is listed as such by Sandage (**51**) in his paper on the extragalactic distance scale.

5. *Conclusions.*—By means of an approximate solution (given in Section 2) of the problem of scattering by a long dielectric cylinder, with axis inclined at an arbitrary angle to the line of sight, extinction curves are computed (in Section 3) for a system of particles with different angular distributions. The angular distributions were determined according to the two existing theories of polarization and in each case it is shown that the observed extinction curve should vary appreciably with polarizability. Predictions are then made and tested against observation (in Section 4) which strongly support the distribution predicted by the Davis–Greenstein theory. The predictions based on the Spitzer–Tukey theory are the inverse of what is observed, but before discarding this theory it should first be asked whether the writer's interpretation of it in determining the angular distribution functions (Section 3) is the only one possible. This interpretation is that the magnetic lines of force are perpendicular to the galactic plane and that the regions of low polarization (e.g. Cygnus) are caused by some depolarization effect. There is only one other galactic magnetic field configuration which would explain the observations on the basis of the Spitzer–Tukey theory

and this is one in which the magnetic lines of force are constrained to lie in a plane perpendicular to the axis of a spiral arm, but are considerably distorted within this plane to give the impression of randomness when looking through it. Then since the long axes of the particles are aligned along the magnetic lines of force, the angular distribution functions become the same as that predicted (unambiguously) by the Davis–Greenstein theory. However, the degree of alignment is much less than assumed by Spitzer and Tukey and consequently a higher field strength than they obtain (10^{-4} gauss) would be necessary to explain the observed degree of polarization. Further, the distortions in the magnetic lines of force necessarily mean a weak field strength, certainly much lower than that (10^{-5} gauss) determined by Chandrasekhar and Fermi (**18**) on the basis of the distortions along the spiral arms. It would therefore seem that this type of configuration is quite untenable and that the only configuration which, on the basis of the Spitzer–Tukey theory, will explain the observed degree of polarization is that adopted above.

We can therefore say that this investigation shows an angular distribution of the axes of the interstellar dust grains as predicted by the Davis–Greenstein alignment mechanism and therefore offers strong confirmation of that theory, and, by inference, of the existence of a galactic magnetic field whose lines of force lie along the axes of the spiral arms. As pointed out in Section 1, this is the type of field configuration expected theoretically.

An important corollary of this investigation is that the ratio R of total to selective extinction is a function of the polarizability $p/E_{(B-V)}$ as expressed by equation (19). This is a new and important result.

The observational tests applied in Section 4 depend on the differences between the theoretical extinction curves for different values of polarizability (reproduced in Figs. 2 and 3). A more profitable and direct approach would be the measurement of extinction curves for different polarizations. This would need to be done for the whole range of accessible wave-length in the manner of Whitford's curve (**2**) and it is strongly urged that this be done for a group of stars of low polarizability in the Great Rift and a group with high polarizability near galactic longitude 100° with, perhaps, another group of intermediate polarizability. The values of R read from these curves should vary by about 60 per cent and will give a better and empirical determination of the constants in equation (19).

Any analysis of these curves to determine particle size etc. should be confined to the case of low polarizability, since this corresponds to the case of incidence perpendicular to the cylinder axis, for which rigorous computations are available. It is interesting to note that the effective diameter of the needles will be somewhat smaller than that derived earlier (about $0{\cdot}5\,\mu$ as compared to $0{\cdot}8\,\mu$).

Acknowledgments.—The basis of this work was carried out during the writer's tenure of a National Research Council (Ottowa) Fellowship at the Dominion Astrophysical Observatory, Victoria, Canada, while on leave of absence from the Royal Observatory, Edinburgh. He would like to record his deep appreciation to Dr R. M. Petrie, Dr A. McKellar and all other members of the Victoria staff for their constant advice and encouragement through all stages of the work.

C.T.R. Division,
Atomic Energy Research Establishment,
Harwell:
1959 *April* 28.

References

(1) H. C. van de Hulst, *Recherches Astron. Obs. d'Utrecht*, **11**, part 1, 1946; part 2, 1949.
(2) A. E. Whitford, *Ap. J.*, **107**, 102, 1948.
(3) A. Güttler, *Zs. f. Astrophys.*, **31**, 1, 1952.
(4) C. Schalén, *Uppsala Medd.*, No. 64, 1936.
(5) C. Schalén, *Uppsala Ann.*, **1**, No. 2, 1939.
(6) L. G. Henyey and J. L. Greenstein, *Ap. J.*, **93**, 70, 1941.
(7) H. C. van de Hulst, *Liège Symposium*, " *Les Particules Solides dans les Astres* "; *Mém. Soc. Roy. Sci. Liège, Série* 4, **15**, 393, 1955.
(8) L. S. Hall, *Science*, **109**, 166, 1949.
(9) W. A. Hiltner, *Science*, **109**, 165, 1949; *Nature*, **163**, 283, 1949.
(10) J. S. Hall and A. H. Mikesell, *Pub. U.S. Naval Obs.*, **17**, part 1, 1950.
(11) W. A. Hiltner, *Ap. J.*, **114**, 241, 1951.
(12) W. A. Hiltner, *Ap. J.*, **120**, 454, 1954.
(13) W. A. Hiltner, *Ap. J. Supp.*, **2**, 389, 1956.
(14) T. Gold, *M.N.*, **112**, 215, 1952.
(15) L. Davis, Jr., *Vistas in Astronomy*, **1**, 336, 1955.
(16) L. Spitzer, Jr., and J. W. Tukey, *Ap. J.*, **114**, 187, 1951.
(17) L. Davis, Jr. and J. L. Greenstein, *Ap. J.*, **114**, 206, 1951.
(18) S. Chandrasekhar and E. Fermi, *Ap. J.*, **118**, 113, 1953.
(19) G. Mie, *Ann. d. Phys.*, **25**, 377, 1908.
(20) R. Gans, *Ann. d. Phys.*, **37**, 881, 1912.
(21) H. C. van de Hulst, *Light Scattering by Small Particles*, chap. 15, John Wiley & Sons, N.Y., 1957.
(22) H. C. van de Hulst, *Ap. J.*, **112**, 1, 1950.
(23) H. C. van de Hulst, *op. cit.*, chap. 11, 1957.
(24) E. Jahnke and F. Emde, *Tables of Functions*, Dover Pub., N.Y., 1945.
(25) J. H. Oort and H. C. van de Hulst, *B.A.N.*, **10**, 187, 1946.
(26) H. C. van de Hulst, *Recherches Astron. Obs. d'Utrecht*, **11**, part 2, Table 10, 1949.
(27) F. D. Kahn, *M.N.*, **112**, 518, 1952.
(28) W. A. Hiltner, *Ap. J.*, **109**, 471, 1949.
(29) J. Stebbins and A. E. Whitford, *Ap. J.*, **102**, 318, 1945.
(30) Lucienne Divan, *Ann. d'Astrophys.*, **17**, 456, 1954.
(31) H. L. Johnson, *Ann. d'Astrophys.*, **18**, 292, 1955.
(32) W. W. Morgan, A. E. Whitford and A. D. Code, *Ap. J.*, **118**, 318, 1953.
(33) P. W. Merrill, *P.A.S.P.*, **46**, 206, 1934.
(34) P. W. Merrill, *Ap. J.*, **83**, 126, 1936.
(35) C. S. Beals and S. H. Blanchet, *M.N.*, **98**, 398, 1938.
(36) R. Wilson, *Ap. J.*, **128**, 57, 1958.
(37) P. W. Merrill, R. F. Sanford, O. C. Wilson and Cora G. Burwell, *Ap. J.*, **86**, 274, 1937.
(38) J. Stebbins, C. M. Huffer and A. E. Whitford, *Ap. J.*, **91**, 20, 1940.
(39) W. W. Morgan, D. L. Harris and H. L. Johnson, *Ap. J.*, **118**, 92, 1953.
(40) J. L. Greenstein and L. H. Aller, *Ap. J.*, **111**, 328, 1950.
(41) D. Duke, *Ap. J.*, **113**, 100, 1951.
(42) Anne B. Underhill, *Pub. Dom. Ap. Obs.*, **10**, 201, 1956.
(43) E. A. Baker, *Pub. Royal Obs. Edinburgh*, **1**, 15, 1949.
(44) W. M. H. Greaves, E. A. Baker and R. Wilson, *Pub. Royal Obs. Edinburgh*, **1**, 115, 1955.
(45) V. M. Blanco, *Ap. J.*, **123**, 64, 1956.
(46) W. A. Hiltner and H. L. Johnson, *Ap. J.*, **124**, 367, 1956.
(47) Lucienne Divan, " *Les Particules Solides dans les Astres* "; *Mém. Soc. Roy. Sci. Liège, Série* 4, **15**, 538, 1955.
(48) H. L. Johnson and W. W. Morgan, *Ap. J.*, **119**, 344, 1954.
(49) W. W. Morgan, H. L. Johnson and Nancy G. Roman, *P.A.S.P.*, **66**, 85, 1954.
(50) S. Sharpless, *P.A.S.P.*, **69**, 239, 1957.
(51) A. Sandage, *Ap. J.*, **127**, 513, 1958.

47 TUCANAE: THE MEMBERSHIP OF TWO RR LYRAE VARIABLES

M. W. Feast, A. D. Thackeray and A. J. Wesselink

(Received 1959 May 25)

Summary

Harvard variables 810, 814 are shown to be the first known RR Lyr variables belonging to the globular cluster 47 Tuc. Their periods are long for their Bailey types. Their radial velocities do not differ significantly from that of 47 Tuc. Their spectra show only a moderate degree of metal weakness.

1. The two Harvard variables HV 810, 814 in the neighbourhood of the globular cluster 47 Tucanae were discovered by Miss Leavitt (**1**) in her survey of variables in the Small Magellanic Cloud. Mrs Nail (**2**), who gives coordinates of the variables relative to the centre of 47 Tuc, found that their periods were short without deriving actual periods; she pointed out that if they were members of the globular cluster and of RR Lyr type then they were too bright by 3/4 magnitude compared with Shapley's distance modulus of 14·72 for 47 Tuc (**3**). It was suggested that they might be foreground W UMa variables.

This paper is concerned with establishing the character of the light variations and with the question whether the variables are in fact members of the globular cluster. These two questions have assumed importance since Radcliffe work (**4**) has suggested that Shapley's distance modulus has been considerably overestimated.

Light-curves and periods

2. HV 810. This star lies only 2′·2 from the centre of 47 Tuc and is therefore unsuitable for accurate photoelectric photometry. Photographs were obtained at the Newtonian focus of the Radcliffe reflector during short spells between July and September 1957. These observations were supplemented by visual estimates of brightness made by all three authors at the Cassegrain focus (while working either photoelectrically or spectroscopically on 47 Tuc). These visual observations covered periods of bright Moon and were useful in bridging the gap between the photographic series.

Step-estimates of brightness from the photographs are listed in Table I (which includes also step-estimates of HV 814). The visual estimates, on an entirely different scale from the photographic series, are listed in Table II.

It was soon established that maxima occurred at intervals very slightly less than 3 days. The true period was found to be one quarter of this interval. Since this is a rather unusual period the photographic and visual estimates (from the 1957 season only) are plotted in Fig. 1 against a period of $2^d{\cdot}946$. It will be seen that three equally spaced maxima are present, one of which is represented only by visual estimates, the fourth maximum having been missed. On four occasions the variable was observed during the rise to maximum. There is clearly no possibility of more than four maxima occurring during the interval of $2^d{\cdot}946$.

All photographic observations are assembled on a period of $0^d{\cdot}73652$ in Fig. 2, in which crosses represent additional estimates made on photographs taken in the years 1948, 1954 and 1958.

TABLE I

Photographic estimates of HV 810 *and* 814

Plate	JD 2430000 +	HV 810 Est.	HV 810 Phase	HV 814 Est.	HV 814 Phase
A 202	2859·466	5	0·41		
203	2859·480	5+	0·43		
217	2888·287	9	0·54		
226	2908·263	9+	0·66		
228	2908·303	8	0·72		
2472	4952·644	4:	0·40		
2594	4986·425	2+	0·27		
3181	6047·517	9	0·96	7+	0·91
3182	6047·531	8	0·98	7+	0·95
3183	6047·547	5+	0·00	7	0·99
3185	6047·583	0	0·04	8	0·09
3187	6047·644	−1	0·13	5	0·25
3188	6047·658	−0+	0·15	5+	0·29
3189	6048·594	5	0·42	5	0·81
3190	6077·552	8+:	0·74		
3191	6107·446	3	0·32	5	0·26
3192	6107·457	3	0·34	4	0·29
3193	6107·482	4	0·37	5	0·36
3194	6107·494	4	0·39	3	0·39
3196	6131·260	9	0·66	5	0·38
3201	6133·340	7+:	0·48	8	0·98
3214	6136·244	5	0·42	6	0·79
3216	6163·228	−1+:	0·06		
3382	6372·656	5	0·41		

Phases Ph computed from formulae:
HV 810 Ph = 1·35774 (JD − 2430000)
HV 814 Ph = 2·69233 (JD − 2430000)

TABLE II

HV 810: *visual estimates*

JD 2430000 +	Est.	Phase
6037·62	5	0·52
6038·50	5:	0·71
6038·65	5+	0·92
6043·50	5	0·50
6043·65	5+	0·70
6050·61	2	0·16
6052·54	5:	0·78
6053·50	0+	0·08
6058·46	5+	0·81
6058·62	2	0·03
6061·45	5+	0·87
6061·59	1	0·06
6067·44	5+	0·01
6067·55	1	0·16
6067·66	>1	0·30
6069·59	5	0·92

Phase Ph computed from
Ph = 1·35774 (JD − 2430000)

The light-curve with rapid rise to maximum clearly marks the variable as an RR Lyr of Bailey *a*-type. The amplitude appears to be about twice that of HV 814, on the basis of step-estimates. Knowing the amplitude of HV 814 (see

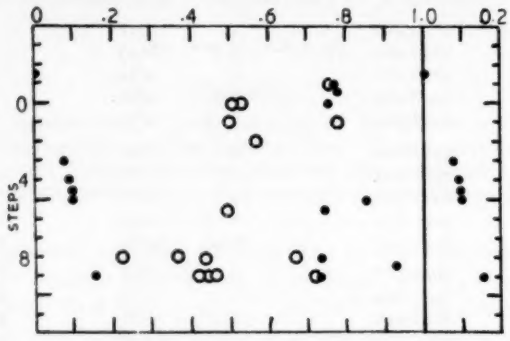

FIG. 1.—*Light-curve of* HV 810 *assembled on period* $2^{d}\cdot946$.
● *photographic series* (1957).
○ *eye estimates at Cassegrain focus, on adjusted scale.*

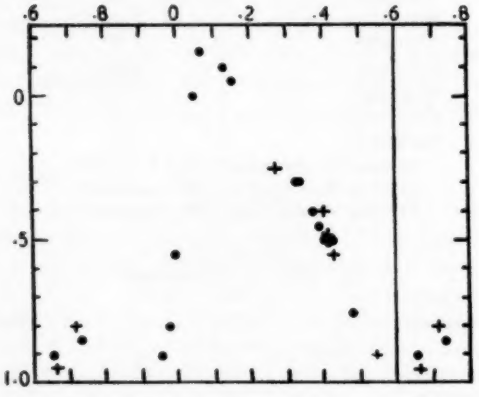

FIG. 2.—*Light curve of* HV 810 (*photographic*).
● 1957
+ 1948, 1954, 1958.

below) and that the median magnitudes of the two variables are about the same (**2**) we find for HV 810 approximately

$$B_{max} = 13\cdot6$$

$$B_{min} = 14\cdot7$$

and for the ephemeris for maxima

$$JD = 2436163\cdot240 + 0\cdot73652E$$

$$M - m = 0\cdot10P$$

3. HV 814. Long series of photoelectric observations of HV 814 were made on several nights at the Cassegrain focus of the Radcliffe reflector. HD 2466 and 2505 were used as comparison stars. The magnitudes determined depend on the

calibration of the integrating photometer of the Radcliffe Observatory. The individual observations, converted to the Johnson *B V* system are listed in Table III.

The period was found by combining the photoelectric data of Table III with the photographic data of Table I; it is to be noted that a long photographic series in Table I, covering a minimum, is available on the night following a long series of photoelectric observations, covering a maximum.

TABLE III

HV 814: *photoelectric observations*

JD 2430000+	*V*	*B*	Phase
6019·574	13·86	14·10	0·68
599	13·98	14·26	0·75
613	13·93	14·30	0·78
636	14·07	14·36	0·85
652	14·14	14·48	0·89
6026·562	13·68	13·88	0·49
577	13·78	13·99	0·53
588	13·71	13·95	0·56
593	13·74	13·99	0·58
609	13·78	14·07	0·62
622	13·88	14·10	0·66
630	13·94		0·68
646	13·88		0·72
6041·535	13·91	14·28	0·81
566	14·02	14·31	0·89
582	14·08	14·41	0·93
652	14·12		0·12
6046·510	13·88	14·26	0·20
532	13·77	14·02	0·26
546	13·80	14·09	0·30
567	13·86	14·09	0·35
581	13·72	13·97	0·39
590	13·73	13·94	0·42
606	13·67	13·91	0·46
619	13·70	13·92	0·49
640	13·75	14·03	0·55
6071·518	13·74	13·93	0·53
6082·448	14·06	14·44	0·96
6109·330	13·90	14·11	0·33
6109·367	13·75	13·97	0·43
382	13·71	13·90	0·47
402	13·66	13·89	0·53
417	13·71	13·89	0·57
422	13·72	13·94	0·58
442	13·76	14·02	0·63
452	13·83	14·08	0·66
462	13·88	14·13	0·69

Phase Ph computed from Ph = 2·69233 (JD − 2430000)

The photoelectric observations alone, in B and V, are plotted in Fig. 3 against phase using a period $0^d.37143$.

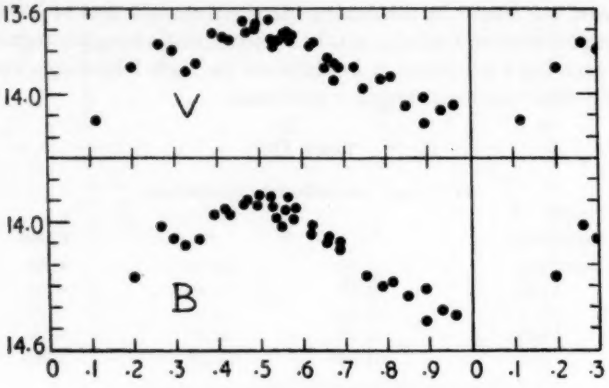

FIG. 3.—*Light curve of* HV 814 (*photoelectric*).

For maximum light we find the ephemeris

$$JD = 2436046.614 + 0.37143E$$

and for the characteristics of the light-curves

	V	B	$B-V$
maximum	13.67	13.89	+0.22
minimum	14.14	14.45	+0.31
median	13.90	14.17	+0.27
range	0.47	0.56	0.09

The period, light-curve and colour establish HV 814 as an RR Lyr variable of Bailey *c*-type. The light curve is nearly sinusoidal; the interval from mid-rise to mid-fall is $0.5P$. The colour rules out the possibility of the variable being of W UMa type. Correction of the observed mean colour (+0.27) by 0.05 appropriate to the galactic latitude (**5**) implies an intrinsic mean colour of +0.22. This lies within the range of colour indices, 0.17 to 0.23, given by Sandage (**6**) for *c*-type variables, but is much bluer than that found for W UMa variables. Moreover, if the observations are assembled on double our period (i.e. $0^d.74286$) alternate maxima and minima show no significant difference.

Spectra

4. *Radial velocities.*—Two spectra of HV 810 and one of HV 814 were obtained with the Cassegrain spectrograph at 86 A/mm at Hγ. The projected slit-width corresponded to 160 km/s at Hγ.

The measured radial velocities, reduced to the Sun, are shown in the accompanying table together with the phases covered by the necessarily long exposures (computed maximum at phase 0.0).

Star	Plate	R.V. km/s	Phase of exposure Beg.	Mid.	End	Exposure: fraction of period
810	Cd3424	−37	0.93	0.08	0.23	0.30
810	Cd3488	− 8	0.11	0.21	0.32	0.22
814	Cd3452	+121	0.13	0.49	0.85	0.72

The number of RR Lyr velocity curves that have been studied in detail is very small and it is not known with any certainty how the velocity curves vary from one star to another. Nor is a mean curve known with any definiteness. However, if we apply the curve given by Mrs C. Payne Gaposchkin (7) for *a*-type variables to HV 810, with integration over about one third of the period, we may expect that for Cd 3424 the measured velocity will be about 20 km/s negative with respect to the γ velocity; for Cd 3488 the measured velocity should not be far from the γ velocity. We derive velocities of -17 and -8 km/s from the two plates. In view of the inaccuracies of measurement and of the corrections for phase, there is no significant departure from the mean velocity of 47 Tuc itself*.

In the case of HV 814, the one spectrum integrates over a large fraction of the period centred on minimum. A velocity curve for a *c*-type variable is given by Tifft and Smith (9). From this we would expect that the measured velocity on Cd 3452 would be positive with respect to the γ velocity by perhaps 10 or 15 km/s. Applying such a correction we find a γ velocity of HV 814 of zero or slightly negative. Again we cannot regard the departure from the velocity of 47 Tuc as significant.

5. *Spectral types.*—The spectral types of both stars appear normal for RR Lyr variables. No work appears to have been published previously on spectra of RR Lyr stars in clusters. The main characteristics of field RR Lyr's brought out in several investigations is that the H lines and the metal lines yield different spectral types, judging by their absolute intensities, the metal types being earlier. This is also found in HV 810, 814. Compared with MK standards of luminosity class III we find:

	H lines	Metals	Phase mid-exp.
HV 810			
Cd 3424	Fo	A5	0·08
Cd 3488	Fo–F2	A5–A7	0·21
HV 814			
Cd 3452	F5–F6	Fo	0·49

This agrees satisfactorily with other work, e.g. Tifft and Smith (9), Munch and Terrazas (10), Preston (11).

The spectral types support the light curves in the conclusion that the stars are cluster type variables.

Membership of 47 Tucanae

6. *Distribution of field variables.*—Of the 1500 variables in the Harvard Small Magellanic Cloud field, 8 are known to be RR Lyr variables in the Galaxy (2). This corresponds to 0·32 per square degree. Mrs Nail (12) also studied fields totalling 400 square degrees at the same galactic latitude as the SMC and found an average of 0·27 RR Lyr's per square degree to the plate limit (about 16m).

The distances of HV 810 and 814 from the centre of 47 Tuc are 2·2 and 21·6 minutes of arc respectively, both within the Harvard adopted radius of 26′·8 for the cluster.

From the quoted densities of field RR Lyr's we predict 0·19 such variables down to 16 m within a circle of radius of 26′·8 or 0·04 down to $14^{m}\cdot0$. We find two RR Lyr variables at 14·0 m within such a circle, or 50 times as many as predicted. Of the 8 RR Lyr variables in the SMC field none is as bright as 14·0

* Kinman (8) has given a value of -24 km/sec from integrated spectra of the cluster. A detailed account of velocity measurements in 47 Tuc will be published shortly. A preliminary velocity of about -15 km/sec has been derived, based on measures of 16 spectra of individual stars at 48 A/mm.

(median mag.) and 5 are a magnitude fainter. Despite the fact that the region of 47 Tuc has probably been searched more completely than others for variables, the above considerations make it highly probable that HV 810 and 814 actually belong to the cluster.

7. *The radial velocities.*—The rather meagre data available concerning radial velocities of HV 810 and 814 suggest that they agree with the velocity of 47 Tuc within about 10 km/s. The velocity of 47 Tuc differs by −120 km/s from the most probable value for a globular cluster at that distance from the solar apex. The probability of a residual between −100 and −140 km/s for one cluster may be assessed at about 0·08. The probability of finding two RR Lyr variables with such a residual is then about $(0{\cdot}08)^2$, since Kinman (**13**) finds no essential difference between the kinematic properties of globular clusters and RR Lyr variables with the same periods as those in the clusters. Even the rough agreement in velocity for a Population II object in this part of the sky therefore adds great force to the argument in favour of cluster membership.

8. *The spectral types and periods.*—It has long been known that globular clusters tend to fall into two groups according to the mean periods of the RR Lyr variables of types *ab* and *c* (**14**). Recently Arp (**15**) has suggested that the long period group is characterized by extreme metal weakness in their spectra (e.g. M 92) while the short period group has more normal metal composition. The evidence for this rests on rather few clusters and the empirical rule is violated by 47 Tuc if HV 810, 814 are members. The two variables have abnormally long periods for their Bailey types; and it is known that the spectra of the giants in 47 Tuc are not extremely metal-weak (**4**). However, 47 Tuc is the only globular cluster known to contain M stars and must be regarded as an abnormal cluster.

Recently Preston (**11**) has investigated the spectra of a considerable number of RR Lyr variables in the general field.

The difference ΔS between the spectral types based on the hydrogen and metal lines is taken as an index of metal weakness. Preston shows that there is a relation between ΔS and period, with a fairly large scatter. Generally stars with large ΔS have long periods (apart from an abnormal group of stars with periods greater than 0·75 days).

If it is assumed that our spectral types for HV 810, 814 are in the same system as Preston's we find a value of $\Delta S = 5$ for both stars. If the two variables are then entered on Preston's plot of ΔS against period (his Fig. 4) they fall in a region relatively scarce in variables. Most variables with these periods have great metal weakness.

We can draw two conclusions: (1) the chance of finding RR Lyr variables with these properties in the general field is small, (2) the fact that we do not find extreme metal weakness in the variables agrees qualitatively with our previous findings for the giants in 47 Tuc (**4**) and adds further support in favour of cluster membership.

Summing up, HV 810 and 814 are established as RR Lyr variables of Bailey *a* and *c* types respectively, with periods long for their Bailey types, but without extreme metal weakness. Considerations of distribution of field variables, radial velocities and of spectral types combine to give conclusive evidence that the two variables belong to 47 Tucanae.

Acknowledgments.—We should like to express our sincere thanks to Dr G. W. Preston (Lick) and Dr T. D. Kinman (Pretoria) for allowing us to see their papers in manuscript.

Radcliffe Observatory,
Pretoria:
1959 *April.*

References

(1) Miss H. S. Leavitt, *H.A.*, **60**, 87, 1907.
(2) Mrs V. McKibben Nail, *H.B.*, 920, 15, 1951.
(3) H. Shapley, *Proc. Nat. Acad. Sci.*, 27, 440, 1941 (H.R. 228).
(4) A. D. Thackeray, *Semaine d'Etude Populations Stellaire, Pont. Acad. Sci.* (Rome) 1957, p. 69.
(5) M. W. Feast, A. D. Thackeray and A. J. Wesselink, *Obs.* **78**, 156, 1958.
(6) A. R. Sandage, *Semaine d'Etude Populations Stellaire, Pont. Acad. Sci.* (Rome), 1957, p. 41.
(7) Mrs C. Payne Gaposchkin, *Variable Stars and Galactic Structure* (London: Athlone Press, 1954), p. 27.
(8) T. D. Kinman, *M.N.*, **119**, 134, 1959.
(9) W. G. Tifft and Harlan J. Smith, *Ap. J.*, **127**, 591, 1958.
(10) G. Munch and L. R. Terrazas, *Ap. J.*, **103**, 371, 1946.
(11) G. W. Preston, *Ap. J.*, **130**, 507, 1959.
(12) Mrs. V. McKibben Nail, *H.B.*, 920, 13, 1951.
(13) T. D. Kinman, *M.N.*, **119**, 559, 1959.
(14) P. Th. Oosterhoff, *Obs.*, **62**, 104, 1939 and *B.A.N.*, **10**, 55, 1944.
(15) H. C. Arp, *A.J.*, **60**, 317, 1955.

RADIO EMISSION FROM THE CYGNUS LOOP

J. E. Baldwin and P. R. R. Leslie

(Received 1959 June 11)

Summary

Observations have been made of the Cygnus Loop using the new 178 Mc/s radio telescope at Cambridge. Good positional agreement was obtained between several of the radio and optical features but an intense extended source lying 1° south of the centre of the Loop is not correlated with any outstanding optical feature. The spectral index is −0·6 and it is suggested that, although emission from some parts of the nebula is thermal, the main component is non-thermal.

---

1. *Introduction.*—Radio emission from the Cygnus Loop was first reported by Hanbury Brown and Walsh (1955) at a frequency of 92·5 Mc/s and more recently by Westerhout (1958) and Eaton and Kraus (1959) at frequencies of 1390 Mc/s and 915 Mc/s respectively. It probably belongs to the small class of filamentary galactic nebulosities having associated non-thermal radio emission. A large number of optical studies of the Cygnus Loop have been made from which the velocity, density and electron temperature of the gas in the filaments and the distance of the nebulosity have been derived (see Minkowski 1957, 1958). Its large angular diameter of about 2°·7 is advantageous for radio measurements since these are chiefly limited by the resolving power of existing radio telescopes, and it therefore provides a particularly favourable opportunity to study the relationship between the optical and the radio emission in this class of objects.

The main series of observations described here have been made with portions of the new radio interferometer at Cambridge working at a frequency of 178 Mc/s (Ryle 1957). These observations have been supplemented with a scan across the source using the fixed portion of the large 38 Mc/s radio telescope and by earlier observations at 81·5 Mc/s and 160 Mc/s.

2. *178 Mc/s observations.*—The fixed portion of the 178 Mc/s interferometer has an extent of 1450 ft in an East–West direction by 65 ft in the North–South direction, giving beamwidths to half power points of 13′·5 arc in right ascension and 4°·6 in declination.

Recordings of the total power received by this instrument over a band width of 4 Mc/s have been made with the beam centred on declinations +28°·0, +31°·0 and +34°·0. These scans across the Cygnus Loop are shown in Fig. 1 where the right ascensions have been reduced to epoch 1950·0. The curve at δ+31°·0 is the mean of two records. Since the signal/noise ratio on the records is high, a comparison of the different records makes it possible to determine the declination of features in the source with an accuracy of about 30′ arc. The positions of the visible filaments, also in coordinates of 1950·0, are sketched in Fig. 2. We shall now discuss the relationship between the main features of the radio scans and the distribution of these filaments.

(i) The steep rise in the radio intensity at α 2043·5 (for δ = +31°) and α 2043 (for δ = +34°) corresponds very closely to the edge of the bright filaments forming the west limb of NGC 6960 at α 2043·7 close to 52 Cygni. The steep rise is most

noticeable on the recording at $\delta + 31°{\cdot}0$ where these filaments lie in the centre of the beam.

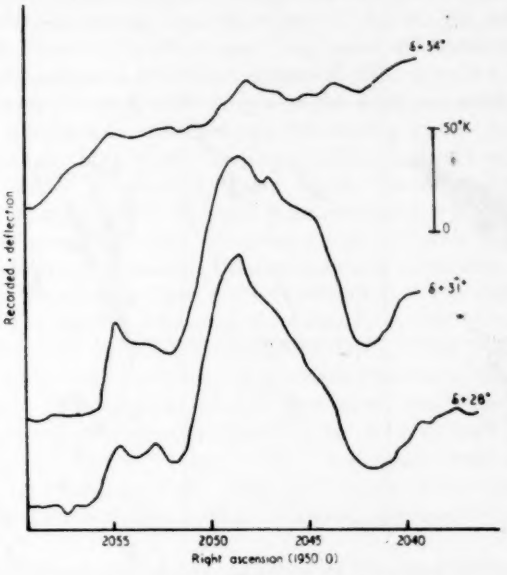

FIG. 1.—*Scans across the Cygnus Loop at 178 Mc/s.*

(ii) The main peak of radio intensity, having a half width of some $1°{\cdot}4$ in right ascension, has its peak at α 2048·5. The amplitudes of the records at $\delta + 31°{\cdot}0$ and $\delta + 28°{\cdot}0$ are nearly equal, indicating that the declination of the main peak is close to $\delta + 29°{\cdot}5$. The source must, however, have an extent northward in declination of at least 2° since it is visible, at a somewhat reduced intensity, on the record at $\delta + 34°$. The position quoted by Hanbury Brown and Walsh (1955), $\alpha\ 20^h\ 49^m\ 30^s \pm 1^m\ 30^s$, $\delta + 29°\ 50' \pm 1°$, agrees within their quoted errors with the position of the centre of this source derived from the present observations :

$$\alpha\ 20^h\ 48^m\ 30^s \pm 15^s,\ \delta + 29°\ 30' \pm 30'.$$

This position lies in the region of sky in which there are a few visible filaments but no outstanding concentration of filaments which could be associated with the radio emission.

(iii) The trough in the radio scan for $\delta + 31°$ at α 2052 corresponds to a part of the nebula showing only a very small amount of optical emission. The lack of optical emission does not appear to be due to localised obscuration.

(iv) The minor peak at α 2055·0 appears with greatest amplitude on the record at $\delta + 31°{\cdot}0$ and with reduced, but equal, amplitudes on the records at $+28°{\cdot}0$ and $+34°{\cdot}0$. The relative amplitudes on the three records indicate a source extending $1\frac{1}{2}°$–2° in declination with its centre at $\delta + 31°$. This region coincides closely with the bright arc of nebulosity NGC 6992–5 at the north following border of the Loop.

(v) The steep fall in intensity at α 2056 occurs at the outer limit of the filaments forming NGC 6992 at α 2055·5.

The steep gradients of intensity on the curve for $\delta + 31°{\cdot}0$ in Fig. 1 at right ascensions 2043·5, 2050·5, and 2056 are unresolved by the 13′·5 beam of the aerial.

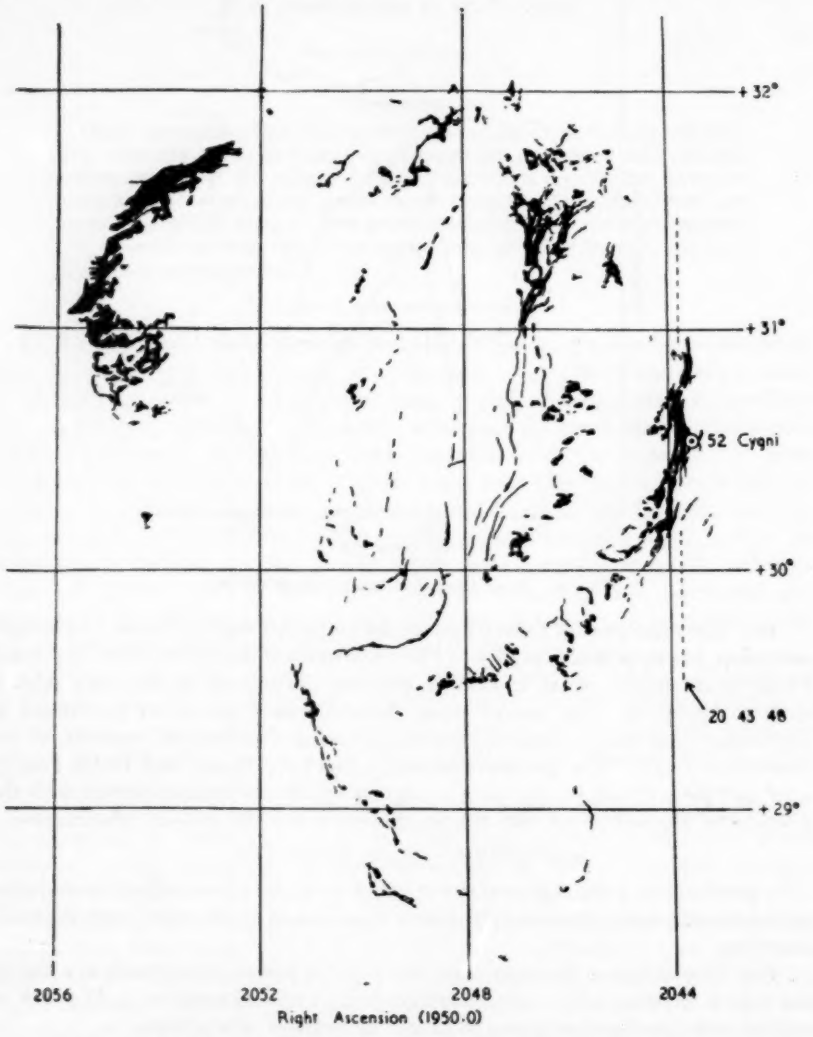

FIG. 2.—*Sketch of the Cygnus Loop in Hα.* 1950 *coordinates.*

and an interferometer of large spacing was therefore used to investigate the presence of structure having an angular size of a few minutes of arc. Observations were made using the moving aerial of the 178 Mc/s instrument in its central position to form an east–west interferometer of 465 λ spacing with the fixed portion of the telescope. These observations revealed a source lying at $\alpha\ 20^{h}\,43^{m}48^{s}$ and having a flux density of 5×10^{-26} w.m.$^{-2}$ (c/s)$^{-1}$ on the record taken at $\delta + 31°{\cdot}0$,

which was too weak to be visible on adjacent declination settings. The right ascension of the source is marked by a dotted line in Fig. 2.

This observation therefore indicates the presence of fine structure in the distribution of radio emission having an angular size $< 5'$ arc in right ascension. It is of course possible that the 'point source' is a quite unrelated object, but the coincidence in right ascension with the filaments of NGC 6960 is sufficiently good to make this unlikely; over the whole area of the Loop, no other sources were found on the interferometer record having a flux density greater than this source. The total emission from the Cygnus Loop at 178 Mc/s derived from the curves of Fig. 1 has a flux density of 430×10^{-26} w.m.$^{-2}$ (c/s)$^{-1}$ of which about 40×10^{-26} w.m.$^{-2}$ (c/s)$^{-1}$ is contributed by the small peak associated with NGC 6992–5.

3. 160 *Mc/s observations.*—The observations at 178 Mc/s did not provide an accurate value for the declination of the main source of emission in the Cygnus Loop, nor a good estimate of its extent in declination. The records taken for measurements of the angular diameters of sources in the 3C survey at 160 Mc/s were therefore examined to provide independent values. The beam width of 1°·2 in right ascension was sufficiently narrow to enable the central peak to be picked out unambiguously. The records, taken with an interferometer spacing of 27 λ on a north-south line show a source at declination $+29° 20' \pm 20'$ having a flux density of only some 50×10^{-26} w.m.$^{-2}$ (c/s)$^{-1}$. The declination estimate is in good agreement with the 178 Mc/s value. The small apparent flux density indicates an extent in declination of about 2°, which is also in agreement with the 178 Mc/s observations.

4. 81·5 *Mc/s observations.*—Re-examination of the observations made during the survey of galactic radio emission at 81·5 Mc/s (Baldwin 1955) has shown the existence of the source associated with the Cygnus Loop centred on α 2048·5. The flux density of the source is $470 \pm 150 \times 10^{-26}$ w.m.$^{-2}$ (c/s)$^{-1}$, the large uncertainty being due to the proximity of the source Cygnus A.

5. 38 *Mc/s observations.*—At 38 Mc/s scans across the Cygnus Loop were made by C. H. Costain using the 3200-ft × 40-ft corner reflector at Cambridge, which has beamwidths to half-power points of 0°·6 in right ascension and 40° in declination. The recording of the total power received by this aerial system, shown in Fig. 3, may be compared with those shown in Fig. 1. Apart from the differences in the galactic radiation underlying the source, which are due principally to the differing extents of the beam in declination in the two measurements, the curves are very similar. In particular: (i) the main peaks of emission occur at the same right ascension—α 2048·5; and (ii) the width of the main source between half brightness points is 1°·4 at 178 Mc/s and 1°·3 at 38 Mc/s.

A striking difference is the absence, on the 38 Mc/s records, of the small peak of emission at 2054·5. This will be discussed further in Section 7.

The flux density of the source at 38 Mc/s is $750 \pm 200 \times 10^{-26}$ w.m.$^{-2}$ (c/s)$^{-1}$. The large uncertainty in this value is caused by the difficulty of separating the relative contributions of the Cygnus Loop and the galactic radiation in Fig. 3.

6. *Spectrum of the radio emission.*—The values of flux density derived from the present observations are as follows :—

Frequency (Mc/s)	Flux Density ($\times 10^{-26}$ w.m.$^{-2}$(c/s)$^{-1}$)
38	750 ± 200
81·5	470 ± 150
178	430 ± 80

These were obtained in each case by comparison of the Cygnus Loop with the sources in Virgo and Taurus whose flux densities were taken from the mean spectral curves published by Whitfield (1957).

All the currently available values of flux density are plotted in Fig. 4. The spectral index of the radio emission is −0·6. Most of the radiation at low frequencies is therefore non-thermal in origin. It is of interest that the slope of the

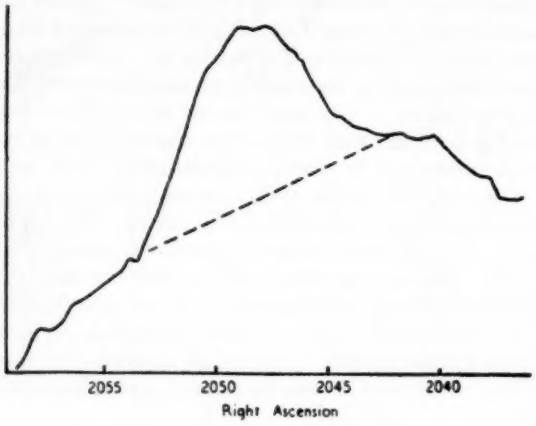

FIG. 3.—*Scan across the Cygnus Loop at 38 Mc/s.*

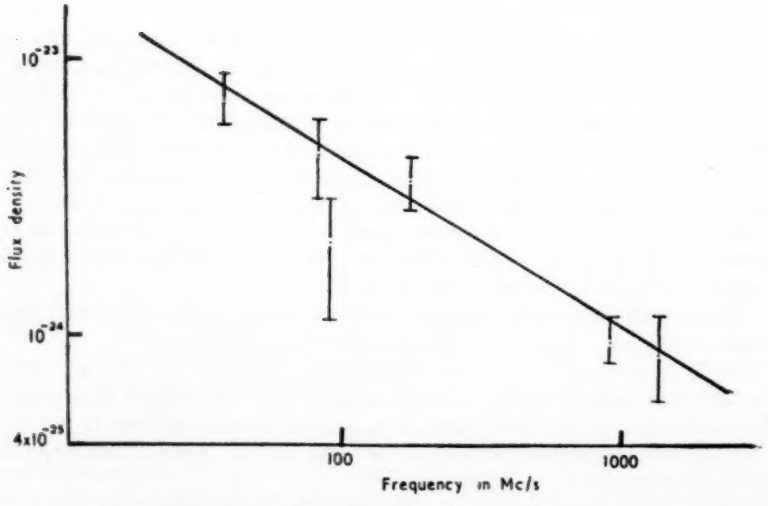

FIG. 4.—*The radio spectrum of the Cygnus Loop. The slope of the mean straight line drawn through the observations is* −0·6.

spectral curve is less steep than the average of all radio sources, but very similar to those of other filamentary galactic nebulae such as IC 443.

The radio position determined by Westerhout (1958) at 1390 Mc/s and by Eaton and Kraus (1959) at 915 Mc/s are :—

	α	δ
1390 Mc/s	$20^h\,46^m\,06^s \pm 2^m\,00^s$	$+30^\circ\,28' \pm 0^\circ{\cdot}3$
915 Mc/s	$20^h\,47^m\,35^s \pm 1^m\,00^s$	$+31^\circ \quad \pm 0^\circ{\cdot}5$

These two positions are consistent within the errors quoted but differ from positions measured at low frequencies and Westerhout has suggested that this shift of position with frequency may be due to the relative importance of thermal emission at high frequencies.

Determinations of the emission measure of the optical radiation from emission nebulae can lead, in the absence of interstellar absorption, to quite accurate estimates of the thermal radio emission from a source. It is of course particularly difficult to use this method of calculation in the case of filamentary nebulae where the emission measure varies between wide limits in an irregular way across the nebula. We can expect to make only an order of magnitude estimate of the thermal radio radiation from portions of the Cygnus Loop.

Observations by Osterbrock (1958) have shown that the maximum electron density in the filaments of the Cygnus Loop is about 500 cm^{-3} assuming that the kinetic temperature is near to 40 000°K. The thickness of typical filaments is 7×10^{-3} pc. The emission measure of one such filament lying normal to the line of sight is therefore about 1750 and the brightness temperature of the thermal radiation at 178 Mc/s corresponding to this value is 150°K.

The brightest mass of filaments in the Cygnus Loop is NGC 6992–5 lying at the N.E. corner of the nebula. We shall assume that over the region showing optical emission there is only one filament in the line of sight. The proportion of the aerial beam occupied by optical emission reaches a maximum when the aerial beam is centred on α 2054·5 when approximately one tenth of the area of the beam is covered with filaments. The thermal radiation should therefore provide an aerial temperature of 15°K. The minor peak in the radio scan at α 2055·0 has an excess brightness over its surroundings of about 30°K. The close agreement of this figure with the 15°K estimated suggests that thermal emission may contribute a significant proportion of the emission at this right ascension. At low frequencies this peak should be a less noticeable feature and at the lowest frequencies it may appear in absorption. The absence of the minor peak on the 38 Mc/s scan supports the thermal origin of its radiation. It does not occur in the list of sources given by Westerhout (1958) but it would probably be too weak to be included in his list. Since the concentration of filaments in NGC 6992–5 is much greater than in the central parts of the Cygnus Loop, thermal radiation can only account for part of the emission in the main source centred on α 2048·5.

7. *Conclusions.*

(i) The main source of radio emission associated with the Cygnus Loop lies at roughly the same right ascension but some 1° south of the centre of the nebula, in a region where there is a relatively small amount of optical emission. The extent of the main component of the radio source is 1°·4 in right ascension and about 2° in declination.

(ii) The radio emission does not extend beyond the limits of the visible nebula in right ascension. The edges of the radio source are sharply defined and coincide very well with the outer edge of the optical shell.

(iii) The emission from the source is mainly non-thermal at 178 Mc/s but a large part of the emission from the region of NGC 6992–5 may be thermal in origin.

Acknowledgments.—The authors would like to thank Mr M. Ryle for his assistance in the observations and Mr C. H. Costain for permission to use his 38 Mc/s recordings.

The investigation was made at the Mullard Radio Astronomy Observatory with the support of a grant from the Department of Scientific and Industrial Research. One of us (P.R.L.) is indebted to the Robert Cormack Bequest Trust for a research fellowship.

The Mullard Radio Astronomy Observatory,
Cavendish Laboratory,
Cambridge:
1959 *June* 4.

References

J. E. Baldwin, 1955, *M.N.*, **115**, 690.
R. Hanbury Brown and D. Walsh, 1955, *Nature*, **175**, 808.
J. J. Eaton and J. D. Kraus, 1959, *Ap. J.*, **129**, 282.
R. Minkowski, 1957. *Proceedings of the Third Symposium on Cosmical Gas Dynamics.* I.A.U. Symposium No. 8.
R. Minkowski, 1958. *Proceedings of the Paris Symposium on Radio Astronomy*, I.A.U. Symposium No. 9.
D. E. Osterbrock, 1958, *Pub. Ast. Soc. Pac.*, **70**, 180.
M. Ryle, 1957, *Nature*, **180**, 110.
G. Westerhout, 1958, *B.A.N.*, **14**, 215.
G. R. Whitfield, 1957, *M.N.*, **117**, 680.

PHOTOMETRY IN THE MAGELLANIC CLOUDS: I. STANDARD SEQUENCES

Olin J. Eggen and Allan R. Sandage

(Communicated by the Astronomer Royal)

(Received 1959 May 8)

Summary

Photoelectric magnitudes and colours on the (U, B, V)-system have been determined for *primary sequence* stars in the Large and Small Magellanic Clouds with the aluminized 18-inch Cape reflector. The magnitude system was established through observations of twenty bright standard stars. Observations of these, and additional, *primary sequence* stars in both Clouds were then secured with the silvered Radcliffe 74-inch reflector, and the magnitude and colour system transferred to *secondary sequences* in two fields of the Large Magellanic Clouds.

The present series of papers* will deal with the results obtained from a combined photographic and photoelectric study of the Magellanic Clouds with the Cape and Radcliffe Observatory telescopes. The first phase of this programme has been concerned with the establishment of preliminary photoelectric sequences to be used in the photographic photometry. These sequences will be strengthened and extended as the needs require. The present paper reports the results of standardization on the (U, B, V)-system of (1) a fundamental sequence in each of the Clouds, and (2) sub-sequences in two regions of the Large Cloud where detailed studies of the variables, clusters and Cloud field stars are being carried out.

Primary sequences.—The primary sequences in the Large (LMC) and Small (SMC) Magellanic Clouds are those used by Arp (1958). That in the SMC is in a region containing stars previously calibrated photoelectrically by Cox and Hallam (1953) and Gascoigne and Kron (Buscombe, Gascoigne and de Vaucouleurs 1955) but only a few stars are common to the present programme. The LMC sequence is near NGC 1866. The lettering system for the stars in the two primary sequences is that of Arp who also has published identification charts (1958, Plates I and II).

The observations of the brighter sequence stars and of twenty standard stars made with the Cape Observatory 18-inch aluminized reflector on 4 nights in December 1958 are given in Table I. The photometer and filters used are those currently in use at the Cape Observatory and will be discussed by the Cape observers. The observing and reduction technique has been described by

* This series of papers will describe some of the results of an investigation financed by the Department of Scientific and Industrial Research, which made a substantial grant to be paid over a period of five years from 1958/9 to the Radcliffe Trustees, with myself as Investigator. Part of the grant has been used to pay the expenses of Drs Eggen and Sandage at Pretoria and of Mr Alexander at the Cape. It is intended to reduce at Herstmonceux the extensive photographic material already obtained, and to obtain further photometric material in South Africa in later years. Part of the grant will be used to finance spectroscopic researches under Dr A. D. Thackeray's direction. R. v. d. R. Woolley.

Eggen (1955). The magnitudes and colours are all reduced to no-atmosphere with extinction coefficients determined each night. The derivation of these coefficients for three nights is illustrated in Figs. 1–3 where the open and filled symbols represent, respectively, the observations of a blue (v Ori) and red (δ Eri) star at various zenith distances, Z. The visual extinction illustrated in Fig. 1 shows little or no dependence of its effect on the deflections, D, through the yellow filter on the colour of the star. The effect of extinction on the observed colours, $(b-v)_n$, is strongly colour-dependent as can be seen in Fig. 2; this colour dependence of the extinction is assumed to vary linearly with colour. The observed ultra-violet colours, $(u-b)_n$, however, show little or no colour-dependence of the

TABLE I

Photoelectric units for the primary sequence and standard stars obtained with the Cape 18-inch aluminized reflector. The three entries under each date are the last two figures of the values for V, $B-V$ and $U-B$, respectively.

Star	Dec 22/3	Dec 23/4	Dec 24/5	Dec 29/30	$\bar{V}$	$\overline{B-V}$	$\overline{U-B}$
α Cet	... ...	... ...	... ...	49 63 93	2·49	+1·63	+1·93
α Pic	23 21 02	... ...	23 21 04	... ...	3·23	+0·21	+0·03
δ Eri	51 90 69	51 91 70	51 90 69	51 91 65	3·51	+0·905	+0·68
ζ Lep	52 10–02	53 14 03	53 10 0	... ...	3·53	+0·11	0·00
ϵ Eri	72 86 60	73 86 58	72 87 51	... ...	3·72	+0·86	+0·56
η Lep	... ...	... ...	... ...	73 32 05	3·73	+0·32	−0·05
ι CMa	36 7 74	39 7 75	36 6 72	... ...	4·37	−0·07	−0·74
HD 66141	... ...	... ...	... ...	38 25 29	4·38	+1·25	+1·29
HD 47442	... ...	... ...	... ...	39 16 06	4·39	+1·16	+1·06
40 Eri	39 79 46	... ...	41 81 45	... ...	4·40	+0·80	+0·455
α Cae	40 32 05	42 32 08	42 32 06	... ...	4·41	+0·32	−0·06
v Ori	62 25 06	62 26 08	62 26 08	62 26 06	4·62	−0·26	−1·07
κ Cet	... ...	... ...	85 68 18	... ...	4·85	+0·68	+0·18
λ Col	83 14 58	88 15 56	86 15 58	... ...	4·86	−0·15	−0·57
α Men	... ...	... ...	08 72 30	... ...	5·08	+0·72	+0·30
HR 875	... ...	... ...	16 10 00	15 08 00	5·16	+0·09	0·00
η Ret	... ...	22 94 53	21 95 70	... ...	5·22	+0·945	+0·62
HD 36003	... ...	... ...	... ...	62 13 17	7·62	+1·13	+1·17
HD 34673	... ...	... ...	... ...	75 03 88	7·75	+1·03	+0·88
SMC							
A	... ...	... ...	87 10 03	88 11 02	6·88	+0·105	+0·025
B	... ...	... ...	15 05 02	17 08 03	7·16	+0·065	−0·025
C	... ...	... ...	44 46 09	... ...	7·44	+0·46	−0·09
D	... ...	... ...	67 31 63	72 35 70	7·70	+1·33	+0·66
E	... ...	... ...	73 12 10	75 12 07	7·74	+1·12	+1·085
F	... ...	... ...	85 89 54	... ...	7·85	+0·89	+0·54
G	... ...	... ...	04 56 00	... ...	8·04	+0·56	0·00
H	... ...	... ...	39 98 77	44 00 79	8·42	+0·99	+0·78
P	... ...	... ...	... ...	29 16 07	10·29	+0·16	−0·17
Q	... ...	... ...	... ...	58 18 54	10·58	+1·18	+0·54
T	... ...	... ...	... ...	83 39 14	10·83	+0·39	−0·14
LMC							
A	02 42 03	08 43 05	00 42 05	03 42 02	7·03	+0·42	−0·04
B	35 09 33	36 08 36	37 07 35	36 07 35	8·36	−0·08	−0·35
C	... ...	35	34 38 ...	38 37 ...	9·36	+1·375	...
D	44 31 09	43 33 11	... ...	44 34 04	9·43	+0·33	−0·08

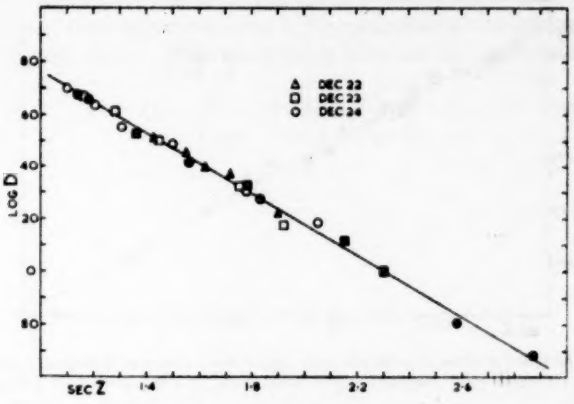

FIG. 1.—*The visual extinction observed on three nights in* 1958 *December with the* 18*-inch reflector of the Cape Observatory. The filled symbols represent observations of a red star* (δ *Eri,* $B-V=+0^{m}\cdot90$) *and the open symbols those of a blue star* (υ *Ori,* $B-V=-0^{m}\cdot26$). *The log D scale is relative only.*

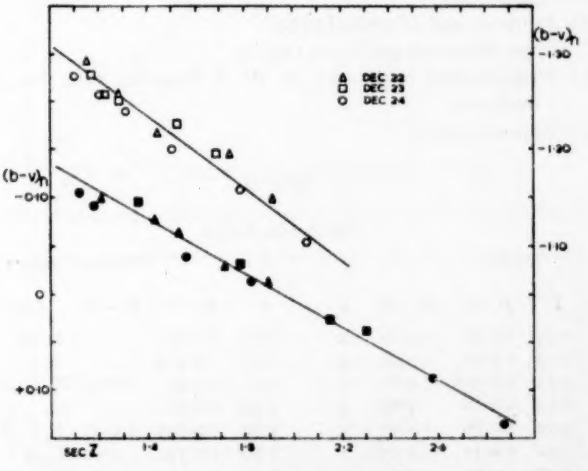

FIG. 2.—*The effect of extinction on the observed blue–yellow colours of* δ *Eridani (filled symbols) and* υ *Orionis (open symbols).*

extinction and they have been reduced to no-atmosphere with a single extinction coefficient. The values of the extinction coefficients used for the observations on the three nights illustrated in Figs. 1–3 are as follows:

$$V=\text{const.}+2\cdot5\,[\text{Log}\,D+0\cdot058\sec Z] \quad \text{(all colours)}$$
$$(b-v)=(b-v)_n-0^{m}\cdot140\sec Z \quad (\delta\,\text{Eri},\ B-V=+0^{m}\cdot90)$$
$$=(b-v)_n-0^{m}\cdot185\sec Z \quad (\upsilon\,\text{Ori},\ B-V=-0^{m}\cdot26)$$
$$(u-b)=(u-b)_n-0^{m}\cdot280\sec Z \quad \text{(all colours)}$$

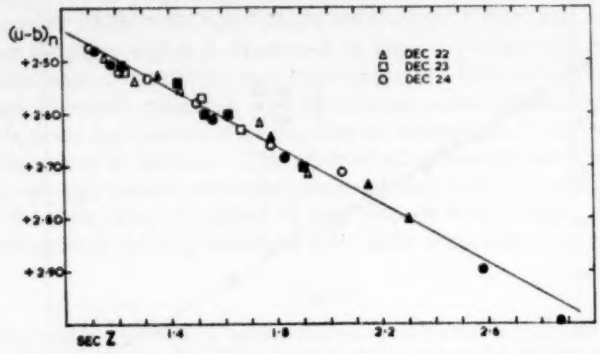

FIG. 3.—*The effect of extinction on the ultra-violet–blue colours of δ Eridani (filled symbols) and υ Orionis (open symbols). The colour scale, $(u-b)_n$, is that of δ Eridani.*

The relationship between the observed colours reduced to no-atmosphere and the adopted values of $B-V$ and $U-B$ for the twenty standard stars is shown in Figs. 4 and 5. The adopted values of V, $B-V$ and $U-B$ for the standard stars are given in Table II where their origins are indicated as follows:

E = Eggen (1955)
J = Johnson and Morgan (1953)
C = Cape Mimeogram No. 1 (1953)
C_1 = Unpublished results by A. W. J. Cousins with the 18-inch Cape reflector
R = Roman (1955)

TABLE II

The standard stars

	18-inch				Standard values				
Star	V	$B-V$	$U-B$	n	V	$B-V$	$U-B$	Obs.	Sp
α Cet	2·45	+1·65	+2·01	2	2·50	+1·65	...	E, C_1	M2 III
α Pic	3·25	+0·21	+0·03	4	3·25	+0·215	...	E, C	A5 III
δ Eri	3·51	+0·905	+0·69	6	3·52	+0·93	+0·69	E, C_1, J	K0 IV
ζ Lep	3·53	+0·10	0·00	3	3·53	+0·10	...	C_1	A3 V
ε Eri	3·72	+0·86	+0·57	3	3·70	+0·895	+0·57	E, C, J	K2 V
η Lep	3·72	+0·31	−0·03	2	3·70	+0·325	0·00	C_1, J	F0 IV
ι CMa	4·37	−0·06	−0·74	3	4·36	−0·07	−0·70	J	B3 II
HD 66141	4·38	+1·24	+1·27	2	4·40	+1·25	+1·24	R	K2 III
α Cae	4·40	+0·31	−0·05	3	4·45	+0·32	...	E, C_1	F2
40 Eri	4·40	+0·80	+0·46	2	4·43	+0·82	+0·44	E, C_1R, J	K1 V
HD 47442	4·41	+1·15	+1·05	2	4·43	+1·15	+1·04	J	
υ Ori	4·62	−0·26	−1·03	6	4·62	−0·25	−1·07	C_1, J	B0 V
HD 83425	4·68	+1·31	+1·47	1	4·66	+1·30	+1·46	R	K3 III
κ Cet	4·85	+0·685	+0·15	2	4·82	+0·68	+0·18	E, C_1, J	G5 V
λ Col	4·86	−0·14	−0·58	3	4·85	−0·135	...	E, C_1	B5 V
α Men	5·08	+0·72	+0·30	1	5·08	+0·72	...	E	G9
HR 875	5·16	+0·08	0·00	3	5·16	+0·09	+0·05	C_1, J	A1 V
η Ret	5·22	+0·95	+0·62	3	5·26	+0·95	...	E	G5
HD 36003	7·62	+1·125	+1·12	2	7·62	+1·065	+1·19	E, R	K5 V
HD 34673	7·76	+1·04	+0·91	2	7·76	+1·04	+0·85	E, R, J	K3 V

The standard values of $U-B$ are from J and from R only. The observations from E and from C were reduced to the (B, V)-system with relationships previously determined (Eggen 1955). The relationship between the observed and standard values are:

$$(U-B) = -1^{m}\cdot 67 + 1\cdot 09\,(u-b)$$
$$(B-V) = \quad 1^{m}\cdot 16 + 0\cdot 96\,(b-v)$$

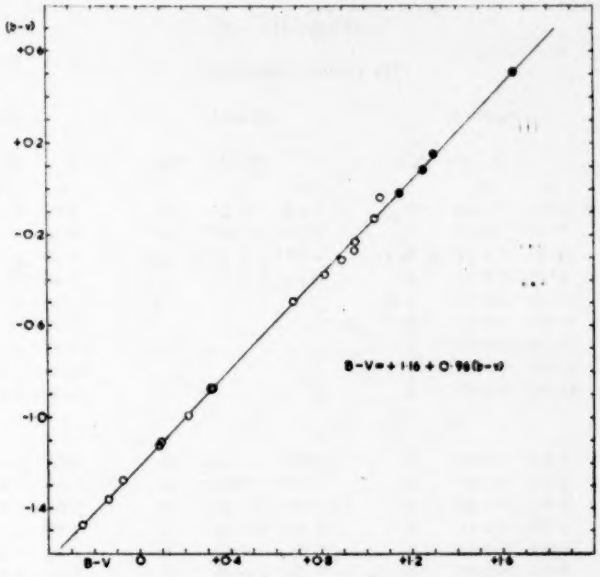

FIG. 4.—*The relationship between the values of* $(b-v)$ *and the standard values of* $B-V$.

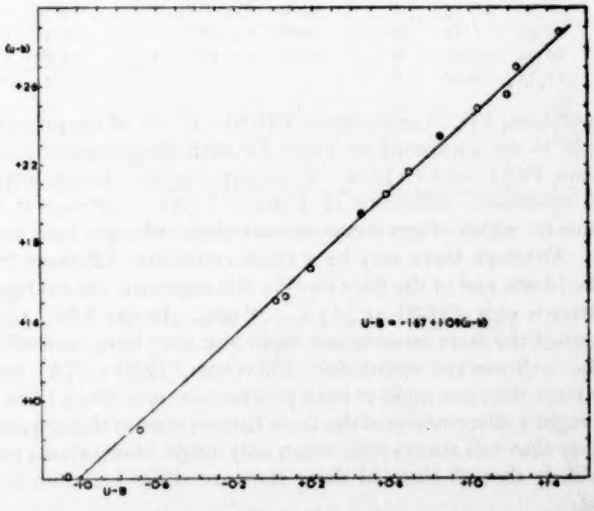

FIG. 5.—*The relationship between the values of* $(u-b)$ *and the standard values of* $U-B$.

The zero-point of the observed visual magnitudes was fixed by the values of V for all twenty standard stars in Table II; no colour equation between the observed and standard values of V was found. The comparison between the final results from the 18-inch programme and the adopted values for the standard stars is given in Table II. The observed magnitudes and colours of stars in the LMC and SMC primary sequences, converted to the (U, B, V)-system are listed in Table III.

TABLE III

The primary sequences

	74-inch			18-inch			Mean		
LMC	V	$B-V$	No.	V	$B-V$	No.	V	$B-V$	No.
	m	m		m	m		m	m	
A	7·02	+0·45	6	7·03	+0·42	4	7·02	+0·44	10
B	8·32	−0·07	6	8·36	−0·08	4	8·34	−0·075	10
C	9·36	+1·38	6	9·36	+1·375	3	9·36	+1·38	9
D	9·45	+0·31	5	9·43	+0·33	3	9·44	+0·32	8
E	11·39	+0·77	5	...	...	...	11·39	+0·77	5
F	11·97	+0·58	3	...	...	...	11·97	+0·58	3
G	12·33	+0·66	4	...	...	...	12·33	+0·66	4
H	12·26	+1·055	4	...	...	...	12·26	+1·055	4
I	13·09	+0·68	3	...	...	...	13·09	+0·68	3
SMC									
A	6·87	+0·09	2	6·88	+0·105	2	6·88	+0·10	4
B	7·15	+0·08	2	7·16	+0·065	2	7·16	+0·07	4
D	7·65	+1·33	2	7·70	+1·33	2	7·68	+1·33	4
E	7·78	+1·11	2	7·74	+1·12	2	7·76	+1·115	4
F	7·81	+0·92	2	7·85	+0·89	1	7·83	+0·91	3
G	8·01	+0·55	1	8·04	+0·56	1	8·03	+0·555	2
H	8·49	+1·00	1	8·42	+0·99	2	8·44	+0·995	3
K	9·80	+0·31	1	...	...	...	9·80	+0·31	1
P	10·30	+0·155	2	10·29	+0·16	1	10·30	+0·16	3
Q	10·55	+1·15	2	10·58	+1·18	1	10·56	+1·16	3
T	10·79	+0·415	2	10·83	+0·39	1	10·80	+0·405	3
g	11·54	+0·09	1	...	...	...	11·54	+0·09	1

The magnitudes, $V(\mathrm{ES})$ and colours, $C(\mathrm{ES}) = B - V$, of the primary sequence stars in Table II are compared in Table IV with the completely independent determinations, $V(\mathrm{A})$ and $C(\mathrm{A}) = B - V$, by Arp (1958). In the SMC there is a well-marked systematic difference of $V(\mathrm{ES}) - V(\mathrm{A}) = +0^{\mathrm{m}}{\cdot}040$ if we consider only those stars for which observations on more than one night have been made in both series. Although there may be a small systematic difference between the colours of the bright and of the faint stars in this sequence, the average difference for all the stars is only $C(\mathrm{ES}) - C(\mathrm{A}) = -0^{\mathrm{m}}{\cdot}005$. In the LMC sequence Arp observed most of the stars on only one night and they have, individually, lower weight. The well-marked systematic difference $V(\mathrm{ES}) - V(\mathrm{A})$ for the stars observed on more than one night in both programmes is $-0^{\mathrm{m}}{\cdot}04$ from three stars. Arp's single night's observations of the three faintest stars in this sequence indicate the uncertainty that will always arise when only single observations are available. It seems unlikely that all three of these stars are either variables or have been misidentified.

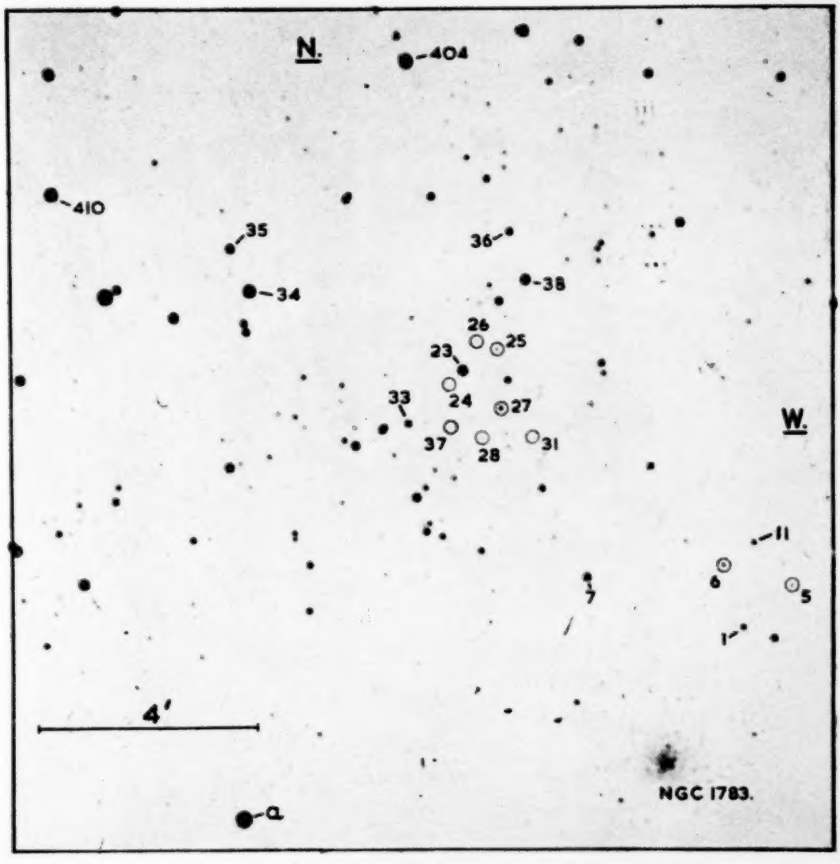

The secondary sequence stars in LMC Field 1.

ERRATA.—*Nos. 25 and 26 should be interchanged.*
Nos. 6 and 11 refer to stars 1·0 cm due east of the indicated positions.

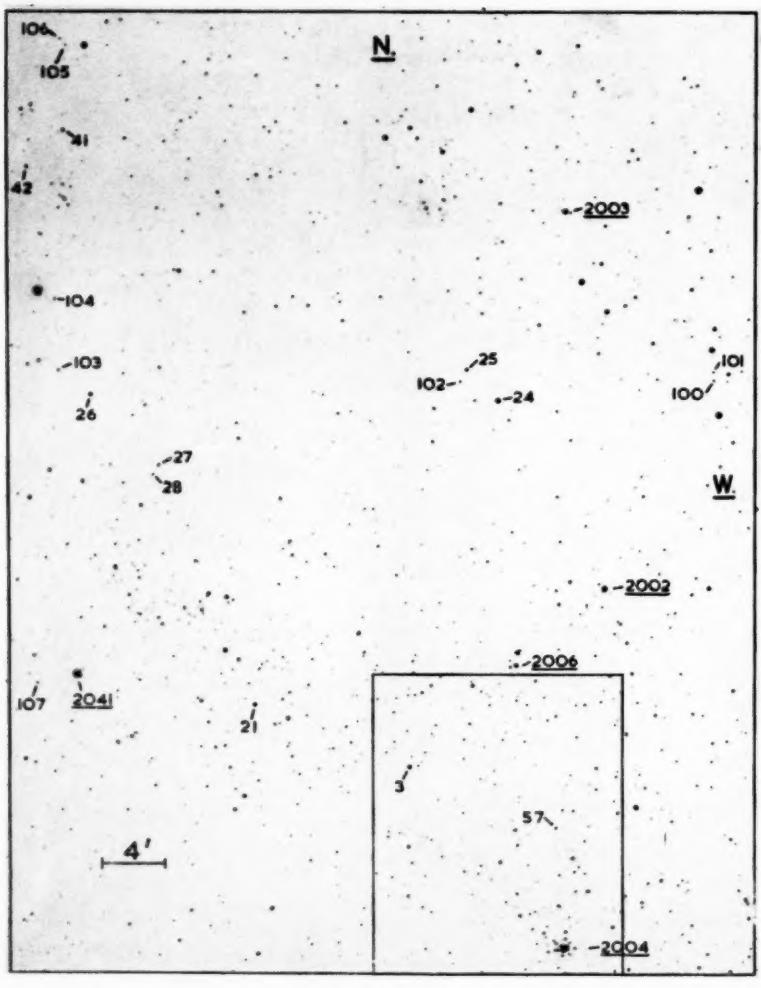

The secondary sequence stars in LMC Field 2. The enclosed area is shown on an expanded scale in Plate 3. Underlined numbers indicate NGC numbers of clusters.

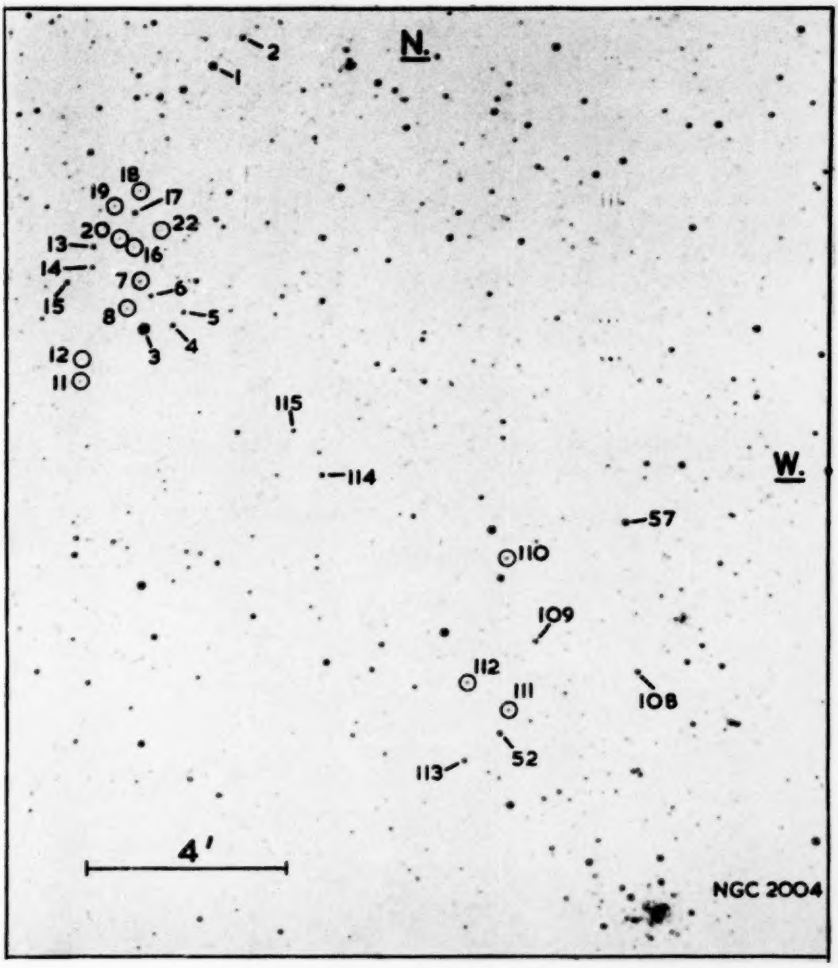

An enlargement of the enclosed area in LMC Field 2 shown in Plate 2.

There are also three stars of the present programme common to some work by Gascoigne and Kron (Buscombe, Gascoigne and de Vaucouleurs 1955) in the LMC and 6 stars in common with the sequence established by Cox and Hallam (1953). The colours determined by these observers cannot be fairly compared with the present results because of differences in the band-pass of the blue filters used and the small number of common stars, but the differences in the visual magnitudes are listed in Table V as $V(ES)-V(GK)$ and $V(ES)-V(CH)$. The mean difference, $V(ES)-V(CH)$ is $0^m.000$ with an average deviation of $\pm 0^m.025$. There is a systematic difference $V(ES)-V(GK)=-0^m.08$. However, Arp's conclusion that the mean value of $V(A)-V(GK)=-0^m.11$ indicates an error in the C12 and D2 regions on which values of $V(GK)$ were based seems a little hasty in view of the systematic difference of $+0^m.08$ in $V(Arp, SMC)-V(Arp, LMC)$, derived from a comparison of the present results with magnitudes determined by Arp by observations on more than one night. A straight mean value of all available photoelectric results for stars P, Q and T in the SMC would leave systematic differences of $V(A)-V(mean)=-0^m.04$ and $V(GK)-V(mean)=+0^m.06$.

TABLE IV

Comparison of the present results for the primary standards with those derived by Arp, by Cox and Hallam and by Gascoigne and Kron. The number of observations is indicated under n.

Star	$V(ES)-V(A)$	$C(ES)-C(A)$	$n(ES)$	$n(A)$	$V(ES)-V(CH)$	$V(ES)-V(GK)$
SMC	m	m			m	m
A	+0.04	−0.010	4	5	...	...
B	+0.05	0.000	4	5	...	...
D	+0.04	+0.005	4	1	+0.01	...
E	+0.03	+0.015	4	5	...	...
F	+0.03	+0.025	3	1	...	...
G	−0.02	+0.035	2	1	0.00	...
H	+0.04	+0.015	3	4	+0.05	...
K	+0.07	−0.010	1	1	...	...
P	+0.05	−0.025	3	2	+0.03	−0.07
Q	0.00	−0.015	3	2	−0.05	−0.09
T	+0.06	−0.020	3	2	+0.03	−0.06
g	0.00	−0.055	1	3	...	...
LMC						
A	−0.03	+0.030	10	3	...	...
B	−0.04	−0.015	10	3	...	...
C	+0.02	+0.010	9	1	...	...
D	+0.01	+0.005	8	1	...	...
E	+0.03	+0.055	5	1	...	...
F	−0.06	+0.045	3	6	...	...
G	+0.05	(−0.155)	4	1	...	...
H	(−0.41)	(+0.035)	4	1	...	...
I	+0.06	(+0.14)	3	1	...	...

Secondary sequences.—Two regions in the LMC, one near NGC 1783 ($\alpha=4^h\,59^m$, $\delta=-66°\,3'$, 1960) and the other near NGC 2004 ($\alpha=5^h\,0^m$, $\delta=-66°\,55'$, 1960) have been selected for an extensive photometric study of the variables, clusters and field stars in the LMC. Secondary photoelectric sequences were established in these regions on three nights at the Cassegrain focus of the silvered 74-inch Radcliffe reflector, using a commercial (General Radio) amplifier

and a refrigerated IP21 multiplier; the filters used were 2 mm GG11 and 2 mm GG13 + 1 mm BG12. The sequence near NGC 1783—in what will be called LMC Field No. 1—contains only 21 stars but stars over the whole magnitude range covered were observed on two and sometimes three nights so that the accuracy of the results for the individual stars is relatively high.

A different approach was made to the sequence near NGC 2004 (LMC Field No. 2) where 44 stars were observed spread over a $\frac{1}{2}^\circ$ field, but except for two of the brightest stars, only a single night's observation was made for each. The resulting sequences in both fields are given in Table V and the stars are identified in Plates 1–3. Observations of primary sequence stars were intermixed with those of the secondary sequence and, because of the varying colour equation of the ageing silver mirror, the transformation from the observed to the (U, B)-system was determined from each night's results. The average colour equation between the observed and standard V-magnitudes was $0^m.06\,(B-V)$.

Approximately 25 yellow and 25 blue plates in each field have been taken by J. Alexander with the Cape 24/18-inch McLean double refractor. The plate and filter combinations were Eastman 103aD + OMAG 301 and Eastman 103aO + Schott GG13. The plates were 16 cm on a side and cover a field of $1^\circ 20'$. To smooth the secondary photoelectric sequence, measurements on six yellow and six blue plates in LMC Field No. 1 and on four plates in each colour in LMC Field No. 2 were made by Sandage with the Sartorious astrophotometer at Herstmonceux. Also, three plates in each colour in LMC Field No. 2 were measured by Woolley with the same instrument. Calibration curves were constructed for each plate using the photoelectric magnitudes listed in Table V. The magnitudes of the sequence stars were then read back from the smoothed calibrations curves and the resulting mean photographic values of V and B for six plates are also listed in Table V.

TABLE V

The secondary sequences

No.	V(PE)	V(PG)	ΔV	B(PE)	B(PG)	ΔB	n
			LMC Field No. 1				
	m	m	m	m	m	m	
a	9·64	...	...	10·66	...	...	2
404	10·83	...	...	10·72	...	...	1
410	11·03	...	...	11·02	...	...	1
34	11·14	11·12	+0·02	11·41	11·46	−0·05	1
23	12·08	12·13	−0·05	12·63	12·63	0·00	3
38	12·17	12·13	+0·04	12·06	11·95	+0·11	1
35	12·68	12·64	+0·04	14·59	14·51	+0·08	1
7	13·12	13·06	+0·06	13·95	13·86	+0·09	3
33	13·42	13·46	−0·04	13·24	13·30	−0·06	1
36	13·50	13·24	+0·26	13·23	13·05	+0·18	1
1	13·90	13·95	−0·05	13·84	13·82	+0·02	1
27	14·50	14·49	+0·01	14·20	14·22	−0·02	2
26	15·15	15·31	−0·16	14·95	15·04	−0·09	1
11	15·16	15·19	−0·03	14·99	14·94	+0·05	1
5	15·30	15·19	+0·11	15·83	15·83	0·00	1
25	15·54	15·69	−0·15	15·45	15·55	−0·10	2
28	15·73	15·68	+0·05	15·59	15·54	+0·05	2
31	15·80	15·80	0·00	15·68	15·72	−0·04	2
6	15·90	15·76	+0·14	15·87	15·64	+0·23	1
24	16·62	16·62	0·00	17·87	17·87	0·00	2
37	17·07	17·07	0·00	17·04	17·04	0·00	2

TABLE V (*continued*)

The secondary sequences

No.	V(PE)	V(PG)	ΔV	B(PE)	B(PG)	ΔB	n
			LMC Field No. 2				
	m	m	m	m	m	m	
24	8·75	...	...	9·26	...	...	1:
3	9·65	...	...	10·19	...	...	2
21	9·78	...	...	9·75	...	...	1:
26	10·25	10·24	+0·01	10·73	10·68	+0·05	1:
25	11·25	11·25	0·00	12·90	12·95	−0·05	1:
1	11·50	11·50	0·00	11·49	11·52	−0·03	3
41	11·83	11·83	0·00	12·40	12·50	−0·10	1:
27	11·84	11·98	−0·14	12·09	12·26	−0·17	1:
42	12·00	11·86	+0·14	12·45	12·36	+0·09	1:
57	12·12	12·28	−0·16	12·13	12·13	0·00	1:
52	12·32	12·54	−0·22	12·97	12·95	+0·02	1
28	12·39	12·44	−0·05	13·49	13·56	−0·07	1:
103	12·48	12·50	−0·02	12·88	12·87	+0·01	1:
102	12·52	12·69	−0·17	12·57	12·67	−0·10	1:
107	12·66	12·52	+0·14	13·51	13·34	+0·17	1:
2	12·86	12·89	−0·03	14·73	14·75	−0·02	2
4	12·93	13·17	−0·24	14·82	14·93	−0·11	1
108	12·96	12·96	0·00	12·96	12·87	+0·09	1:
100	13·07	13·01	+0·06	13·66	13·56	+0·10	1:
104	13·07	13·06	+0·01	13·66	13·65	+0·01	1:
17	13·08	13·23	−0·15	12·92	13·01	−0·09	1
113	13·09	13·24	−0·15	12·74	12·96	−0·22	1:
114	13·16	13·12	+0·04	15·23	14·82	+0·41	1:
13	13·19	13·20	−0·01	15·00	14·83	+0·17	1
109	13·21	13·20	+0·01	13·68	13·69	−0·01	1:
15	13·31	13·24	+0·07	13·25	13·14	+0·11	1
101	13·38	13·33	+0·05	13·60	13·77	−0·17	1:
5	13·72	13·80	−0·08	13·47	13·62	−0·15	1
115	13·72	13·86	−0·14	13·44	13·73	−0·29	1:
14	13·92	13·86	+0·06	14·61	14·61	0·00	1
106	14·12	14·16	−0·04	14·78	14·66	+0·12	1:
105	14·22	14·45	−0·23	14·81	14·87	−0·06	1:
110	14·38	14·26	+0·12	15·71	15·76	−0·05	1:
111	14·47	14·58	−0·11	15·60	15·36	+0·14	1:
112	14·54	14·38	+0·16	15·17	15·00	+0·17	1:
7	15·21	15·10	+0·10	14·78	14·88	−0·10	1
11	15·33	15·43	−0·10	15·30	15·20	+0·10	1
20	15·37	15·41	−0·04	15·18	15·21	−0·03	1
8	15·65	15·36	+0·29	15·20	15·08	+0·12	1
18	15·67	15·74	−0·07	15·51	15·52	−0·01	1
19	15·75	15·76	−0·01	15·42	15·49	−0·07	1
16	16·01	15·96	+0·05	15·70	15·69	+0·01	1
12	16·20	16·16:	+0·04	16·09	16·01:	+0·08	1
22	16·45	16·48	−0·03	16·43	16·44	−0·01	1

A plot of the residuals V(PE)$-V$(PG) and B(PE)$-B$(PG) against the photoelectrically determined values of $B-V$ and V shows no significant colour or magnitude equation between the photoelectric and the photographic values. However, the size of the residuals is larger by a factor of two from the results obtained in similar studies with the Mt Wilson reflectors using smaller plates. This may be explained either by random inhomogeneities in the photographic

emulsion over the large area of the 16 cm square plates or by small systematic distance to centre corrections caused by comatic aberration in the McClean refractor. Special offset plates are being measured by Woolley to determine the distance to centre effect but the present residuals indicate that the effect will probably be smaller than $0^{m}\cdot1$.

The secondary sequence stars listed in Table V and identified by Plates 1–3 will be used as standards in later papers of this series for studies of the cepheid variables, and for the $(V, B-V)$-diagrams for selected clusters and for the background of the LMC.

We are greatly indebted to R. H. Stoy and A. D. Thackeray for making available the observing time on, respectively, the Cape and Radcliffe Observatory instruments. Thanks are also due to Dr G. E. Kron for constructing the cold-box used with the multiplier on the 74-inch reflector, to Dr A. J. Wesselink for the use of the Cassegrain photometer on the 74-inch reflector, and Dr A. W. J. Cousins for furnishing some magnitudes and colours before publication.

Royal Greenwich Observatory,
Herstmonceux Castle,
Sussex:
1959 *May* 7.

Mount Wilson and Palomar Observatories,
California Institute of Technology,
Carnegie Institute of Washington,
Pasadena, California.

References

Arp, H. C., 1958, *A. J.*, **63**, 118; *Pub. Goethe Link Obs.*, No. 20.
Buscombe, W., Gascoigne, S. C. B., and de Vaucouleurs, G., 1955, *Supplement to the Australian Journal of Science*, **17**.
Cox, A. N., and Hallam, K. L., 1953, *Ap. J.*, 118, 314; *Pub. Goethe Link Obs.*, No. 11.
Eggen, O. J., 1955, *A. J.*, **60**, 65; *Lick Obs. Bull.*, No. 552.
Johnson, H. L., and Morgan, W. W., 1953, *Ap. J.*, **117**, 313.
Roman, N. G., 1955, *Ap. J. Supp. Series* **II**, 195.

NOTICE TO AUTHORS

Presentation of Papers at Meeting

At some meetings of the Society the background and conclusions of selected papers are presented and then discussed. In order to assist the Secretaries in the selection of papers for such meetings, authors are asked to let the Society know, when submitting papers, whether they would be willing to give an account of their paper, if requested.

The attention of authors resident abroad is drawn to the fact that the Society welcomes information about their work. The Secretaries would be happy to consider having such work described at a meeting, in accordance with the author's wishes, either by a Secretary or other Fellow.

Publication of Papers

1. *General.*—It is the aim of the Society to be of the greatest possible service in disseminating astronomical results and ideas to the scientific community with the utmost possible speed. Contributors are accordingly urged to give the most careful consideration to the presentation of their work, for attention to detail will assuredly result in a substantial saving of time.

It is the practice of the Society to seek a referee's opinion on nearly every paper submitted for publication in *Monthly Notices*; experience has shown that frequently the comments of referees have enabled authors to improve the presentation of their work and so increase its scientific value.

2. *Communication.*—Papers must be communicated to the Society by a Fellow. They should be accompanied by a summary at the *beginning* of the paper conveying briefly the content of the paper, and drawing attention to important new information and to the main conclusions. The summary should be intelligible in itself, without reference to the paper, to a reader with some knowledge of the subject; it should not normally exceed 200 words in length. Authors are requested to submit MSS. in duplicate. These should be typed using double spacing and leaving a margin of not less than one inch on the left-hand side. Corrections to the MSS. should be made in the text and not in the margin. By Council decision, MSS. of accepted papers are retained by the Society for one year after publication; unless their return is then requested by the author they are destroyed.

3. *Presentation.*—Authors are allowed considerable latitude, but they are requested to follow the general style and arrangement of *Monthly Notices*. References to literature should be given either in the traditional form of a numbered list at the end of the paper, or as prescribed in *Notes on the Preparation of Papers to be Communicated to the Royal Society*.

4. *Notation.*—For technical astronomical terms, authors should conform closely to the recommendations of Commission 3 of the International Astronomical Union (*Trans. I.A.U.*; Vol. VI, p. 345, 1938). Council has decided to adopt the I.A.U. 3-letter abbreviations for constellations where contraction is desirable (Vol. IV, p. 221, 1932). In general matters, authors should follow the recommendations in *Symbols, Signs and Abbreviations* (London: Royal Society, 1951) except where these conflict with I.A.U. practice.

5. *Diagrams.*—These should be designed to appear upright on the page, drawn about twice the size required in print and prepared for direct photographic reproduction except for the lettering, which should be inserted in pencil. Legends should be given in the manuscript indicating where in the text the figure should appear. Blocks are retained by the Society for 10 years; unless the author requires them before the end of this period they are then destroyed. Enough copies or prints of the diagrams should accompany each manuscript.

6. *Tables.*—These should be arranged so that they can be printed upright on the page.

7. *Proofs.*—Authors are liable for costs of alteration exceeding 5 per cent of composition. It is therefore in their own and the Society's interests to seek the maximum conciseness and simplification of symbols and equations consistent with clarity.

CONTENTS

PAGE

Meeting of 1960 January 8:

Announcement of award of Gold Medal to Professor V. A. Ambartsumian .. 1

Announcement of award of Eddington Medal to Dr R. d'E. Atkinson .. 1

Announcement of award of Jackson Gwilt Medal and Gift jointly to Mr F. M. Bateson and Mr A. F. A. L. Jones 1

Fellows and Junior Members elected 1

Antoni Przybylski, On the mean absorption coefficient in the computation of model stellar atmospheres of solar type stars 3

F. Hoyle, On the main-sequence band and the Hertzsprung gap 22

J. Crampin and F. Hoyle, Problems concerning Pleione 33

D. H. P. Jones, The radial velocities of five stars in the ζ Persei aggregate .. 43

R. Wilson, The relation between interstellar extinction and polarization 51

M. W. Feast, A. D. Thackeray and A. J. Wesselink, 47 Tucanae: the membership of two RR Lyrae variables 64

J. E. Baldwin and P. R. R. Leslie, Radio emission from the Cygnus Loop .. 72

Olin J. Eggen and Allan R. Sandage, Photometry in the Magellanic Clouds: I. Standard sequences 79

Printed in London by Taylor & Francis, Ltd., 1960 February